Inês de Brito Trindade

Degree in Forensic Science

Emerging human pathogens from the *Shewanella* genus: understanding the molecular mechanism behind ferric iron-siderophore reduction

Dissertation presented to obtain the Master degree in Biochemistry for Health.

Supervisor: Ricardo O. Louro

Co-supervisor: Bruno M. Fonseca

Jury:

President: Dr. Pedro Matias

Opponent: Dr. Alice Pereira

Members of the Jury: Dr. Margarida Archer

Instituto de Tecnologia Química e Biológica António Xavier

September 2016

Emerging human pathogens from the *Shewanella* genus: understanding the molecular mechanism behind ferric iron-siderophore reduction.

Acknowledgements

"Never doubt that a small group of thoughtful committed citizens can change the world. Indeed, it is the only thing that ever has." Margaret Med

Foremost, I would like to express my sincere gratitude to my thesis supervisors Dr. Ricardo Louro and Dr. Bruno Fonseca for making this thesis possible. Dr. Ricardo Louro, it has been an honor to be your master's student. Your motivation, and commitment to highest standards were inspirational. Thank you for your positive attitude, guidance and support. You showed me the way to "fly".

I would like to thank my lab colleagues for the knowledge shared, support, and for the fun moments that we spent in the lab.

I would also like to express my gratitude to the following:

- Thank you Dr. Elin Moe for allowing me the pleasure of setting up crystallization experiments, and for believing in me. I had a great time!
- Thank you Dr. Masaki Fujita for sending us the siderophores all the way from Japan. This was a crucial part of this thesis, and I hope to return this gesture.
- Thank you Dr. Teresa Catarino for making part of this project and for your support. Thank you for your enthusiasm and for your working ethics!
- Thank you Isabel for helping me with the purifications and for your wisdom. It is always the biggest pleasure to work with you!
- Thank you Dr. Américo Duarte for the wise advices and for providing us the ferredoxin.
- Thank you all my friends, family, and specially to Fatima, my guardian angel.

Lastly, but most importantly, I owe my deepest recognition to Paulo Oliveira for walking this journey by my side. Thank you for your love, support, patience, enthusiasm and for reminding me about the basic needs of a human being!

Abstract

Keywords: Electrochemistry; Iron uptake; Nuclear Magnetic Resonance; *Shewanella;* Siderophore-interacting protein; Stopped-flow kinetics.

Shewanella are Gram-negative rod-shaped bacteria that colonize diverse environments. Nevertheless, over the past years, reports have increasingly identified particular *Shewanella* spp. as opportunistic human pathogens. Reaching up to almost 300 cases of accounted infections, higher frequency was found in warm climates and usually includes the exposure to sea water.

To date there is virtually no research on *Shewanella*'s pathogenicity, however iron acquisition during infection of a host plays an important role and it is a challenge that every pathogen encounters. Siderophore-mediated iron acquisition provides pathogens with the ability of circumventing the host's immune defense and for this reason the siderophore pathway has been extensively explored. One of the least explored processes is siderophore recycling, the reduction of the ferric siderophores mediated by siderophore-interacting proteins. These fall into two subfamilies, the SIP flavoproteins and the FSR proteins containing an iron-sulfur cluster.

Hereby, a siderophore-interacting protein (SIP) from *Shewanella frigidimarina* was produced and biochemically characterized. Electrochemical data show that the reduction potentials are adequate to reduce ferric siderophores associated with *Shewanella* and display Redox-Bohr effect. NMR data show that both NADH and NADPH bind SIP with dissociation constant in the range that is typical for redox partners. However, stopped-flow data show that the reduction of ferric siderophores by SIP using these electron donors required the presence of ferrozine to drive the reaction. Interestingly, our data revealed that within the SIP subfamily, this is the first reported SIP that can utilize a ferredoxin as electron donor. This novelty was further explored by preparing crystals to determine the molecular structure of SIP.

Overall, this thesis reports the comprehensive characterization of the SIP from *S. frigidimarina* revealing novel aspects of the reactivity of this important class of enzymes for the colonization of iron limited environments.

Resumo

Palavras-chave: Aquisição de ferro; Eletroquímica; Estudos cinéticos de Fluxo-Interrompido; Proteínas de interação com sideróforos (SIP); Ressonância Magnética Nuclear; *Shewanella*.

Shewanella são bactérias Gram-negativas em forma de bastonete que colonizam ambientes diversos. Ao longo dos anos, tem se verificado o aumento do número de infeções oportunistas causadas por algumas espécies de Shewanella. Aproximadamente 300 casos de infeções foram reportados, com maior frequência em climas quentes e perante a exposição marítima.

O conhecimento sobre a virulência de *Shewanella* é presentemente limitado. No entanto, a aquisição de ferro mediada por sideróforos permite aos patogeneos contornar a resposta imunitária do hospedeiro, e por este motivo a via metabólica dos sideróforos tem sido intensamente estudada. Um dos processos menos explorado é a reutilização dos sideróforos. Este consiste na redução do complexo sideróforo-Fe^{3+} mediada por proteínas de interação com sideróforos (SIP). Estas proteínas estão organizadas em duas famílias, uma de flavoproteinas (SIP) e outra de proteínas que contêm um centro de ferro-enxofre (FSR).

Nesta tese produziu-se e caracterizou-se uma *SIP* de *S.frigidimarina*. Os dados eletroquímicos revelam que os potenciais de redução desta proteína são adequados para reduzir complexos de sideróforo-Fe^{3+} produzidos por *Shewanella* e observa-se efeito Redox-Bohr. Os dados de RMN revelam que NADH e NADPH se ligam à SIP com uma constante de dissociação da ordem de grandeza dos micromolar. No entanto, os dados de Fluxo Interrompido demonstram que a redução de sideróforos pela SIP utilizando estes dadores de eletrões requer a presença de ferrozina para promover a reação. Os nossos dados revelam ainda pela primeira vez uma proteína da família das SIPs com a capacidade de utilizar uma ferredoxina como dador de electrões. Estas novidades funcionais foram também exploradas preparando cristais da SIP para determinar a sua estrutura tridimensional.

Globalmente, esta tese apresenta a caracterização abrangente da SIP de *S.frigidimarina* revelando aspetos inovadores da reatividade desta classe de proteínas que tem um papel fundamental na colonização de ambientes limitados em ferro.

Table of contents

List of figures

List of tables

List of abbreviations

ABC	ATP binding cassette
BIFs	Banded iron formations
BLAST	Basic local alignment search tool
FAD	Flavin adenine dinucleotide
FER	Ferrioxamine E
FSR	Ferric siderophore reductase
FMN	Flavin mononucleotide
GOE	Great oxidation event
LC-MS	Liquid chromatography
MY	Million years
NAD(P)H	Dihydronicotinamide-adenine dinucleotide (phosphate)
NMR	Nuclear magnetic resonance
PAL	Present atmospheric levels
PFV	Protein film voltammetry
PGE	Pyrolytic graphite edge
ROS	Reactive oxygen species
SIP	Siderophore-interacting protein
SD	Standard deviation
SDS-PAGE	Sodium dodecyl sulfate - polyacrylamide gel electrophoresis

1. Introduction

The bioselection of elements is driven by four fundamental rules: the abundance of the element, its efficiency, its fitness for a specific task, and the evolutionary pressure (Ochiai, 1986, Silva & Williams, 1991, Crichton & Pierre, 2001).

Highlighting the exclusive characteristics of iron, throughout evolution this transition metal was kept as a crucial element across the three domains of life (eukarya, eubacteria, and archaea) (Ilbert & Bonnefoy, 2013, Koonin, 2014).

After aluminum, iron is the most abundant metal, and the fourth most abundant element in the Earth's crust (Ilbert & Bonnefoy, 2013). Ferric, Fe(III), and ferrous, Fe(II), are the two most common forms of iron, even though it can exist in oxidation states that range from -2 to +6. In nature, iron is not commonly found in its free form, instead, it tends to coordinate with various organic and inorganic ligands, providing the Fe(II)/Fe(III) redox couple with the ability to substantially span the entire biologically relevant range of redox potentials, from -0.5 V to 0.6 V, making this redox pair suitable and adjustable for incorporation in diverse biological pathways (Crichton & Pierre, 2001, Pierre, et al., 2002, Ilbert & Bonnefoy, 2013).

Essentially, iron is able to incorporate two key roles for life: an energetic role, as it can be used as an electron donor and acceptor for some organisms such as *Shewanella onedensis* MR-1 and *Geobacter sulfurreducens* and a structural/redox role, as it is incorporated in many vital metalloproteins (Schröder, et al., 2003,.Ilbert & Bonnefoy, 2013).

Despite the abundance of this transition metal, after the Great Oxidation Event (GOE) previously readily available ferrous iron precipitated into ferric iron leading microorganisms to face iron limitation (Holland, 2006). The amount of iron in the human body provides bacterial pathogens with an opportunity for iron acquisition and proliferation promoting what has been regarded as "the ongoing battle for iron" between bacterial pathogens and their vertebrate hosts (Skaar, 2010, Caza & Kronstad, 2013).

1.1. The Great Oxidation Event

Oxygen in the atmosphere is the most influential factor in the redox state of a water body such as the ocean (Ochiai, 1986). In today's oxygen-rich atmosphere, 21% of free oxygen (O_2) exist, and for this reason, Fe(II) is readily oxidized to a low solubility (10^{-17} M) Fe(III) (Ochiai, 1986, Ilbert & Bonnefoy, 2013).

Nevertheless, this was not always the case, through isotopic data it is possible to confirm that both the ocean and atmosphere were oxygen deprived for almost 70% of the Earth's history (Lyons, et al., 2014). Possibly, as a consequence of the activity of photosynthetic cyanobacteria, approximately 2.4 billion years (BY) ago the first buildup of oxygen took place, and this became known in the literature as the GOE (Ilbert & Bonnefoy, 2013). GOE has been regarded as one of most compelling stories of Earth's history, subject of intense research and controversy (Huston & Logan, 2004).

Notwithstanding, after GOE, 2,4 billion years ago, oxygen levels still represented only 0.001% of the present atmospheric levels (PAL). It was only after the second oxidation event (550 MY later) that oxygen levels rose to about 20% of PAL, enough oxygen to sustain respiration (Ilbert & Bonnefoy, 2013, Zhang, et al., 2016). Different models have been proposed to represent the timeline and increase of oxygen from GOE to PAL (Fig. 1.1 B) including the classical two-step model, where oxygen levels increased modestly at GOE and then lagged for about two billion years before dramatically rising to PAL, and the emergent model, which defends a more dynamic increase in the atmospheric oxygen levels which rise after GOE and decrease back to lower levels probably due to the existing biogeochemical conditions which together with low oxygen availability postponed the emergence and diversification of eukaryotic organisms and large animals (Lyons, et al., 2014).

The timing and mechanisms for the increase in oxygen are still a matter of debate. However, the rise of oxygen surely had a profound impact in the redox structure of both, ocean and atmosphere which ended up determining today's bioavailability of iron (Lyons, et al., 2014).

The history of iron in the ocean has been studied in banded iron formations (BIFs) deposited around 3 BY and in embedded sulfate deposits (Williams, 2012, Huston & Logan, 2004). From these, three stages can be distinguished (Fig. 1.1 B): stage I, up until 2.5 BY which is defined by the precipitation of BIFs caused by an anoxic and sulfidic ocean, altering the BIFs composition from a mixture of Fe_2O_3 and Fe_3O_4 to substantially all Fe_2O_3; stage II, a period between 1 and 2 BY marked by no observed BIFs, a period of coexisting sulfidic and ferruginous conditions beneath oxic surface waters and stage III, represented by the reappearance of Fe_2O_3 BIFs, probably resultant from the second oxidation event which caused a dramatic change in the ocean's chemistry, shifting it to fully oxygenated conditions (Ilbert & Bonnefoy, 2013, Williams, 2012). These three stages represent the rapid environmental changes as a consequence of the two great oxidation events, having a close correspondence with the evolution from single-cell to multiple-cell organisms (Figure 1.1 A) (Williams, 2012). In the ocean, the redox potential shifted from -0.4 V to 0.4 V and the iron's concentration changed from 10^{-6} M Fe(II) to free 10^{-17} M of Fe(III) and 10^{-10} M of Fe(III)-complexes (Williams, 2012) (Ilbert & Bonnefoy, 2013). Nowadays, "iron-rich"

environments contain in reality, a free iron concentration lower than 1 µM, the considered threshold to sustain life (Schröder, et al., 2003).

Allegedly, the biochemistry and geochemistry coevolved, but with iron-containing cofactors reaching to lower reduction potentials the demand for iron never followed its bioavailability (Ilbert & Bonnefoy, 2013).

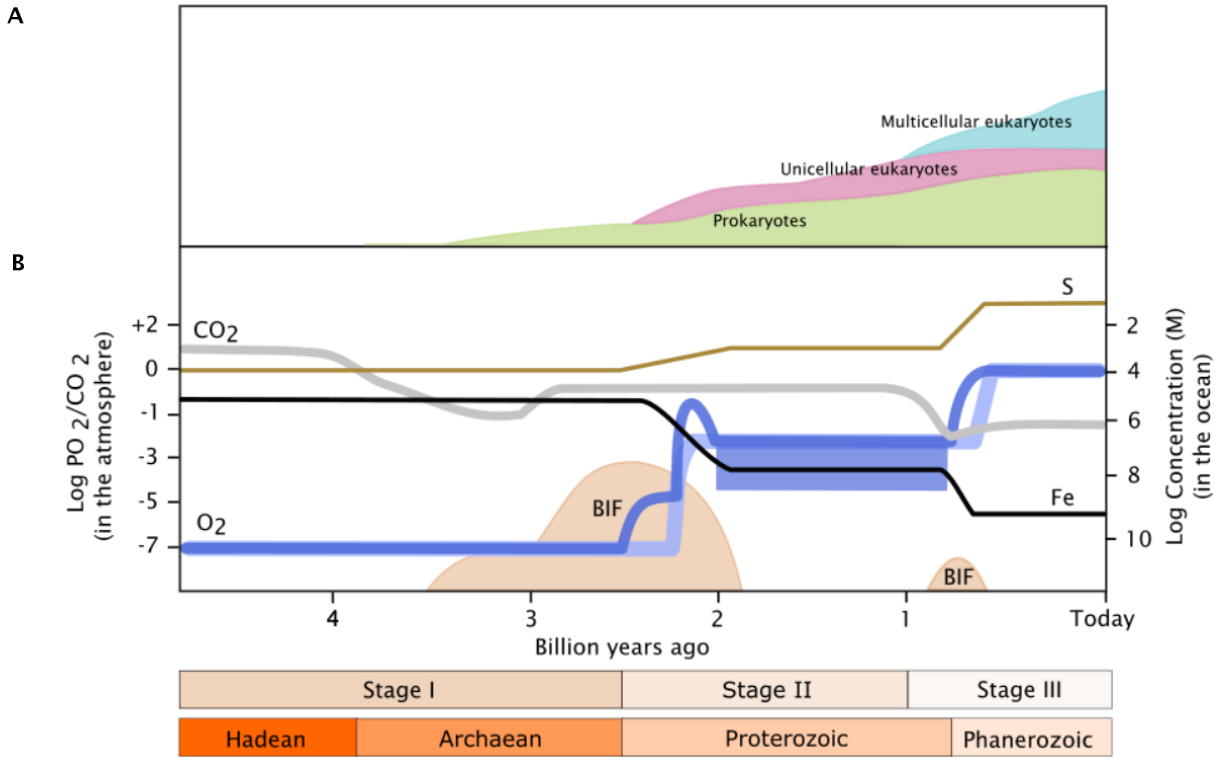

Figure 1.1: Biogeochemical evolution of the earth from 4 billion years until today. A) Evolution of prokaryotes to multicellular eukaryotes. B) Evolution of elements through time in the atmosphere (left axis) and in the ocean (right axis). Different shades of blue for O_2 correspond to different models: dark blue represents the emergent model described by Lyons et al. 2014 and light blue corresponds to the classical two-step model. Figure adapted from the literature (Williams, 2012, Ilbert & Bonnefoy, 2013 and Lyons, et al., 2014).

1.2. Iron, an essential element for life

In humans, iron plays a fundamental role in cellular function since it is an essential component of uncountable hemeproteins including oxygen transport proteins (hemoglobin, myoglobin, neuroglobin), heme-containing enzymes (cytochromes, catalase, peroxidase), non-heme enzymes (aconitase, ferrochelatase) and proteins involved in iron transport, and storage (transferrin, ferritin, hemosiderin) (Tandara & Salamunic, 2012). Given its importance, iron deficiency and iron overload diseases are the most common disorders affecting humans (Tandara & Salamunic, 2012). For instance, excessive iron in the brain has been associated with neurodegenerative disorders including Parkinson's and Alzheimer's disease (Tandara & Salamunic, 2012). Other iron mismanagement disorders include anemia of chronic disease (ACD) which has been associated

with various types of infections, solid cancers, hematologic malignances and autoimmune disorders (Tandara & Salamunic, 2012).

The average human contains approximately 3 to 5 g of iron, of which around 60% is incorporated in hemoglobin within erythrocytes, 10% is incorporated in muscle myoglobin, and the remaining is stored in hepatocytes and in reticuloendothelial macrophages (Chifman, et al., 2014). Even though 20 to 25 mg of iron are required for the synthesis of hemoglobin, the daily intake of iron is usually only about 1 to 2 mg and the remaining is recycled each day by macrophages (Caza & Kronstad, 2013). Dietary iron uptake occurs in the intestine, either as ferrous iron (after reduction by intestinal ferric reductase), or as duodenal cytochrome B or as heme. In the blood, iron is present in hemoglobin and in heme which derive from ruptured erythrocytes and enucleated erythroblasts (Kristiansen, et al., 2001). In plasma, approximately 2 to 3 mg of iron are bound to transferrin (Tandara & Salamunic, 2012). Transferrin can bind two iron atoms, one in each globular lobe with a K_a of about $10^{20}\ M^{-1}$ for ferric iron at physiological pH, leaving plasma with a free iron concentration of about $\sim 10^{-24}$ M.

Iron in the cell is stored in ferritins, iron storage proteins that can accumulate up to 4500 atoms of iron, which are eventually released to incorporate various metalloproteins (cytochromes, catalase, hemoglobin, myoglobin, aconitase, succinate dehydrogenase) or during iron deficiency (Williams, 2012).

Overall, the metabolism of iron and iron's biological function originates from its chemical properties as a transition metal (Tandara & Salamunic, 2012). At physiological pH it becomes poorly soluble as ferric iron and highly reactive as ferrous iron, making this metal not only the most vital, but also the most toxic of the necessary metals. (Tandara & Salamunic, 2012, Andrews, 2005). Based on Fenton and Haber-Weiss reactions (Fig.1.2) iron is able to catalyze the generation of radicals including reactive oxygen species (ROS) (hydroxyl radicals $OH^{\cdot}$; superoxide $O_2^{\cdot-}$; hydrogen peroxide H_2O_2), organic reactive species (peroxyl $ROO^{\cdot}$; alkoxyl $RO^{\cdot}$; thiyl (RS); thiyl-

Fenton and Haber-Weiss reaction

$$Fe(II) + H_2O_2 \rightarrow Fe(III) + OH^- + OH^{\cdot}$$

$$Fe(III) + O_2^{\cdot-} \rightarrow Fe(II) + O_2$$

$$H_2O_2 + O_2^{\cdot-} \rightarrow OH^- + OH^{\cdot} + O_2$$

Generation of organic radicals

$$Fe(II) + ROOH \rightarrow Fe(III) + OH^- + RO^{\cdot}$$

$$Fe(III) + ROOH \rightarrow Fe(II) + H^+ + ROO^{\cdot}$$

$$RSH + OH^{\cdot} \rightarrow RS^{\cdot} + H_2O$$

$$RSH + ROO^{\cdot} \rightarrow RS^{\cdot} + ROOH$$

$$RS^{\cdot} + O_2 \rightarrow ROO^{\cdot}$$

Generation of heme-catalyzed oxygen radicals

$$Heme\text{–}Fe(II)\text{–}O_2 + H_2O_2 \rightarrow Heme\text{–}Fe(IV)\text{–}OH^{\cdot} + O_2 + OH^-$$

$$Heme\text{–}Fe(IV)\text{–}OH^{\cdot} + ROOH \rightarrow Heme\text{–}Fe(III) + ROO^{\cdot} + H_2O_2$$

Figure 1.2: Generation of organic and heme-catalyzed radicals based on the Fenton and Haber-Weiss reactions (Papanikolaou & Pantopoulos, 2005).

peroxyl RSOO˙) and free radicals by direct interaction with oxygen. Radicals are highly reactive species which damage cellular macromolecules, promoting cell death, and tissue degeneration (Papanikolaou & Pantopoulos, 2005). To avoid toxicity, and to ease solubility and transport, iron is usually protein-bound and its internal equilibrium is strictly regulated inside the cell and in the systemic circulation (Andrews, 2005,Chifman, et al., 2014, Papanikolaou & Pantopoulos, 2005). Systemic iron homeostasis is maintained by the hormone hepcidin and receptor ferroportin whereas intracellular iron regulation is maintained by iron-regulatory proteins (IRP1 and IRP2) that bind iron responsive elements (IREs) (Chifman, et al., 2014). The iron intracellular network alone includes 151 chemical species and 107 reactions and transport systems (Chifman, et al., 2014).

From the available dietary iron in the intestine to the iron intracellular network, great opportunities exist for microbial exploitation in the forms of colonization, commensalism and invasion (Caza & Kronstad, 2013).

In bacteria, iron plays vital roles in biological processes that include photosynthesis, N_2 fixation, H_2 production and consumption, oxygen transport, free radical scavenging, Krebs cycle and DNA biosynthesis (McHugh, et al., 2003). Iron-based metabolisms such as anoxygenic photosynthesis are spread across bacteria and archaea and these may have been some of the earliest metabolisms on Earth contributing to the deposition of BIFs (Wu, et al., 2014). Iron is also involved in biomineralization, a process that involves the formation of inorganic materials by proteins, carbohydrates and lipids (Crichton & Pierre, 2001). Examples include the transformation of haemosiderin through the formation of a ferritin core, and the formation of magnetite (Fe_30_4) by magnetotatic bacteria, a crucial component of magnetosomes, specific intracellular structures which confer these bacteria the ability to swim along the geomagnetic field (Yan, et al., 2012).

Iron homeostasis in bacteria is constantly dependent on the prevailing environmental conditions, ecological niche and phylogeny (Andrews, et al., 2003). Essentially, bacterial iron homeostasis is maintained employing the following five strategies: securing various iron scavenging systems, maintenance of intracellular iron stores, development of redox stress resistance systems, control of iron consumption under iron-limited conditions, and possession of an iron-responsive regulatory system that controls the iron metabolic pathways (Andrews, et al., 2003).

Based on *E. coli*, bacterial iron requirements for optimal growth range from 10^{-7} M to 10^{-5} M. Therefore, in the wild environment, iron deprived bacteria face essentially three possibilities (Fig. 1.3): lowering the external pH to promote the solubilization of ferric iron, performing ferric iron reduction and/or releasing siderophores as solubilizing agents (Andrews, et al., 2003).

Bacterial incorporation into a host provides an ecological niche with further possibilities for iron acquisition (Caza & Kronstad, 2013). Nevertheless, inside the host, as bacterial numbers increase, the host response is to withdraw iron by inducing inflammation (Caza & Kronstad, 2013). The complexity of bacterial iron acquisition systems inside the host and the host's defense mechanisms for avoiding the proliferation of pathogens can be represented as an ongoing battle for iron (Doherty, 2007).

1.3. Ongoing battle for iron: Microbial mechanisms for iron acquisition

Bacteria have developed multiple iron acquisition pathways which often coexist within a bacterial species, providing a range of specificities and affinities for different forms of available iron, a means to survive in diverse habitats and to compete with other surrounding bacteria (Cartron, et al., 2006, Wandersman & Delepelaire , 2004).

Given its solubility, the ferrous iron is considered the preferred form of iron utilized by bacteria (Cartron, et al., 2006). Some microorganisms exclusively use this form of iron which is the case of obligate anaerobes *Bifidobacterium bifidum*, *Legionella pneumophila* and *Streptococcus mutans* (Wandersman & Delepelaire, 2004). In comparison to Fe(III), Fe(II) is extremely soluble (0.1 M for ferrous iron and 10^{-18} M for ferric iron at pH 7) and it is able to diffuse freely through the outer membrane porins of Gram-negative bacteria. Once in the periplasmic space it is subsequently transported by an ATP binding cassette (ABC) ferrous iron transporter. This is regarded as the ferrous iron transport system (Feo), which was first identified in facultative anaerobic *Escherichia coli* K-12 (Wandersman & Delepelaire , 2004, Cartron, et al., 2006, Kammler , et al., 1993, Hantke, 1987). Enterobacterial Feo systems comprise three proteins: FeoA, FeoB and FeoC. The role of FeoA it is not fully understood, FeoB acts as a permease and FeoC has been proposed to regulate FeoB (Lau, Krewulak, & Vogel, 2015). Other ferrous transport systems have been identified including the sitABCD system identified in *S.enterica* and *E.coli*, the YfeABCD system identified in *Y.pestis* the Fur-regulated EfeUOB found in specific strains of *E.coli* (Caza & Kronstad, 2013).

Ferrous iron uptake proceeds independently of the ferric iron uptake and inside the host and in reducing conditions, iron homeostasis is strictly regulated. Upon bacterial infection the first line of defense is nutritional immunity, the withholding of nutrients to prevent bacterial proliferation (Skaar, 2010). This involves the sequestration of free ferrous and ferric iron into carrier proteins (lactoferrin, transferrin, ferritin) and the binding to the protoporphyrin ring in hemoproteins (Skaar, 2010). The pH maintenance can also play an important role in immunity by guaranteeing the insolubility of ferric iron. Additionally, iron sequestration is covered within a pH

range of 3 to 5.5 with lactoferrin, a carrier protein present in body fluids including tears, milk and saliva, which is able to scavenge iron at a relatively lower pH around ~ 3.0, and with transferrin which scavenges iron at around pH ~5.5 with an association constant of $10^{36}\,M^{-1}$ (Skaar, 2010, Schaible & Kaufmann, 2004). Defense against infection also involves the action of hepcidin and siderocalin. (Wandersman & Delepelaire, 2004) Hepcidin binds ferroportin and promotes its degradation, trigging a series of events that lead to the blockage in intestinal iron absorption and cellular iron efflux (Anderson, et al., 2002; Nemeth, et al., 2004). This host nutritional immunity leaves bacteria with virtually no accessible iron and therefore the possession of specialized iron transport systems that scavenge free iron is crucial to override the iron limitation imposed either by the environment and/or by the host (Crosa, 1989).

So far three strategies for importing and utilizing ferric iron have been identified: i) direct extracellular reduction (Deneer, et al., 1995); ii) acquisition of iron-bound proteins (Wandersman & Delepelaire , 2004) and iii) synthesis and extracellular release of siderophores (Neilands, 1981). Direct extracellular reduction was described in 1995 by Denner et al in *Listeria monocytogenes* where intact cell suspensions were exposed to ferric iron and immediately produced chromogenic ferrozine Fe^{2+}-complexes (Deneer, et al., 1995). Acquisition of iron-bound proteins occurs during infection and it can involve two types of mechanisms: a direct contact mechanism and an indirect mechanism. The first involves direct contact to host heme sources and the secretion of hemolysins and/or hemoglobin proteases. Hemolysins to lyse red blood cells releasing heme-containg proteins such as hemoglobin, and hemoglobin proteases, to degrade hemoglobin releasing heme. The second involves the use of hemophores, extracellullar proteins that are specialized in binding heme and bringing it to a specific outer membrane receptor (Caza & Kronstad, 2013, Wandersman & Delepelaire , 2004). Finally, the utilization of siderophores (from the greek, “iron bearer”), small molecules (500-1500 Daltons) synthesized by bacteria, plants and fungi under iron limiting conditions (10^{-6} M) that are released and utilized for iron scavenging. Not always requiring specific receptors for each iron source, this perhaps explains why siderophores are the most common employed strategy for microbial iron acquisition (Raines, et al., 2015, Miethke & Marahiel, 2007, Pierre, et al., 2002).

1.4. Siderophores – “small iron carriers”

The first discovery of siderophores (mycobactin, ferrichrome and progen) was made in the period between 1949 and 1952 (Francis, et al., 1949, Neilands, 1952, Hesseltine, et al., 1952). These small molecules are metal chelators that have a high thermodynamic affinity for ferric iron (Hider & Kong, 2010). Chelation of iron prevents its hydrolysis and precipitation, and allows for specific recognition and uptake at the cell surface (Harrington & Crumbliss, 2009).

The chelation through siderophores allows the possibility of controlling the redox properties of the iron center interfering in its release mechanism (Harrington & Crumbliss, 2009). In comparison with free aqueous Fe(II), iron-siderophore complexes have lower reduction potentials ranging from -82mV (rhizoferrin) to -990mV versus NHE for (FeIII-enterobactin) (Harrington & Crumbliss, 2009). This prevents damage caused by free Fe(II) in the organism and ensures that iron is released to a specific iron-requiring site within the cell and not to another location (Harrington & Crumbliss, 2009). Nevertheless, the utilization of siderophores is not exclusive to siderophore-producing bacteria. Some bacteria including *Bacillus subtilis* have the ability to uptake and reduce xenosiderophores (siderophores produced by other bacteria) (Miethke, et al., 2013, Miethke & Marahiel, 2007).

Based on their psychochemical properties, siderophores can be grouped to the following types: hydroxamates, catecholates (phenolates), carboxylates, amphiphilic and mixed-type siderophores (Hider & Kong, 2010, Martinez, et al., 2003, Saha, et al., 2016). Hydromaxate siderophores (Fig.1.3) are the most commonly found and consist of C(=O)N-(OH)R groups, where R is usually an amino acid or a derivative. Represented by ferrichrome these type of siderophores bind ferric iron with binding constants ranging from 10^{22} to 10^{32} M^{-1} forming a hexadentate octahedral complex with Fe^{3+} through the oxygen atoms in the hydroxamate groups. Catecholate siderophores (Fig.1.3) represented by enterobactin (also known as enterochelin) form a hexadentade octahedral complex by binding iron to the two oxygen atoms from each catechol group, $C_6H_4(OH)_2$, with binding constants in the range of 10^{52} M^{-1}. Carboxylates are siderophores that bind iron through carboxyl and hydroxyl groups. These are represented by achromobactin (Fig.1.3) and these have been isolated from *Rhizobium*, *Staphylococcus* and fungi. Amphiphilic

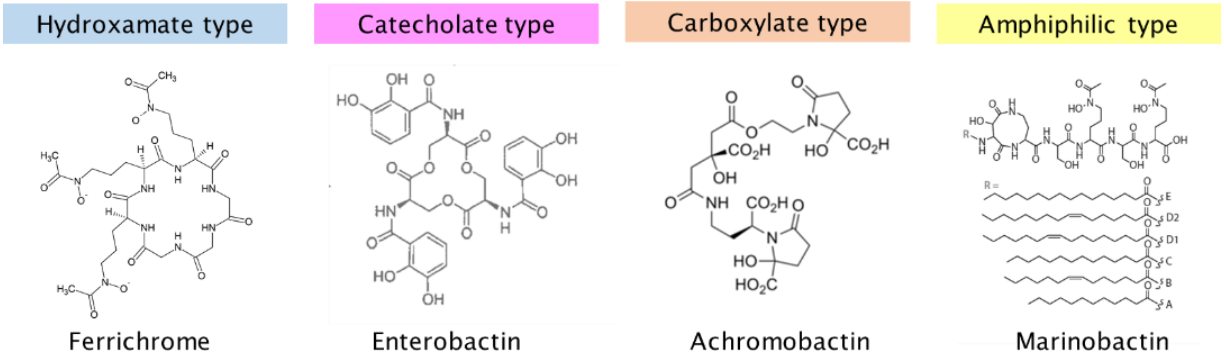

Figure 1.3: Structural representation of different groups of apo-siderophores. Adapted from Miethke & Marahiel, 2007 and Martinez & Butler, 2007.

siderophores, represented by marinobactin (Fig.1.3) are siderophores commonly found in marine bacteria and that contain unique structures which consist of a head group that coordinates iron(III) and a group of fatty acid chains (Martinez & Butler, 2007). Some siderophores present a mixture of the chemical features that are specific to each class of siderophores and for this reason these siderophores are regarded as "mixed-type" siderophores. (Miethke & Marahiel, 2007)

1.5. The siderophore pathway and potential applications

Since its discovery, the siderophore pathway has been considered for its range of applications in the following areas: microbial ecology, agriculture, biosensors and medicine (Saha, et al., 2016).

In the field of microbial ecology siderophores can be used to enhance the growth of uncultured microorganisms and to manipulate the microbial community in soils (Saha, et al., 2016). Currently only 0.1 to 1 % of microbes can be cultivated in the laboratory, a microbiology problem regarded as the "the great plate count anomaly" which results from the difficulty of replicating in the laboratory some of the basic microbial requirements (Saha, et al., 2016, Lewis, et al., 2010). In their natural habitats bacteria live in unique environments with exclusive resources and microbial communities (Saha, et al., 2016, Lewis, et al., 2010). As an important cooperative trait, chemical dependence can exist between neighboring microorganisms that allows for the regulation of the community and its successful establishment in the environment (Saha, et al., 2016, Lewis, et al., 2010). Several strategies have been employed and the co-culture approach of Lewis and Espstein revealed siderophores as the first class of growth factors for uncultured bacteria (Saha, et al., 2016, Lewis, et al., 2010). It has been reported that the production of siderophores can be an altruistic behavior where siderophore-producing bacteria are invaded with bacteria that do not produce siderophores but have the ability to utilize them to meet their iron requirements (O'Brien, et al., 2014). In this way, siderophores allow the proliferation of multiple microorganisms but also alter and exert control in the soil microbial community.

Similarly to promoting the growth of microorganisms, siderophores can be also be used for promoting plant growth. Acting simultaneously but not necessarily, as potential biocontrol agents and/ or used for soil bioremediation. As seen in the previous sections, iron is a fundamental element, participating in essential roles that include photosynthesis and DNA repair. Iron starvation can reduce the quantity and quality of crop production. Utilization of certain type of bacteria such as different *Pseudomonas* species can promote plant growth by secreting siderophores such as pyoverdine. This provides plants with an iron source but also reduces the iron availability for plant pathogens (Saha, et al., 2016).

Despite its greater affinity for iron, siderophores can also bind with lesser affinity to toxic metals such as V^{4+}, Cr^{3+}, Al^{3+}, Eu^{3+} Pb^{2+}, Sn^{2+}, and Tb^{3+}. This property of siderophores plays an important role in detoxifying the environment for the microbial community. Lower affinity binding causes heavy-metal bound siderophores not to enter the cell efficiently, preventing in this way the uptake of heavy metals (O'Brien, et al., 2014).

Siderophores can also be used as iron biosensors, integrated devices with the ability of quantifying iron using a biological recognition element attached to a transducer (Saha, et al., 2016). For instance, pyoverdine from *Pseudomonas aeruginosa* has been regarded as a promising detector for iron(III) being able to detect iron in solution down to 10 ng/mL and in the immobilized form up to 3 ng/mL (Saha, et al., 2016).

Antibiotic-resistant bacteria are a major threat in the treatment of infectious diseases. The research target is in finding new ways to combat bacterial virulence and "Trojan -horse" antibiotics have been regarded as way of circumventing permeability-mediated drug resistance. A Trojan-horse siderophore-based antibiotic consists of a siderophore joined with an antibiotic which can further bind iron forming an antibiotic-siderophore-Fe(III) complex. The use of siderophores allows for selective delivery of the antibiotic by exploiting siderophore's ability to carry iron inside the bacterial cell by interacting with specific receptors at the cell surface. The interesting particularity of this strategy is that this was not a human invention, siderophore antibiotics named sideromycins exist in the nature and examples include: albomycins, salimycins, ferrimycins, micromycins and danomycins (Górska, et al., 2014, Nagoba & Vedpathak, 2011). For instance, albomycin, is a thioribosyl pyrimidine antibiotic joined to an iron-complexing moiety similar to ferrichrome that inhibits tRNA synthetase. This natural Trojan horse antibiotic is taken up by the the ferrichrome transport system FhuA-FhuB-FhuC and binds in the same binding site as ferrichrome (Górska, et al., 2014, Nagoba & Vedpathak, 2011. This siderophore, as other examples included in Table 1.1 are already used to treat microbial infection.

The use of siderophores in medicine extends further to the treatment of iron overload, antimalarial activity, wound-healing, removal of transuranic elements and in cancer therapy (Saha, et al., 2016). (Kumari, et al., 2016)

Table 1.1: Examples of siderophores and their role in medicine. Adapted from Górska, et al., 2014.

Siderophore	Diseases
Albomycin	Microbial infection
Carboxymycobactin	Prevention of reperfusion injury
Desferrioxamine	Thalassemia, prevention of pancreatic injury, sideroblastic anemia, iron overload cardiomyopathy, skin exposed to nitrogen mustard, retrobulbar hematoma, Skeletal muscle ischemia, neuroblastoma and prostate cancer.
Ferrimycin	Microbial infection
Tris-catecholate siderophore and ampicillin conjugates	Microbial infection

1.6. The siderophore pathway

Extensive progress has been made in understanding the molecular mechanisms of the siderophore pathway due to its potential utilization and inspiration in the development of new semi-synthetic drugs (Miethke & Marahiel, 2007).

Siderophore biosynthesis, secretion, uptake and iron release require tight regulation of both enzymes and transport systems (Miethke & Marahiel, 2007). Regulation commonly involves gene regulation at the transcriptional level by the ferric uptake repressor Fur in Gram-negative bacteria and diphtheria toxin regulator (DtxR) in Gram-positive bacteria (Miethke & Marahiel, 2007).

The biosynthesis of siderophores is catalyzed by nonribosomal peptide synthetases (NRPS) via either dependent or independent NRPS mechanisms. NRPS are large multienzyme complexes that assemble and activate a broad range of amino, carboxy, and hydroxy acids providing great variability in macrocyclic peptidic products (Miethke & Marahiel, 2007).

Only a few siderophore transport mechanisms have been identified and these include transporters from the major facilitator family (MFS), the resistance, nodultation and cell division (RND) and the ATP-binding cassette (ABC) superfamily (Miethke & Marahiel, 2007). Once iron incorporates the siderophore, cellular uptake can occur in two distinct ways: either the ferric-siderophore is reduced at the extracellular surface releasing ferrous iron or the ferric-siderophore complex is incorporated by ABC-type transporters and outer membrane (OM) receptors at the extracellular membrane of Gram-negative bacteria. OM receptors can either be specific, e.g. FepA (*E.coli*), IroN (*S.enterica*) and Pfc (*P.aeruginosa*) or can be general, such as the receptor IutA and ABC-transporter FhuBCD (*E.coli*) which can internalize different siderophores (Caza & Kronstad, 2013).

Of the siderophore pathway, the mechanisms of siderophore export and iron release are the least studied (Miethke & Marahiel, 2007).

1.7. Iron release from the ferric siderophores

Three main mechanisms have been proposed for the release of iron from the ferric-siderophore complexes: the hydrolysis of the ferric-siderophore, proton-assisted dissociation of the complex and reduction of the ferric iron (Harrington & Crumbliss, 2009). The hydrolysis of the ferric-siderophore by esterases has been observed for various siderophores including bacillibactin (by BesA esterase), enterobactin (esterase Fes) and fusarinine C (by esterase Sidj). (Abergel, et al., 2009) (Gründlinger, et al., 2013). This strategy involves great metabolic cost since it causes a constant production of new siderophores for iron acquisition. On the other hand,

despite ensuring the recycling of the siderophore, proton-assisted dissociation of the siderophore complex requires extreme low pH to guarantee complete dissociation. Siderophores have Redox-Bohr effect, the potential increases as the pH is lowered and in some cases ferric siderophores are sequestered by intracellular compartments that have a lower pH, perhaps as a strategy to facilitate ferric siderophore reduction (Harrington & Crumbliss, 2009).

The reduction of the ferric iron is proposed to occur via small molecule reducing agents or by assimilatory ferric reductases. The reduction potential of ferric siderophores indicates that their reduction by biological reducing agents is unfavourable. However, despite working only at the range between -200mV to -400mV, reduced flavins, using NAD(P)H exhibit ferric siderophore reductase activity (Coves & Fontecave, 1993, Pierre, et al., 2002). The metal release from the ferric siderophores is facilitated by reducing iron(III) to iron(II), which decreases the stability of the complex and facilitates the kinetics of ligand exchange allowing time- and site- specific delivery of the metal (Harrington & Crumbliss, 2009).

1.8. Ferric siderophore reduction

Ferric reductase activity was first detected for more than 30 years ago and it has been studied in multiple organisms including: *Archaeoglobus fulgidus* (Vadas, et al., 1999) , *Azobacter vinellandi* (Huyer & Page, 1989), *Bacillus halodurans* (Miethke, et al., 2011), *Escherichia coli* (Miethke, et al., 2011), *Legionella pneumophila* (Poch & Johnson , 1993), *Listeria monocytogenes* (Deneer, et al., 1995), *Magnetospirillum gryphiswaldense* (Xia, et al., 2007), *Mycobacterium paratuberculosis* (Homuth, et al., 1998), *Neisseria gonorrhoeae* (Faou & Morse, 1991), *Paracoccus denitrificans* (Sedláček, et al., 2009), *Pseudomonas aeruginosa* (Hallé & Meyer, 1992), *Pseudomonas fluorescences* (Hallé & Meyer , 1989), *Riemerella anatispetifer* (Tu, et al., 2014), *Rhodopseudomonas sphaeroides* (Moody & Dailey, 1985), *Shewanella putrefaciens* (Bamford, et al., 2008), *Thermobifida fusca* (Li, et al., 2015), *Vibrio cholerae* (Butterton & Calderwood, 1994). Of these, only a few enzymes have been isolated and fully characterized (Schröder, et al., 2003). Overall, great diversity has been found for ferric iron reductases ranging from their cellular location, substrate, specificity and electron donors (Schröder, et al., 2003). Ferric reductases have been identified in the cell's cytoplasm, periplasm and cytoplasmic membrane (Schröder, et al., 2003). Whereas most Gram-negative bacteria contain ferric reductases that are either located in the cytoplasm or periplasm, some bacteria have several ferric reductases that are localized in different cell compartments (Poch & Johnson , 1993) (Schröder, et al., 2003). Other bacteria are even able to excrete ferric reductases into the media or expose them at the cell surface. The most common electron donors are NADH and NADPH with some enzymes being able to use both. A few can use as electron donors: glutathione or ferredoxin (Miethke, et al., 2011). Most bacterial

ferric reductases are flavin reductases which use non-covalently bound flavins such as FMN (flavin mononucleotide), FAD (flavin adenine dinucleotide) or riboflavin. Almost all ferric reductases exhibit a wide range of substrate specificity versus Fe(III)-compounds, including: ferric-siderophores (produced or xenosiderophores), ferric-citrate, free Fe^{3+}, transferrin, ferritin, Fe^{3+}-EDTA, Fe^{3+}quinate. Given the importance of this mechanism for iron uptake, efforts have been put in understanding and classifying these type of enzymes. In 1994 it was proposed that ferric reductases were in fact flavin reductases due to the lack of substrate specificity found in this type of enzymes (Fontecave, et al., 1994). Flavin reductases, such as the NAD(P)H: flavin oxidoreductases which catalyze the reduction of free flavins (FMN, FAD, riboflavin) using NAD(P)H (Fontecave, et al., 1994).

Given the large number of not fully characterized ferric reductases, attention will be given only to ferric reductases that demonstrated the ability to reduce ferric-siderophores (Table 1.2). This type of enzymes since the beginning of the 21st century has been regarded not only as ferric reductases but also as SIPs (and even SUPs, siderophore-utilization proteins).

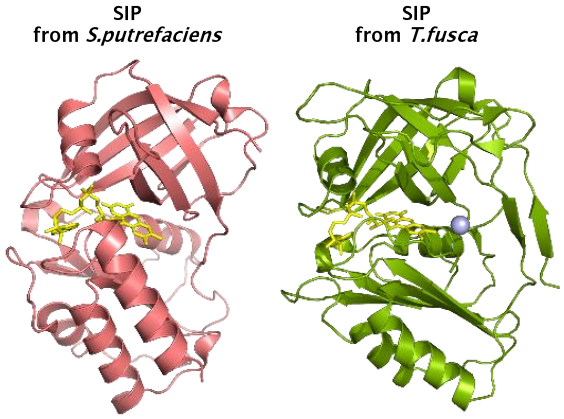

Figure 1.4: Structural representation of SIPs: The first identified SIP from *S.putrefaciens* (PDB entry: 2GPJ) and SIP from *T.fusca* (PDB entry: 4YHB).

ViuB has been claimed as one of the first SIPs ever described in the literature (Miethke, et al., 2011). A product of the ferric vibriobactin utilization gene, a ≈30 KDa protein with the ability to utilize ferrisiderophores in a similar way as Fes, an esterase from *E.coli* but not showing hydrolytic activity (Butterton & Calderwood, 1994). Nevertheless, the term "SIP" appeared only in 2006 with the first determined structure of a SIP from *Shewanella putrefaciens*, PDB entry 2GPJ (Fig.1.4).

Since then, other genes coding for ferric reductases have been found clustered around the genes for siderophore biosynthesis nd transport, including genes coding for *E.coli* YqjH, ItrAB from *M.tuberculosis*, FscN from *T.fusca* and Fhuf from *E.coli* (Butterton & Calderwood, 1994, Li, et al., 2016, Miethke, et al., 2011, Matzanke, et al., 2004). In 2008, Bruner et al. identified and characterized a siderophore-producing gene cluster from the Gram-positive *T. fusca.* This gene cluster produces fuschachelin, a mixed catecholate/hydroxamate and contains components commonly found in iron acquisition including NRP synthetases (FscFGHI), biosynthetic enzymes (FscABCDEK), transport (FscM) and iron utilization (FscJ) genes and two proteins involved with intracellular iron reduction. Based on the fuscachelin gene cluster, in 2015, Kunhua Li et al. proposed that the two proteins involved with intracellular iron reduction were representatives of two superfamilies of ferric siderophore

reductases.The two proposed families are the siderophore-interacting protein (SIP) family and the

Table 1.2: Ferrisiderophore reductases, source, ferrisiderophore substrate, electron donor, electron acceptor and cell location.

Organism	Name	Electron acceptor	Electron donor	Ferric-siderophore	location	Reference
Agrobacterium tumefaciens	-	FMN	NADH	Ferriagrobactin Ferriferrioxamine B Ferrienterobactin (others)	Cytoplasm (soluble fractions)	(Lodge, et al., 1982)
Azotobacter vinelandii	ferric reductase	FMN	NADH	azotobactin azotochelin desferrioxamine B	cytoplasm (soluble fractions)	(Huyer & Page, 1989)
Bacillus halodurans	FchR	[2Fe-2S]	ferredoxin	Fe[III]-aerobactin Fe[III]-schizokinen Ferrichrome Ferrioxamine E	-	(Miethke, et al., 2011)
Bacillus megaterium		-	NAD(P)H	Ferrischizokinen Ferrioxamine B ferrioaerobactin	cytoplasm	(Arceneaux & Bryers, 1980)
E.coli	flavin reductase	Riboflavin , FAD, FMN	NAD(P)H (depends on electron acceptor)	ferrichrome ferrienterobactin ferricrocin ferricoprogen ferriaerobactin (others)	cytoplasm	(Coves & Fontecave, 1993) (Fontecave, et al., 1987)
E.coli	YqjH	FAD cofactor	NADPH	Ferric enterobactin Ferric vibriobactin	cytoplasm	(Miethke, et al., 2011)
E.coli	Fhuf	[2Fe-2S]	-	Ferrioxamine B Coprogen Ferrichrome	Cytoplasm	(Matzanke, et al., 2004) (Müller, et al., 1998)
Mycobacterium Smegmatis	Ferrimycobactin NAD(P)H oxidoreductase	-	NAD(P)H	ferrimycobactin	plasma membrane	(Brown & Ratledge, 1975)
Mycobacterium tuberculosis	ItrAB (ItrA domain)	FAD	-	exomycobactin	plasma membrane	(Ryndak, et al., 2010)
Neurospora Crassa	NADH:sideramine oxidoreductase	-	NADH	Ferrichrome Ferrirubin Coprogen B ferrioxamine	Soluble fraction	(Ernst & Winkelman, 1977)
Paracoccus denitrificans	FerA (ferric reductase A)	FMN	NADH	ferriparabactin	cytoplasm	(Sedláček , et al., 2009)
Pseudomonas aeruginosa	ferripyoverdine reductase	FMN	NADH	ferripyoverdine	cytoplasm	(Hallé & Meyer, 1992)
Thermobifida fusca	FscN	FAD cofactor	NADH	fuscachelin	cytoplasm	(Li, et al., 2015)
Vibrio Cholerae	ViuB	-	-	vibriobactin	cytoplasm	(Butterton & Calderwood , 1994) (Wyckoff, et al., 2015)

ferric siderophore reductase family (FSR). The SIP family, containing a bound flavin and using NAD(P)H as reducing agents (Fig.1.5), and the FSR family, which contains an unique C-terminal C-C-x10-C-x2-C 2Fe-2S cluster (Li, et al., 2015). So far, no structure has been determined for the FSR family of proteins and few studies exist due to the difficulty of expressing and purifying this type of proteins (Li, et al., 2015).

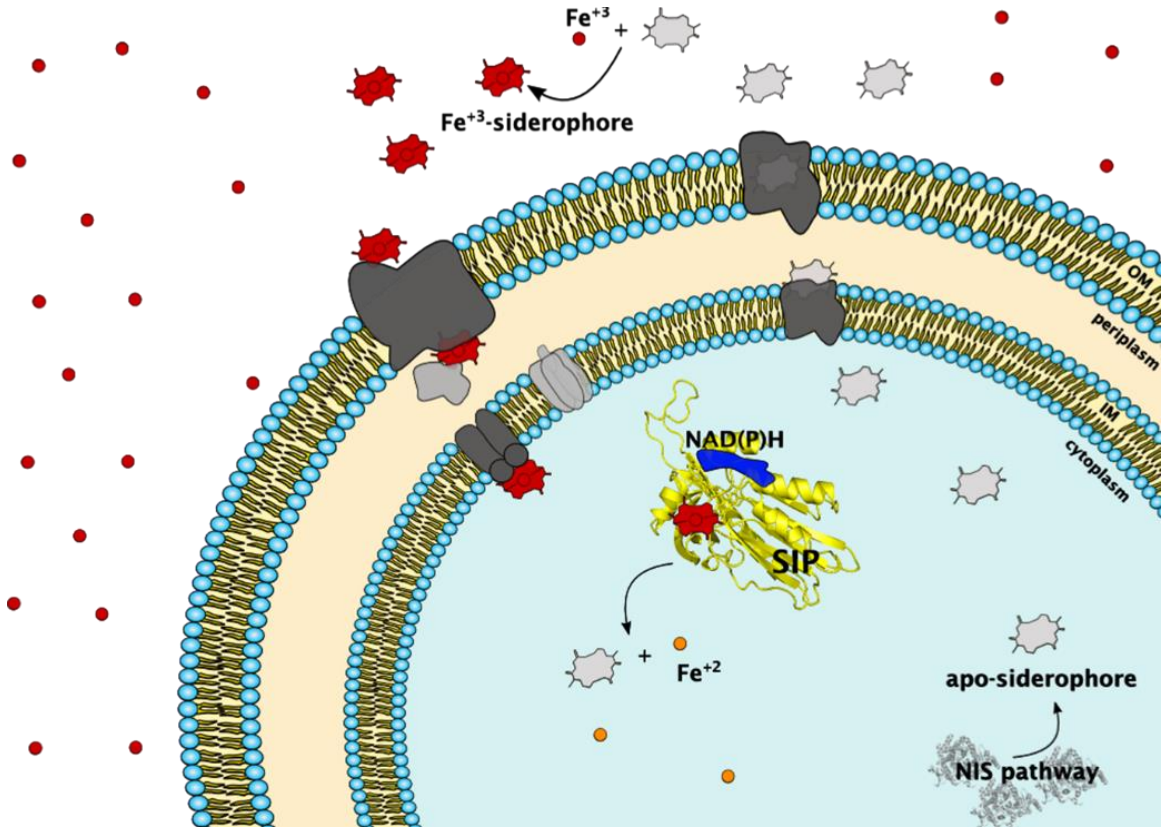

Figure 1.5: Representation of SIP-mediated ferric siderophore reduction.

In the SIP family, two structures have been determined, one from *S. putrefaciens* and another from *T. fusca* (Fig.1.4). In this family of proteins, YqjH from *E. coli* and FscN from *T. fusca* are the most studied proteins. Based on N-terminal and C-terminal sequence alterations, the SIP family can be divided further in two subfamilies: group I and group II. FscN from *T.fusca* belongs to group I subfamily due to containing 15-20 additional amino acids predicted as C-terminal α-helical elements with the HH(K)x_5DE sequence. This protein contains a noncovalently bound flavin cofactor whereas YqjH from group II subfamily, contains a covalently bound flavin cofactor. Group II SIPs have a relatively shorter C-terminal and based on bioinformatic analysis this group of SIPs was proposed to utilize NADPH whereas group I was proposed to utilize NADH. No direct reduction using NAD(P)H was observed for FscN nor reduction of "generic iron chelates" such as ferric citrate, ferrichrome and ferric aerobactin. Reduction was only observed in the ferene assay using NADH to reduce the natural substrate ferric fuscachelin to yield ferrous iron as the end product, reporting an activity of 40nmol of Fe^{2+} min^{-1} mg^{-1}. As for *E.coli* YqjH, it is able to catalyze the reduction of various ferric siderophores and iron chelators including ferric enterobactin, ferric vibriobactin and ferric citrate using NADPH with an activity of 22 nmol of Fe^{2+} min^{-1} mg^{-1}. YqjH-mediated iron reduction proceeded via single-electron transfer exhibiting double-displacement-type (ping-pong) kinetics through the formation of a transient flavosemiquinone. Site-direct mutagenesis of this protein revealed key residues for substrate binding and reductase activity

(K55 and R130). In the case of FscN no significant reduction was observed to allow the determination of mechanistic details in FscN. Structural determination of FscN, reveals similarity of this protein with flavohemeproteins such as cytochrome b_5 reductase which catalyze the transfer of one electron from NADH to heme. Having no heme-protein genes in the biosynthetic siderophore cluster and showing the atypical feature of containing representatives of both SIP and FSR families, it is possible that FscN interacts with the FSR protein (FscP) in a synergistic way allowing siderophore utilization (Li, et al., 2015, Miethke, et al., 2011).

1.9. Emerging pathogens from the *Shewanella* genus

Shewanella was first described in 1931, as *Acrhomobacter putrefaciens*, an unknown bacterium found in putrefied butter (Derby & Hammer, 1931). Its name was later changed to *Pseudomonas putrefaciens* by Long and Hammer, which found this organism widely distributed in water supplies and in the soil explaining the presence of this bacterium in the sweet milk and cream used for butter production (Long & Hammer, 1941).

The name *Shewanella* emerged later in honor of Dr. J Shewan, for his work in fish microbiology. *Shewanella* belong to the order of Altermonadales, family of Shewanellaceae and class of Gamma proteobacteria. So far, the genus *Shewanella* includes over 50 different species, all of which these present the following morphologic traits: Gram-negative rod shaped and motile bacteria by a single unsheated polar flagellum (Satomi, 2014).

The main interest in *Shewanella* started with the isolation of manganese reducing *Shewanella oneidensis* (previously known as *Alteromonas putrefaciens*) in 1988 from the lake Oneida in New York (Myers & Nealson, 1988). Since then, the interest in *Shewanella* has been focused in its ability to transfer electrons to solid metal oxides and to use more than ten different electron acceptors. These characteristic traits readily reflect the versatility and adaptability of this microorganism which has been isolated from both aquatic and sedimentary systems and it is able to use various carbon sources (pyruvic acid, xylose, galacturonic acid, asparagine, glucose, malic acid, putrescine, lactose) as well as uncommon electron acceptors, including chromium [Cr(VI)], iodate, uranium [U(VI)], technetium, neptunium, plutonium, selenite, tellurite, and vanadate and nitroaromatic compounds (Fredrickson, et al., 2008) (Drewniak, et al., 2015).

The versatility of Shewanella extends further: over the past years, particular species of *Shewanella* mainly *Shewanella putrefaciens* and *Shewanella algae* have been reported as opportunistic human pathogens. Despite being an unusual cause of disease in humans, emergent reports of *Shewanella* infections have been increasing, reaching up to 260 cases in the period between 1973-2012 (Vignier, et al., 2013). Some of these cases are described in Table 1.3 together with extra 17 cases that were reported in the literature after 2012.

Most cases identify S.*putrefaciens* and *S.algae* as the main causative agents, although other species including *S.haliolitis*, *S.onedensis* and *S.xiamenensis* have also been reported in the literature (Janda, 2014). Overall, it is possible that more cases exist, not only due to their occurrence in mixed flora bacterial infections but also due to similarity between bacterial phenotypes which might have wrongly attributed *Shewanella*'s infections to *Pseudomonas* and *Vibrio vulnificus* (Holt, et al., 2005, Janda, 2014).

Table 1.3: Examples of reported cases of infections caused by *Shewanella.*

Number of patients	Affected site/Type of infection	Portal of entry	possible source	Agent identified	Reference
1	sacroiliac joint (osteomyelitis)	subcutaneous infusion	-	*S.putrefaciens*	(Pope, et al., 1982)
1	wrist, ankle (bactereamia and oligoarthritis)	peritoneal dialysis	tap water	*S.putrefaciens*	(Roger, et al., 1991)
1	articulation of the foot (arthritis)	cellulitis of the foot	puncture by a sea-urchin	*S.putrefaciens*	(Levy & Tessier, 1998)
1	tibia (osteomyelitis)	open fracture	stagnant water	*S.algae*	(Botelho-Nevers, et al., 2005)
31	bloodstream, surgical site, intra-abdominal and hepatobiliary infections	Drainage catheter	measuring cup	*S.algae and S.putrefaciens*	(Oh, et al., 2008)
1	purulent pericarditis	-	-	*S.algae*	(Tan, et al., 2008)
1	lumbar rachis	cutaneous lesion	seawater	*S.algae*	(Gressier, et al., 2010)
1	foot (ulcer)	injury	-	*S.algae and Staphylococci*	(Sharma & Kalawat, 2010)
1	interdigital ulceration	-	-	*S.algae*	(Sharma & Kalawat, 2010)
1	chest ulcer	-	-	*S.algae ad E.coli*	(Sharma & Kalawat, 2010)
1	gastroenteritis	-	-	*S.putrefaciens*	(Sharma & Kalawat, 2010)
1	burn	cutaneous lesion	-		(Sharma & Kalawat, 2010)
1	tibial infection	tibial fracture	Ship strike	*S.algae*	(Lee, et al., 2013)
16	cellulitis, superinfection of open fracture with necrosis and arthritis, osteitis, erypsipelas, superinfection of ulcer, repiratory distress, stercocal peritonitis, abscess and pneumonia	ulcer, open fractures, blister, amputation, birth, digestive, wound and lung	-	*Monomicrobial (8cases) and multimicrobial (8cases)*	(Vignier, et al., 2013)
1	hemorrhagic bullae and leg ulcers	-	seawater	*S.algae*	(Wagner, et al., 2013)
1	infective endocarditis	-	-	*S. putrefaciens*	(Constant, et al., 2014)
1	intracranial infection	operation of cerebral hemorrhage	-	*S.putrefaciens*	(Duan, et al., 2014)
1	Bacterial Peritonitis with Bacteremia	-	-	*S.algae*	(Kim, et al., 2014)
1	bacterimia	vein	intrapermanent catheter	*S.putrefaciens*	(Lee , et al., 2014)
1	wound infection	puncture wounds	cobra bite	*S.algae*	(Liu, et al., 2014)
1	dysentery	digestive	freshwater red tilapia fish	*S.putrefaciens*	(Stephen, 2014)
1	wound infection in navel area	-	seawater	*S.algae*	(Taberzadeh, et al., 2014)
1	neonatal sepsis	birth	-	*S.algae*	(Charles, et al., 2015)
7	surgical wound infection, acute cholangitis, respiratory colonisation	-	-	*S.algae* (5 cases) *S.putrefaciens* (2 cases)	(Muñoz-Gallego, et al., 2016)

Shewanella infections have a higher frequency in warm climates and usually include the exposure to saline waters (Holt, et al., 2005). Marine-associated bacterial infections are remarkably uncommon, although they can be acquired via the consumption of seafood products (shark meat, clams, mackerel), exposure of traumatized tissues to marine pathogens in recreational activities (swimming, ocean bathing, diving), occupational exposure (crabbing and fishing) and through unintentional contact with marine pathogens by marine-related hobbies (cobra bite, sea urchin puncture, fish fin) (Janda, 2014). Most *Shewanella* infections involve: ears, skin and soft tissue with or without bacteremia (Holt, et al., 2005). The most significant case described in the literature is an outbreak of *Shewanella* infections in a General Unit in Korea (Oh, et al., 2008).

The outbreak of *Shewanella* infections in a General Unit in Korea was reported in 2008 and included both *S.algae* and *S.putrefaciens*. With an attack rate of 5.8%, infections were caused by a shared measuring cup. This was the first time that infections in humans or clinical isolates of this pathogen had been reported in the Republic of Korea. This outbreak involved 31 case patients, 25 cases caused by *S.algae* and 6 cases caused by *S.putrefaciens.* The following signs and symptoms were recorded: fever in 23 patients, abdominal pain and purulent drainage in 9 patients and chills in 6 patients. *S.algae* and *S.putrefaciens* were isolated from diverse sources including blood, bile, ascitic fluid, skin and soft tissue and stool. Of the 31 infected patients, 7 were colonized with either *S.algae* or *S.putrefaciens*, whereas the remaining were all healthcare-acquired infections. Of the later, 5 patients developed a bloodstream infection and 19 developed a surgical site infection. Two risk factors were identified including the use of an external drainage catheter and the presence of hepatobiliary disease, a risk factor previously reported in other studies (Oh, et al., 2008).

Some cases present *S.algae* as being more virulent then *S.putrefaciens*, but in most cases this divergence cannot be accounted for. Nevertheless, it is important to note that automated identification systems are unable to distinguish between these two species of *Shewanella* (Holt, et al., 2005, Oh, H. et al 2008). Studies in mice indicate that *S.algae* is more virulent than *S.putrefaciens*, possibly as a consequence of producing mucoid cultures with hemolytic substances or exotoxins (Khashe & Janda, 1998). The main phenotypic attribute of *S. putrefaciens* is the production of hydrogen sulfide gas (H_2S) on triple sugar iron agar (TSI) slants (Khashe & Janda, 1998, Botelho-Nevers, et al., 2005). In contrast to *S.putrefaciens*, *S.algae* is not able to produce acid from maltose but it is also able to reduce nitrite (Holt, et al., 2005). S*. putrefaciens* and *S. onedensis* have the ability to form biofilms and this can also turn into a factor of pathogenicity (Holt, et al., 2005).

In general, *S.algae*'s infections epidemiology and clinical symptoms present similarity with infections involving *Aeromonas* and *Vibrio* (Holt, et al., 2005). This species presents resistance to penicillin, amoxicillin, ampicillin and it is susceptible to ticarcillin, ceftazidime, ciprofloxacin, imipen, colistin, tobramycin, tetracycline and carbenicilin (Botelho-Nevers, et al., 2005, Beleneva, et al., 2009). The introduction of this bacterium in the coelomic cavity of sea urchins *Strongylocentrotus nudus* caused the death of this organism within 3-8 days after inoculation (Beleneva, et al., 2009). The pathogenic effect of *S.algae* only occurs if the cutaneous epitheliumis disrupted allowing it to penetrate to lower tissue layers (Beleneva, et al., 2009).

Iron homeostasis in *Shewanella* is regulated by an orthologue of global transcription factor Fur, its major role being to mediate the transcription of genes involved in siderophore biosynthesis and iron acquisition systems (Yang, et al., 2009). Additionally, the disruption of siderophore alcaligin biosynthesis protein leads to severe growth deficiency of *Shewanella* under low iron conditions (Yang, et al., 2009). The *Shewanella*'s genome codes for both SIPs and FSRs (Pruitt, et al., 2005). The genome of some species of *Shewanella* including *S.algae* and *S.frigidimarina* only codes for one of the two families of siderophore interacting proteins. Other species of Shewanella including *S. baltica* have genes coding for both a FSR and SIP (Pruitt, et al., 2005).

Shewanella also produces siderophores, exoenzymes, tetrodoxins and is able to resist or tolerate bile salts. In 1994, a study showed that in 51 species of *Shewanella*, 30 produced siderophores in heat-sterilized fish juice. This ability was present in strains isolated from different environments including wounds, and aquatic sources. Strains that produced siderophores were positive for the Csáky test, indicating the presence of hydromaxate siderophores (Gram, 1994). The 30 strains that produced siderophores included all 6 strains isolated from mesophilic environments (wounds, infections, flamingos) and 7 isolated from aquatic sources (Gram, 1994). The capacity of producing siderophores favored growth under iron limiting conditions but did not exhibit inhibitory effects on the growth of other microorganisms (Gram, 1994). Studies indicate that the ferric reductase ability of *S.putrefaciens* is associated with the outer-membrane. These properties usually have an important role for virulence, although little research has been published studying assimilatory iron acquisition and its role in the emergent pathogenicity of *Shewanella*.

Understanding the molecular mechanisms that provide *Shewanella* with such metabolic diversity to survive and thrive in different environments can promote the use of this microorganism in bioremediation applications, energy production and its use as a model organism. Few studies have explored the capacity of *Shewanella* of producing and utilizing siderophores. Understanding the mechanistic details of siderophore-mediated utilization in this

microorganism can not only promote further insight on its emergent virulence of this microorganism but it can also unravel new applications that explore the combination of siderophore use, bioremediation and energy production.

2. Materials and Methods

2.1. Production of SIP from Shewanella frigidimarina

The gene and amino-acid sequence of SIP (table 2.1) was obtained from the National Center for Biotechnological Information (NCBI) (Pruitt, et al., 2005). The molecular weight and isoelectric point of this protein were calculated using ProtParam (ExPASY) (Gasteiger , et al., 2005). This information served as a guide throughout the experimental part of this thesis.

Expression of SIP

SIP was previously expressed by Dr. Bruno Fonseca (Trindade, et al., 2016) (Blommel, et al., 2007). Cell stocks of *E. coli Tuner* (DE3) pLacI containing the SIP (SFRI_RS12295) gene construct were first grown overnight in Luria-Bertani (LB) medium supplemented with 35 mg/L chloramphenicol, and 100 mg/L ampicillin at 30˚C and 170 rev.min^{-1}. Two percent of this culture served as inoculum and protein overexpression was achieved using an autoinduction method (Studier, 2005, Blommel, et al., 2007). The autoinduction medium consisted of 50 mL of stock solution 20×NPS [1 M Na_2HPO_4, 1 M KH_2PO_4, 500 mM $(NH_4)_2SO_4$], 20 mL stock solution 50×5052 (25% glycerol, 2.5% glucose, 10% α-lactose monohydrate) to 1 L LB medium supplemented with 1 mM $MgSO_4$, 35 mg/L chloramphenicol, and 100 mg/L ampicillin. The cells were allowed to grow for 30 hours at 30˚C and 170 rev.min^{-1}.

Table 2.1- Main characteristics of SIP.

Definition (NCBI name)	FAD-binding 9, siderophore-interacting domain protein [*Shewanella frigidimarina* NCIMB 400]
Genbank	ABI72237.1
Organism	*Shewanella frigidimarina* NCIMB 400
Reference for Gene sequence/ gene symbol	NC_008345.1/ Sfri_2392
Amino-acid sequence	MNNQSAKKSPTRLTYISDIIEISPY LRRLVLSGEQLANFPADQQGAY VKVLIPQPGETTVNMTLTGPNAA IKRSYTIREFDPVRGQLSLDFVINK HTGPATDWAKLANVGDTVAIAG PGPLKMNRFDFNDYLLFGDSTSI NAVDALIKRLPATAKGHIIMLVN SHQEQALLSQHPLLKTHWLVLN DSITAEQQIDWLLDKLELFGDLP AVTQVFVGLEATQVRVIKQYLLE QQQLPLSSISATGYWKRNTDAD TFGKQKQMQPL
Number of amino-acids/ Molecular Weight (g/moL) (ProtParam)	264/ 29 382
Charged amino-acid residues (positive/negative) (ProtParam)	25/ 25
Theoretical PI (ProtParam)	6.97

Cell harvest and disruption

Cells were harvested by centrifugation (10 min at 11305 x g) and then frozen at -80 ˚C. Thawed cells were resuspended in 20 mM Tris-HCl buffer pH 7.6 together with a protease inhibitor cocktail (Roche) and DNase I (Sigma), prior to a three-pass cell disruption at 6.9 MPa using a French Press. The lysate was centrifuged at 11305x g to remove undisrupted cells and

then ultracentrifuged at 204 709 x g for 90 min at 4 °C to remove cell membranes and debris. The supernatant was dialyzed overnight against 20 mM Tris-HCl buffer pH 7.6 and concentrated using an Amicon Ultra Centrifugal Filter (Millipore) with 10 kDa cutoff.

Purification of SIP

SIP was purified from the supernatant using two ion-exchange chromatography columns previously equilibrated with 20mM Tris-HCl buffer pH 7.6: a strong anion exchanger Q-Sepharose fast flow column (GE Healthcare) followed by a strong cation exchanger SP-Sepharose fast-flow column (GE Healthcare). A stepwise elution method from 0% to 100% of 1M NaCl at a flow rate of 1 $mL.min^{-1}$ was used for both columns. After the first column, fractions containing SIP were dialyzed overnight against 20 mM Tris-HCl buffer pH 7.6 and concentrated using an Amicon Ultra Centrifugal Filter (Millipore) with a 10 kDa cutoff before injection in the second column.

After each column, eluted fractions were examined through SDS-PAGE (12% gel with BlueSafe staining from NZYTech) and UV-Visible spectroscopy to select fractions containing purified SIP.

2.2. Characterization of SIP

Sequence analysis tools

Using the SIP sequence presented in table 2.1 a BLAST was performed using NCBI (Altschul, et al., 1990). A global-multiple protein alignment was performed with MUSCLE using the following protein sequences: ABI72237.1 (GenBank) from *S. frigidimarina*, ABP73812.1 (GenBank) from *S. putrefaciens*, WP_011292284.1(NCBI Ref.Seq.) from *T. fusca*, WP_059260114.1(NCBI Ref.Seq.) from *V. cholerae*, ALY14613.1 (GenBank) from *E. coli*, AHF22078.1 (GenBank) from *R. anatipestifer* (Edgar, 2004, Pruitt, et al., 2005). Binding motifs were identified as previously published (Li, et al., 2015).

A structural model of SIP was created with SWISS-MODEL (ExPASY) using PDB entry 2qpj with 30% identity as template, a SIP from S. *putrefaciens* (Arnold, et al., 2006). This model structure was also submitted through the DALI server platform for multiple structural alignment (Holm & Rosenström, 2010).

UV-Visible spectroscopy

UV-Visible absorbance spectra of purified SIP were acquired using a Shimadzu UV-1800 UV-Vis spectrophotometer at room temperature using a 1 cm path-length quartz cuvette. Absorbance was measured in the fast-scan rate mode between 250-700 nm. Quantification of SIP was performed based on the FAD spectral peak and using the extinction coefficient of free FAD ε_{450}= 11 300 M^{-1} cm^{-1} (Macheroux, P. 1999).

Protein film voltammetry (PFV)

Protein film voltammetry experiments were performed on a pyrolytic graphite edge (PGE) electrode purchased from IJ Cambria Scientific.

Experiments were conducted at 25ºC using a three-electrode electrochemical cell configuration with the PGE (working electrode), a platinum wire (counter electrode) and an Ag/AgCl (3 M KCl) (reference electrode) inside a Coy anaerobic chamber using a CHI electrochemical analyzer from CHI Instruments controlled by the manufactures' software (version 10.12). Oxygen levels were kept stable at approximately 8 ppm.

The electrode was cleaned (3 M nitric acid and distilled water) and freshly polished before every experiment. The polishing routine consisted in 10 min of hand-polishing with aqueous slurry 1.0 µm alumina followed by a 10 min sonication.

SIP was immobilized in the freshly polished PGE electrode by pipetting 3 µl of a 500 µM solution of SIP in 20 mM potassium phosphate buffer 100 mM KCl pH 7.6. To guarantee protein immobilization, the electrode was left to dry for approximately 15 min. Protein excess and/or unattached protein was removed by rinsing the electrode with distilled water. The electrode was then immersed in 2 mL of a mixed buffer solution containing 5 mM HEPES, 5 mM CHES, and 5 mM MES at the following pHs: 5.5; 6; 7;8 and 8.5. For each pH experiment, voltammograms were acquired at the following scan rates ($mV.s^{-1}$): 10, 13, 17, 21, 28, 36, 41, 48, 60, 78, 100, 130, 170, 210, 280, 360, 410, 480, 600, 780, 1000, 1300, 1700, 2100, 2800, 3600, 4100, 4800, 6000, 7800, 9100,10 000. After each experiment, the solution was removed and the pH was measured. These experiments were performed in duplicate by cleaning the electrode and repeating the same routine as previously described.

All data were first analyzed with Excel and QSoas and the trumpet-plots were fitted using the Butler-Volmer model using Jellyfit with the following parameters: n = 1, potential step $1x10^{-6}$, temperature 25ºC and for every data potential a standard deviation (SD) of 0.005 was assumed (Fourmond , 2016, Jeuken, et al., 2002). Potentials were reported in mV versus the standard hydrogen electrode (SHE) by addition of 210 mV to those measured (Friis, et al., 1997).

NMR spectroscopy

NMR spectroscopy experiments were performed at CERMAX, Centro de Ressonância Magnética António Xavier.

SIP samples were prepared in 20 mM phosphate buffer 100 mM KCl pH 7.6 containing 10% of $^{2}H_2O$ (99.9 atom %).

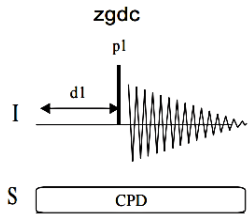

Figure 2.1 – Schematic representation of pulse sequence "zgdc" adapted from Parella, 2006. Each scan consists of a pre-scan delay (d1), followed by a read pulse (p1) and acquisition. Composite Pulse Decoupling in the proton channel is applied throughout.

Using the standard Bruker pulse program "zgdc" (Fig.2.1), one-dimensional proton-decoupled ^{31}P SIP spectra were acquired with 15 360 scans, d1 of 1.3 s and p1 of 9.5 µs at 25ºC on a Bruker Avance II 500 MHz equipped with a SEX probe for ^{31}P detection.

2.3. Characterization of ferric-siderophores

Preparation of avaroferrin, bisucaberin, putrebactin and ferrioxamine E

Avaroferrin, bisucaberin and putrebactin were kindly provided by Dr. Masaki Fujita from the Laboratory of Bioorganic Chemistry, Hokkaido University (Japan). These siderophores were provided in the apo-form (no iron) in three separate vials in the powder form, purified as described in the literature (Fujita & Sakai, 2014). Accordingly with Dr.Masaki Fujita, not all siderophores were completely pure (Appendix nº1) and were hardly soluble in any solvent. For this reason, the apo-siderophores were dissolved in 2 mL of DMSO, resulting in stock solutions of approximately 6.7 mM for (AVA) avaroferrin (MW = 387 g/mol, 5.4 mM for (BIS) bisucaberin (MW = 419 g/mol) and 5.7 mM for (PUT) putrebactin (MW = 373 g/mol) (Fujita & Sakai, 2014).

Iron-containing siderophores were prepared for every experiment in working stocks of 500 µM in 20 mM phosphate buffer 100 mM KCl pH 7.6. Each 500 µM ferric-siderophore solution was prepared from the starting stock plus equivalent amounts of $FeCl_3$ (highly concentrated acidic solution) resulting in an iron-siderophore molar ratio of 1:1.

Ferrioxamine E (FER) (1,12,23-Trihydroxy-1,6,12,17,17,23,28-hexaazacyclotritriacontane-2,5, 13,16,24,27-hexone iron(III) complex) was purchased from Sigma-Aldrich. A stock solution of 2 mM was prepared in 20 mM potassium phosphate buffer 100 mM KCl pH 7.6.

UV-Visible Spectroscopy

UV-Visible absorbance spectra of 100 μM avaroferrin, bisucaberin, putrebactin and ferrioxamine E were acquired using a Shimadzu UV-1800 UV-Vis spectrophotometer at room temperature using a 1 cm path-length quartz cuvette. Absorbance was measured in the fast-scan rate mode between 250-700 nm.

Cyclic voltammetry

Cyclic voltammetry experiments were performed using a pyrolytic graphite edge (PGE) electrode purchased from IJ Cambria Scientific. The electrode was cleaned and freshly polished before every experiment following the same routine as previously described for SIP's PFV (Section 2.2).

In each experiment, the freshly polished PGE electrode was first immersed in the buffer (20 mM phosphate buffer 100 mM KCl pH 6, 7 and 8 used to prepare the 500 μM siderophore-containing solution to draw a baseline of the capacitive current and then immersed in the siderophore-containing solution. Scans were acquired at 100 $mV.s^{-1}$ in triplicate.

Experiments were conducted at 25° C using a three-electrode electrochemical cell configuration with the PGE (working electrode), a platinum wire (counter electrode) and an Ag/AgCl (3M KCl) (reference electrode) inside of a Coy anaerobic chamber using a CHI electrochemical analyzer from CHI Instruments controlled by the manufactures' software (version 10.12). Oxygen levels were kept stable at approximately 8 ppm.

All data was analyzed using Excel and QSoas (Fourmond , 2016). Potentials were reported in mV and with respect to the SHE by addition of 210 mV to those measured (Friis, et al., 1997).

2.4. NMR interaction studies

The interaction of NAD(P)H with SIP was studied through NMR spectroscopy based on a two-state exchange model (Fig. 2.2) where A represents the protein, SIP, B represents the ligand, NAD(P)H, and A.B represents the protein-ligand complex (Furukawa , Konuma, Yanaka, & Sugase, 2016)

A

$$A + B \underset{K_{off}}{\overset{[B]K_{on}}{\rightleftarrows}} A.B$$

B

$$K_D = \frac{K_{off}}{K_{on}} = \frac{[A][B]}{[A.B]}$$

Figure 2.2: Two-state exchange model. A represents the protein, B represents the ligand and A.B the protein-ligand complex. A) Schematic representation of the two-state exchange model with K_{on} as the forward rate and K_{off} as the backward rate. B) Equation used to calculate the dissociation constant of (K_D): [A] representing free concentration of SIP, B representing free concentration of NAD(P)H and [A.B] representing the concentration of bound SIP and NAD(P)H (Furukawa et al 2016).

Both NAD(P)H and SIP were prepared in 20 mM Tris-HCl 100 mM KCl pH 8 containing 10% of $^{2}H_2O$ (99.9 atom %). Samples of 100 µM of NAD(P)H were titrated against increasing concentrations of SIP. To determine the concentration of free and bound species triplicate experiments using a ratio of 0.8 (NAD(P)H: SIP) were performed.

As previously described in the characterization of SIP, experiments were performed at 25ºC on a Bruker Avance II 500 MHz equipped with a SEX probe for ^{31}P detection. Using the standard Bruker pulse program "zgdc" one-dimensional proton-decoupled ^{31}P spectra (1024 scans) were collected for each NAD(P)H:SIP ratio.

Collected spectra were visualized and analyzed using TopSpin 3.5 (Bruker). The concentration of free and bound species was determined from the relative intensity of each peak and the dissociation constant (K_D) was calculated using the formula described above (Fig. 2.2).

2.5. Kinetic studies

The following experiments were carried out using stopped-flow technique: reduction of SIP with NADPH, NADH, sodium dithionite and ferredoxin; reduction of ferredoxin; reduction of ferric siderophores and the ferrozine assay. The experiments were performed in a HI-TECH Scientific Stopped-Flow equipment (SF-61DX2) installed inside an anaerobic glove box (Mbraun MB150-GI). The temperature of the drive syringes and mixing chamber was maintained at 25ºC using a water bath and the pH controlled with 20 mM potassium phosphate buffer 100 mM KCl pH 7.6. The time course of the reactions was monitored using a photodiode array. All solutions were prepared inside the anaerobic chamber with degassed water and all experiments were performed in

triplicate. Data were analyzed using Excel and fittings were performed and analyzed using Kinetics Studio version 2.32 (TgK Scientific).

Reduction of SIP with NAD(P)H, sodium dithionite and Ferredoxin

Experiments were performed at multiple time-scales and at different concentrations for each reducing agent. The reduction of SIP with NAD(P)H was attempted by mixing 1 mM NAD(P)H with 20 μM SIP acquiring spectra for a total 3600 s (60 min).

Reduction of SIP with sodium dithionite was performed by mixing 100 μM sodium dithionite with 20 μM SIP. Reduction rates were obtained from experiments at the 6000 s time-scale with a total of 200 spectra acquired.

Ferredoxin from *Clostridium tetanomorphum* was a kind gift of Dr. Américo Duarte from the Bacterial Energy Metabolism Lab at ITQB-NOVA. To confirm the purity of this protein, an SDS-PAGE gel (15%) was performed. The reduction of ferredoxin with sodium dithionite was first performed in excess (1:10). Time evolution of ferredoxin's reduction was followed during 0.75 s, 75 s and 150 s. The rate constant was obtained from fitting the 400 nm kinetic trace from experiments at the 45 s time-scale. The reduction of SIP with ferredoxin was carried out after reducing ferredoxin. To avoid direct reduction of SIP with sodium dithionite the reduction of ferredoxin was carried in a 1:1 ratio and was left to react for 10 minutes before initializing the experiments of reduced ferredoxin against SIP. Reduction of SIP with ferredoxin was performed by mixing 20 μM of reduced ferredoxin with 20 μM SIP. Reduction rates were obtained from experiments at the 75 s time-scale with a total 200 spectra acquired.

The reduction rate constants of SIP with different reducing agents were obtained from fitting kinetic traces using the data collected at 470 nm and 600 nm which presented the clearest spectral changes.

Reduction of ferric siderophores

Reduction of ferric siderophores (AVA, BIS, PUT and FER) with reduced SIP was performed after reducing SIP with sodium dithionite in a 1:1 ratio. The reduction of ferric siderophores was performed by mixing 20 μM SIP with 100 μM ferric siderophores and it was followed in the time scales: 0.3, 3.0, 7.5, and 150 s. The reduction rate constant was obtained from the fitting of kinetic traces at 600 nm from experiments at the 150 s time-scale.

The ferrozine assay

The ferrozine assay consisted in monitoring the formation of ferrous iron using an iron chelator with high affinity for Fe(II), ferrozine, ($C_{20}H_{13}N_4NaO_6S_2$) purchased from Fluka. The assay was performed with the following components: the Fe(II) chelator (0.5 mM ferrozine), the putative siderophore reductase (10 µM SIP), a reducing agent (0.5 mM NAD(P)H, 50 µM sodium dithionite or 10 µM reduced ferredoxin) and 50 µM for each ferric siderophore (avaroferrin, bisucaberin, putrebactin, ferrioxamine E). The formation of Fe(II)-ferrozine complexes was analyzed by measuring the absorbance at 562 nm and the total amount of ferrous iron produced was estimated using a molar absorption coefficient of 30 000 mol^{-1} cm^{-1} (Viollier, et al., 2000). Each experiment was performed in triplicate and controls were performed containing all the previous described components with the exception of SIP.

Due to possible rust contamination of the stopped-flow equipment this assay was also performed in a Shimadzu UV-1280 UV-Vis spectrophotometer following the same conditions above mentioned (anaerobic glove box and 25ºC) with the addition of magnetic stirring inside the plastic cuvettes with assay volumes of 1.5 mL.

2.6. SIP crystallization and structural determination

Screening crystallization experiments were performed by the sitting drop vapor diffusion method on a Honeybee Cartesian crystallization robot (Genomic Systems) using a 10 mg/mL SIP solution in 20 mM Tris-HCl 50mM NaCl pH 7.6. Ninety-six conditions were tested using MDL3 plates (100 nl protein solution and 40 µL reservoir solution) and the JCSG plus crystallization screen (Molecular Dimensions).

Optimization experiments were performed by hand using the hanging-drop vapor diffusion method varying the concentration of PEG 3350 from 18 to 22% and of magnesium formate dihydrate from 0.18 M to 0.22 M.

Diffraction data and structural determination was carried out by Dr. Elin Moe from the Structural Genomics Lab and Dr. Pedro Matias from the Industry and Medicine Applied Crystallography Lab at ITQB-NOVA.

3. Results and Discussion

3.1. SIP from *Shewanella frigidimarina*

Production and Purification of SIP from *S. frigidimarina*

Grown cultures (2 L) were centrifuged to yield a total of ~20 g of biomass. The biomass was solubilized in 20 mL of 20 mM Tris-HCL pH 7.6. Crude cell extract was obtained through a three-passage disruption in the French Press. Non-disrupted cells and debris were removed by centrifugation and the remaining supernatant was ultracentrifuged to remove cell membranes. Soluble extract was concentrated and dialyzed before injection in the Q-sepharose Fast-Flow column. A total of eight fractions were collected and analyzed by UV-Visible spectroscopy. Based on previous purifications, color and UV-Visible profile, three fractions (Fig. 3.1 A) that eluted at 150 mM NaCl (15% buffer B, 20mM Tris-HCl 1M NaCl pH 7.6) were selected as potential candidates for containing the protein of interest. The content of these three fractions was verified by SDS-PAGE and based on sample volume, color and band intensity between 25 and 35 KDa on the SDS-PAGE gel (Fig.3.1 B) fraction 2 was selected for further purification.

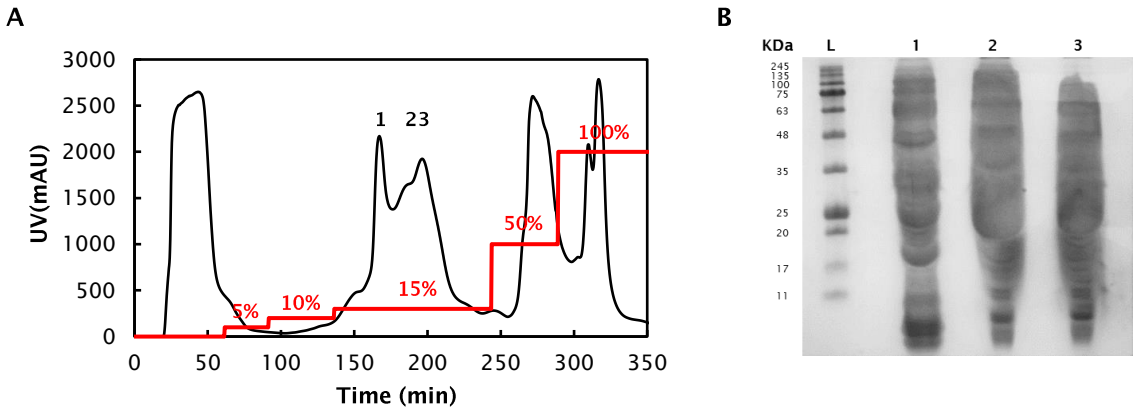

Figure 3.1: Purification of SIP. A) Elution profile of SIP and contaminants in Q-Sepharose Fast Flow column at flow rate 1mL.min^{-1}. Red numbers represent the percentage of buffer B (20 mM Tris-HCl 1 M NaCl pH 7.6) and numbers in black represent collected fractions for SDS-PAGE analysis. B) SDS-PAGE gel of fractions 1, 2 and 3.

Fraction 2 was dialyzed overnight against 20 mM Tris-HCl buffer (pH 7.6) and concentrated before injection into SP-Sepharose Fast-Flow Column.

Based on color, fractions eluted with 50 mM (5% B, tube nr. 5) and with 100 mM NaCl (10% tubes nr.13 to nr.33) (Fig. 3.2 A) were inspected by UV-Visible spectroscopy. Based on absorbance ratio A470nm/A280nm (~ 6.5) and UV-Visible profile, collection tubes from nr. 15 to nr. 31 were analyzed by SDS-PAGE (figure 3.2 B). Tubes nr. 25 to nr. 28 and nr. 29 appeared to only contain one band (Fig. 3.2 B). This band was relatively thick and this may be due to highly concentrated samples. To ensure that this was only one band, further analysis was conducted. Tubes nr. 26,

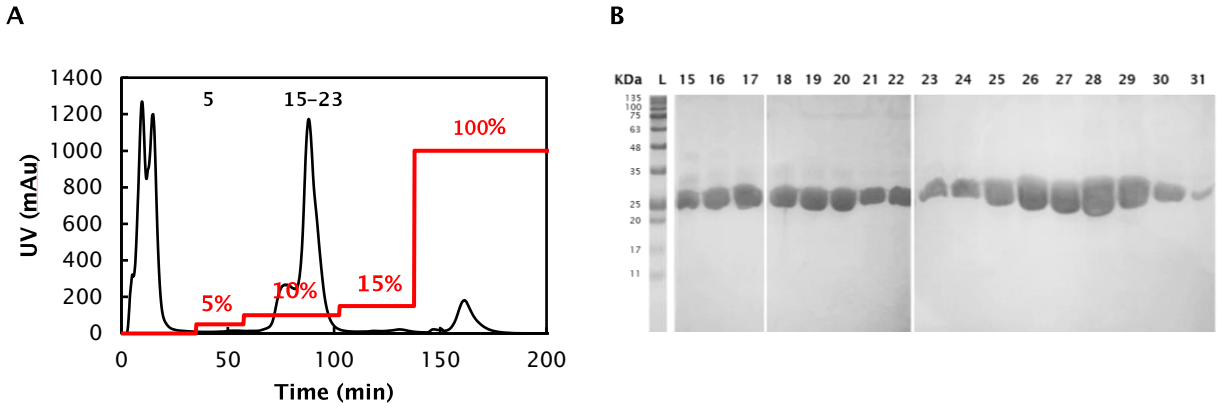

Figure 3.2: Purification of SIP. A) Elution profile of SIP and contaminants in SP-Sepharose Fast Flow column at flow rate 1mL.min-1. Red numbers represent the percentage of buffer B (20 mM Tris-HCl 1 M NaCl pH 7.6) B) SDS-PAGE gel of fractions of collection tubes nr. 15 to nr. 31.

27 and 28 were grouped together to form fraction A. Tubes nr. 23, 24, 25, 29, 30 and 31 were grouped as fraction B and finally tubes from nr. 15 to nr. 23 were grouped as fraction C. Fraction C appeared to contain a contaminant and for this reason this was saved for later purification. Fraction A was analyzed by SDS-PAGE and UV-Visible. In agreement with the sequence-based molecular weight of this protein (≈29 KDa) only one band was found in the SDS-PAGE gel (Fig. 3.3 A) migrated slightly above the 25 KDa marker. The UV-Visible spectrum (Fig. 3.3 B) of this fraction presented the typical features of a flavoprotein and it was similar to the spectrum of FscN from *T.fusca*. SIP (Fig. 3.3 B) presenting absorption maxima at 275, 387, 470 nm and distinct shoulders at 445 and 500 nm (Li, Chen, & Bruner, 2015).

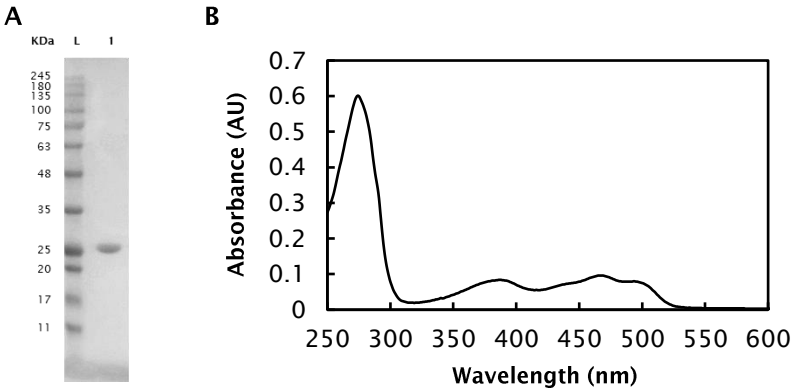

Figure 3.3: SDS-PAGE gel of purified SIP (A) and UV-Visible profile of pure protein presenting absorption maximum peaks at 275, 387 and 470 nm (B).

Using the extinction coefficient of free FAD (ε_{450}= 11 300 $M^{-1}.cm^{-1}$) fraction A was estimated to contain a total of ~40 mg of SIP (Macheroux, P. 1999). Fraction A was considered pure, and was used in the subsequent experiments. Fraction B was saved at -80ºC for further purification.

In conclusion, SIP eluted from Q-sepharose Fast-Flow with 15% B, approximately 150 mM NaCl and eluted with 10%B in SP-Sepharose Fast-Flow column, approximately 100 mM NaCl.

FAD-containing SIP

The presence of a FAD prosthetic group was confirmed using ^{31}P NMR.

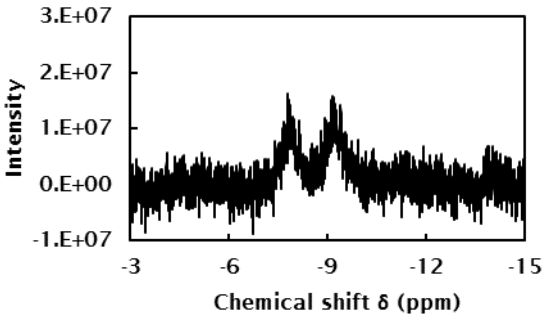

Figure 3.4: ^{31}P NMR spectrum of purified SIP containing resonances at -7.87 ppm and -9.18 ppm corresponding to the pyrophosphate moiety of FAD (Fig.3.5).

SIP ^{31}P NMR spectrum presented two resonances at -7.87 and -9.18 ppm (Fig.3.4) which correspond to the two phosphorus nuclei of the pyrophosphate moiety of FAD (Fig.3.5). Resonances of free FAD at pH 7.6 appear at -9.87 and -10.55 ppm. (Otvos, Krum, & Masters, 1986). In comparison to what is described for free FAD, in SIP there is an increase in the chemical shift and an increase in the separation between the two resonances (Fig.3.4). These differences may be attributed to the insertion in the protein moiety which provides a different conformation on the phosphorous atoms.

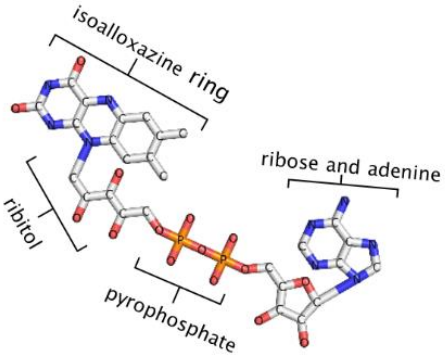

Figure 3.5: Structural representation of the FAD and its components.

SIP electrokinetics

The redox chemistry of flavoproteins is confined to the isoalloxazine ring of the flavin. Sidechains such as the adenine moiety serve solely as an anchor placing the coenzyme at the active site (Ghisla & Massey, 1989)

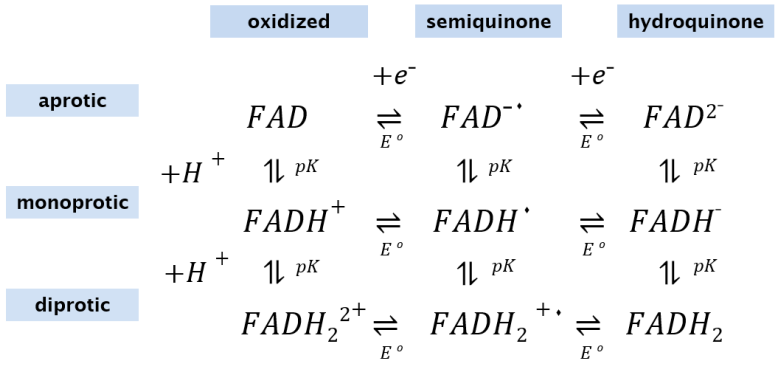

Figure 3.6: Potential mechanism for a flavin center highlighting the pathway for proton-coupled electron transfer with respective reduction potentials (E^0) and acid dissociation constants (pK) (Smith, Davis, & Barber, 2003).

Flavins are biological redox centers with the ability to couple one- and two-electron transfer with proton transfer. (Smith, Davis, & Barber, 2003). Flavins have three oxidation states, oxidized (FAD), semiquinone ($FAD^{-\cdot}$) and the hydroquinone (FAD^{-2}) state which can exist in three different ionization

states giving a total nine possible species (Fig.3.6). These electron transfer reactions and protonation steps are characterized by equilibrium constants, the reduction potential and the acid dissociation constant, respectively (Fig.3.6.) These processes can be studied through voltammetric techniques (Smith, Davis, & Barber, 2003).

A well-defined voltammetric response from SIP was obtained. Figure 3.7 (A) shows the typical acquired SIP protein-film voltammogram and its background-subtracted voltammogram. SIP voltammograms were acquired for each pH at scan rates ranging from 10 to 10000 $mV.s^{-1}$.

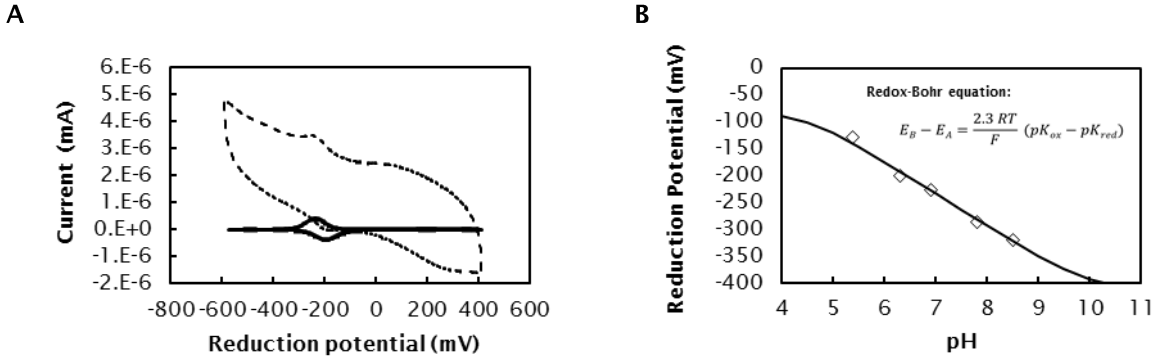

Figure 3.7: Typical SIP PFV voltammogram at 100 $mV.s^{-1}$ pH 7, dashed lines represent raw voltammograms and solid lines represent background-subtracted voltammograms (A). Dependence of the reduction potential of the FAD center in SIP participating in the Redox-Bohr effect, diamonds represent measured reduction potentials (mV vs SHE) at 100 $mV.s^{-1}$ at the following pHs: 5.4; 6.3; 7.0;7.8 and 8.5. Solid line represents the simulation of the pH dependence of the reduction potentials (B).

Throughout each pH experiment no significant protein diffusion was observed. However, a non-ideal peak separation of approximately 30mV between the reduction and oxidation peaks at low scan rate was found. Using QSoas, the background current was subtracted for every voltammogram and the full width at half height and mid-point potentials were determined (Table 3.1). Results show that SIP presents Redox-Bohr effect, the reduction potential increases as the pH is lowered (Fig.3.7 B) and table 3.1). No fitting was possible due to lack of data in the extreme pH values, although the simulation of pH dependence of the reduction potentials (Fig.3.7) shows that the pK values must be lower than 4.5 (pK_{ox}) and higher than 10 (pK_{red}) (Louro, Catarino, Salgueiro, LeGall, & Xavier, 1996). The reduction potential changes 57±2 mV for every pH unit.

Table 3.1: Electrokinetic parameters of SIP for each pH.

pH	width at half height peak (mV)	E(0) (mV)	$K_0/s-1$ (ChiSq)
5.4	86±6	-130	31 (60)
6.3	96±1	-201	59 (26)
7.0	94±6	-228	20 (29)
7.8	102±6	-286	97 (33)
8.5	110±3	-320	86 (136)

The Nernstian equilibrium portraits reversible reactions where the reductive and oxidative waves are symmetrical, currents reach maximum at the formal reduction potential, where the peak separation is zero and the half-weight peak is 3.53RT/nF (R is the ideal gas constant, T is temperature in Kelvin, n is the number of electrons and F is the Faraday constant) (Armstrong, Heering, & Hirst, 1997). Accordingly, at 25ºC the full width half weight peak for one electron

transfer (n=1) is 90 mV. The half-height width of the anodic and cathodic waves (Table 3.1) is within the theoretical value. Altogether, the half-height width and the change in reduction potential with pH are in agreement to what has been reported in the literature for a flavodoxin changing from the oxidized to the semiquinone state (Paulsen, Stankovich, Stockman, & Markley, 1990).

The half-height width shows a slight deviation from the theoretical values increasing with the increase in pH. This deviation from the ideal behavior has been reported in the literature together with the non-ideal separation between oxidation and reduction peaks (Armstrong, Heering, & Hirst, 1997). Increased half height peaks can occur due to thermodynamic dispersion which causes a general broadening of the peaks (Hirst, 2006) . Trumpet plots were fitted (Fig.3.8) using

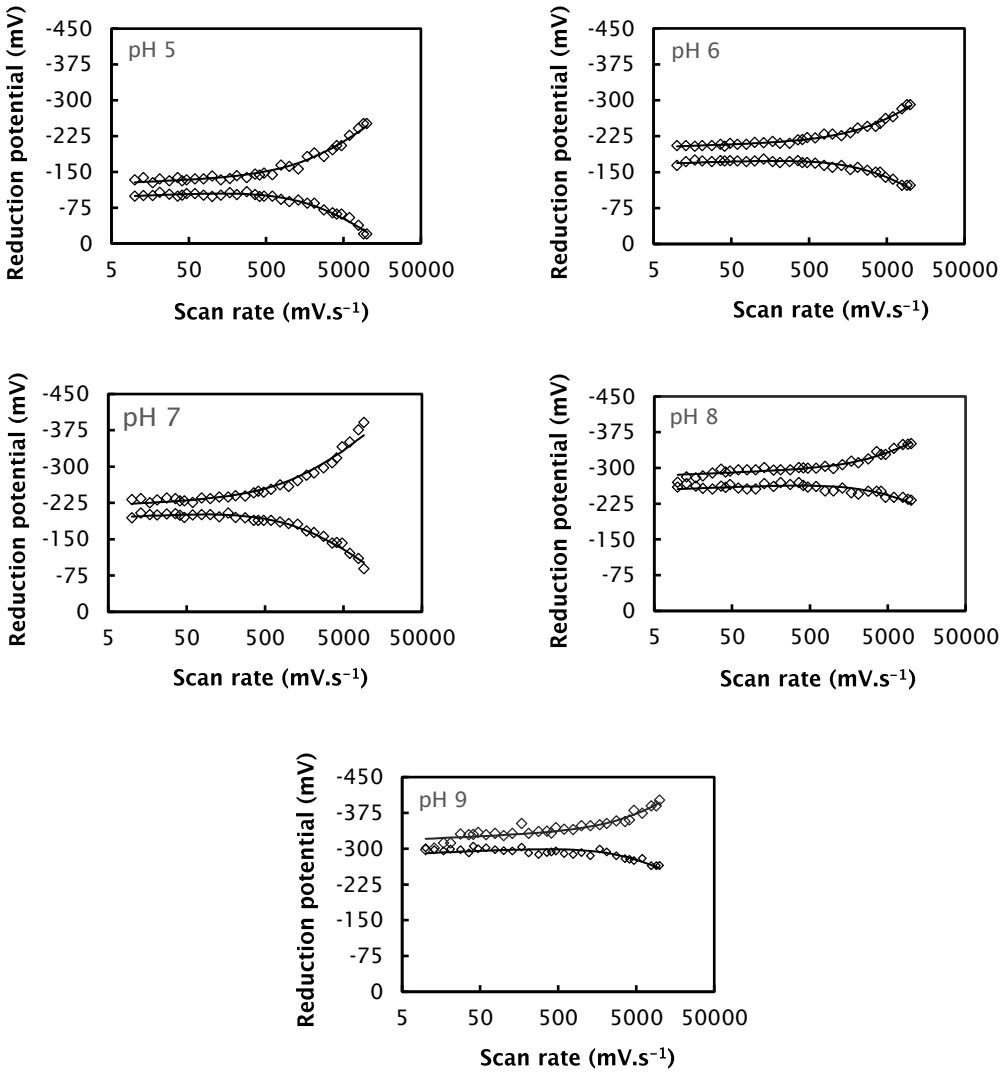

Figure 3.8: Butler-Vulmer trumpet-plots of SIP at different pHs, reflecting the influence of scan rate on the reduction and oxidation peak. Diamonds represent acquired data and solid lines represent respective fitting.

the Butler-Volmer model for one electron transfer (Jeuken, et al., 2002, Heering, et al., 1998). The rate of interfacial electron transfer was determined for each pH (Table 3.1). Fit results are shown with respective Chi-square(ChiSq) representing the goodness of the fit (Table 3.1).

Overall, an increase in the interfacial electron transfer with pH was observed, except for neutral pH which presented the slowest rate of interfacial electron transfer. Given that pH 7 corresponds to the theoretical isoelectric point of SIP, it is possible that this has an effect on its interaction with the electrode surface of the PGE electrode, rich in hydrophilic and acidic oxides (Armstrong, Heering, & Hirst, 1997).

Sequence Analysis of SIP

SIP's protein BLAST shows that SIP presents conserved motifs for FAD, phosphate and NAD(P)H binding and that it belongs to the family of siderophore interacting proteins in the FNR-like reductases superfamily. Homologous SIP proteins were found among proteobacteria (gamma, delta and beta) including: *Paraglaciecola mesophila, Psuedoaltermonas atlantica, Ferrimonas kyonanensis, Psychromonas artica, Alcanivorax dieselolei, Photobacterium marinum, Vibrio caribbeanicus*, *Storangium cellulosum* and in high GC content Gram-positive bacteria including *Sacharopolysphora rectivirgula*. SIP Homologous proteins were also found in other species of *Shewanella*, including: *S. decolorationis, S. baltica, S. putrefaciens* and *S. xiamenensis*.

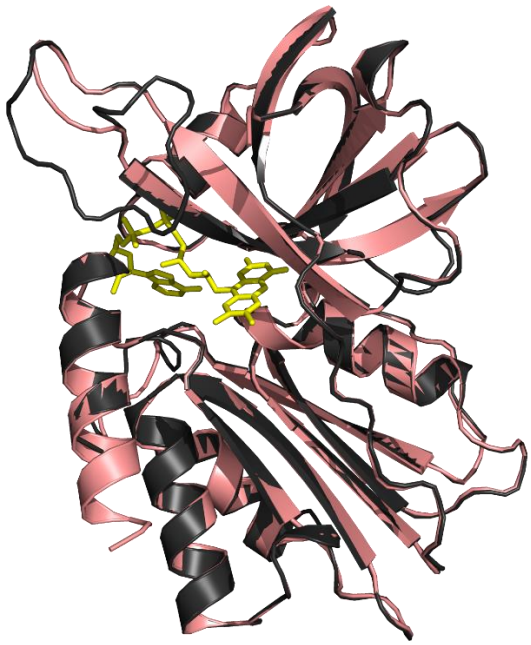

Figure 3.9: Structural model of SIP (colored in black) from *S. frigidimarina*, and model template *S.putrefaciens* SIP structure (colored in salmon together with FAD in yellow).

A structural model of SIP was obtained with 89% sequence coverage with a GMQE (Global Model Quality Estimation) of 0.62 and a QMEAN4 of -3.91. The superimposition of the SIP model with the template structure shows a similar arrangement of the secondary structure elements (Fig.3.9). The main differences are noted in the N-terminal loop and in the C-terminal helix. These differences have been previously reported in the literature for other SIPs, and they were also encountered in the multiple alignment of putative SIPs (Fig. 3.10). The two different subfamilies of SIPs can be distinguished mainly on C-terminal differentiation. (Miethke, Hou, & Marahiel, The

siderophore-interacting protein YqjH acts as a ferric reductase in different iron assimilation pathways of Escherichia coli, 2011) (Li, Chen, & Bruner, 2015) Group I SIPs include FscN from *T. fusca* and Group II SIPs include YqjH from *E.coli* (Fig.3.10).SIP contains a relatively longer C-terminus (Fig.3.10) and for this reason is possible that SIP from *S. frigidimarina* belongs to Group I SIPs which utilize NADH as an electron donor to reduce ferric siderophores. In general, all SIPs present highly conserved FAD binding motifs, both metal and putative substrate binding motifs are fairly conserved, while the NAD(P)H binding motifs are less conserved (Fig. 3.10).

Using the structural homology program DALI, SIP's structural model displayed structural homology with siderophore-interacting proteins (namely from *S.putrefaciens and T.fusca*), flavohemoglobins, flavodoxin NADPH-reductase, NADH:ubiquinone oxidoreductase and ferredoxin NADP-reductase.

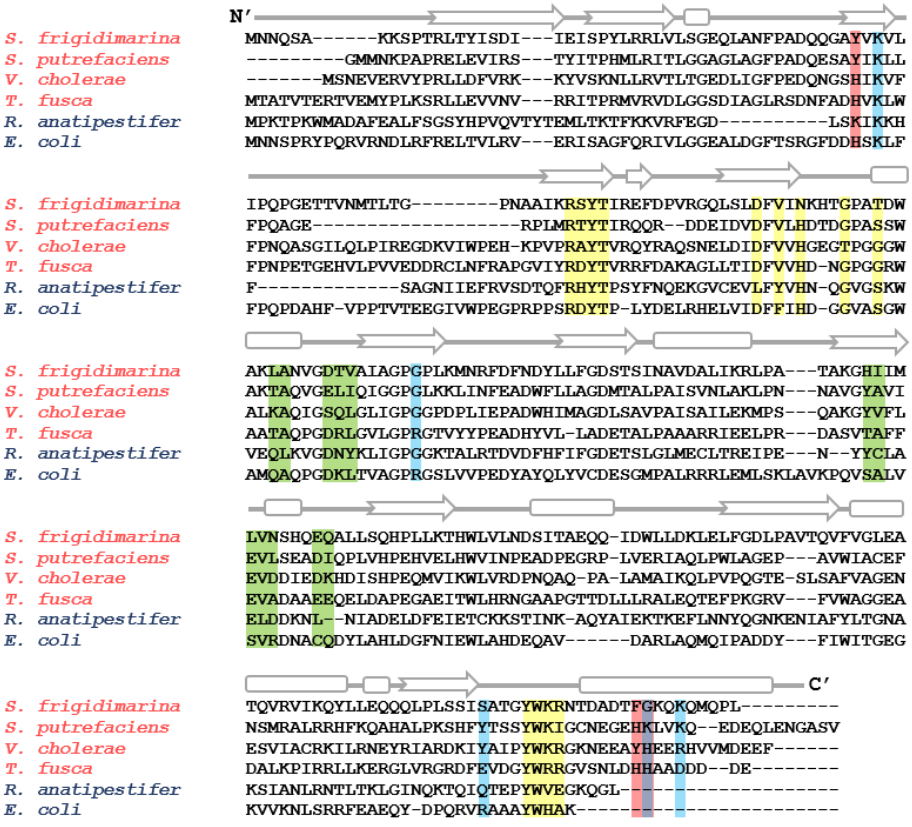

Figure 3.10: Global multiple-protein sequence alignment (MUSCLE, EMBL-EBI) of putative siderophore-interacting proteins: SIP from *S. frigidimarina,* SIP from *S. putrefaciens* ,ViuB from V. cholerae, FscN from *T.fusca*, SIP from *R.anatipestifer* and FhuF from *E. coli*. Red highlighted residues are associated with metal binding, blue for residues associated with putative substrate binding, yellow residues for the FAD binding pocket, green highlighted residues associated with the NAD(P)H binding pocket. Secondary structure from *S. putrefaciens* with arrows for beta-strands and boxes for alpha-helixes. Group 1 SIPs are typed in red and Group II SIPs are typed in blue.

3.2. Ferric siderophores

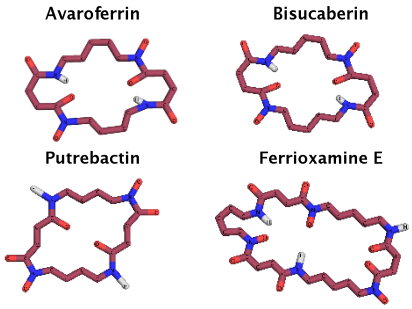

Figure 3.11: Structural representation of apo-siderophores used in this thesis. Structures obtained from ChemSpider and stick representation was obtained with PyMOL.

The addition of iron to apo-siderophores partially solubilized in DMSO (avaroferrin, bisucaberin, putrebactin), resulted in an immediate color development from dark red (acidic solution without buffer) to orange (buffered solution). All siderophores used in this thesis were siderophores of the hydroxamate type (Fig.3.11) (Spasojević, Armstrong, Brickman, & Crumbliss, 1999). These siderophores were produced by the heterologous expression of a biosynthetic gene cluster from *S.algae* cloned from deep-sea sediment genomic DNA (Fujita & Sakai, 2014). Ferrioxamine E was isolated from *Streptomyces antibioticum* and it has the ability to resuscitate stressed viable-but-nonculturable *Salmonella typhimurium* (Reissbrodt, Heier, Tschape , Kingsley , & Williams, 2000).

All siderophores including ferrrioxamine E presented a similar UV-Visible spectrum (Fig.3.12) with maximum absorption at ~430 nm. This is in agreement to what has been found for other hydroxamate siderophores (*e.g.* alcaligin produced by *Bordetella* spp.) (Nishio, Hou, Raymound, O'Sullivan, & Esker, 1998) (Spasojević, Armstrong, Brickman, & Crumbliss, 1999).

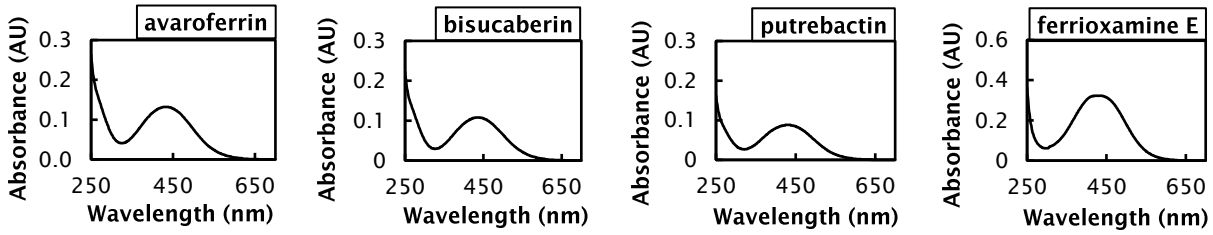

Figure 3.12: UV-Visible spectrum of the ferric siderophores: avaroferrin, bisucaberin, putrebactin and ferrioxamine E at pH 7.

Cyclic voltammograms were obtained for ferric putrebactin, ferric avaroferrin and ferric bisucaberin (Fig. 3.13). Two reduction and two oxidation peaks were found for each of these siderophores. Considering that these siderophores are analogous to alcaligin, this might be explained due to the speciation found in this type of siderophores. Alcaligin and BIS exhibit different iron coordination upon pH change, forming 1:1 ferric complexes (FeL^{+}) at acidic pH, and 2:3 ferric complexes (Fe_2L_3) at alkaline pH. At neutral pH using a 1:1 mixture of iron to apo-siderophore (ligand, L), there is insufficient apo-siderophore to enable the formation of Fe_2L_3 and therefore complex FeL+ hydrolyzes to form a third complex (FeLOH) (Nishio, Hou, Raymound, O'Sullivan, & Esker, 1998).

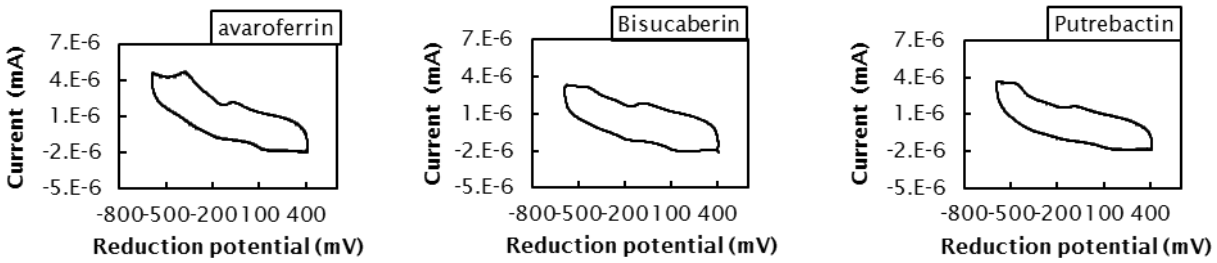

Figure 3.13: Cyclic voltammograms of AVA, BIS and PUT at pH ~7, acquired at 100 mV.s^{-1}.

Altogether, this suggests the existence of at least two species in solution for each ferric siderophore, one with lower reduction potential and another with a higher reduction potential (Table 3.2). Mid-point reduction potentials were determined using the average of the oxidation and reduction peaks. A high peak separation (around ~ 250mV) and difference in signal amplitude between the oxidation and reduction peaks was observed. The decrease in the signal amplitude of the reoxidation peak and the shift towards a more positive potential can be explained by the reduction of the ferric siderophore complex which leads to the formation of ferrous iron and consequent dissociation of the complex (Spasojević, et al., 1999).

Table 3.2: Reduction potentials of ferric siderophores determined in a 1:1 ratio of metal to apo-siderophore.

Siderophore	pH, temp.	$E_{1/2}$ (mV vs SHE)	Reference
Avaroferrin	7.25 , 25ºC	-295 and +25	This study
Bisucaberin	7.30, 25ºC	-311 and +35	This study
Ferrioxamine E	10.5, n/d	-478	(Nishio, Hou, Raymound, O'Sullivan, & Esker, 1998)
Putrebactin	7.27, 25ºC	-309 and +33	This study

Of the measured reduction potentials, the species with the positive potential can be easily reduced by SIP (Table 3.1) whereas the reduction of the species with negative potential is an uphill process. To further understand the range of possible reduction potentials of the ferric siderophores used, supplementary studies should be conducted at different pHs and at different mixing ratios of apo-siderophore to ferric iron.

The presence of the various species of ferric siderophores varies with the ratio of apo-siderophore to metal due to the different stability constants of the different complexes in solution varying with pH. It is possible to achieve one single ferric siderophore species in solution, although only in extreme pH conditions and in excess of apo-siderophores (Spasojević, Armstrong, Brickman, & Crumbliss, 1999). These conditions narrow the experimental range mimicking the physiological pH and require high amounts of apo-siderophores. However, in certain cases, ferric siderophores are intracellularly imported in very acidic small vesicles, and for these cases it is of biological relevance to study ferric siderophores and ferric siderophore reduction in acidic conditions (Sutak, Chamot, Tachezy, Camadro, & Lesuisse, 2004).

Understanding the electrochemical behavior of ferric siderophores may be relevant for understanding the mechanism of cellular ferric siderophore reduction. Not only the structural organization of the apo-siderophore structure upon the binding of the metal, but also the

surrounding pH and the ratio of apo-siderophore to iron change the reduction potential of ferric siderophores. These factors can be determinant to the cellular fate and iron release from siderophores.

3.3. Interaction studies

Interaction of SIP with NAD(P)H

NADH and NADPH are not symmetrical molecules (Fig. 3.14 B). However, from the presented ^{31}P NMR spectra it can be observed (Fig. 3.14 A) that the two central phosphorus atoms appear identical from the NMR point of view by having only one resonance at -11.25 ppm. NADPH having an extra phosphorus presented an extra resonance at 3.47 ppm.

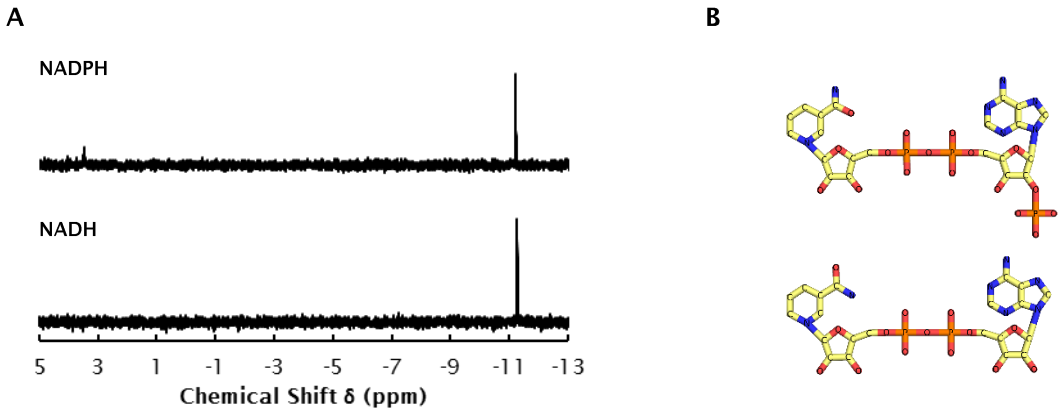

Figure 3.14: Proton-decoupled ^{31}P NMR spectra of NADPH and NADH, 100 µM in 20mM Tris-HCl pH 8 (A). Both spectra present a resonance at -11.25 ppm and NADPH having an extra phosphate group presents an extra resonance at 3.47 ppm. Structural representations of NADPH and NADH drawn with PyMOL (B).

Figure 3.15 illustrates the variation of ^{31}P NMR spectra upon the addition of a concentrated SIP solution to a 100 µM NADPH solution. Upon increasing amounts of SIP to the solution of either NADH or NADPH a pattern change was observed, a symmetry break from spectrum A to spectrum G (Fig.3.15). In function of SIP's concentration, the spectrum evolves from a A_2 in the free NAD(P)H to a AB system in the bound NAD(P)H. The chemical shifts of the two phosphorus atoms change from -11.25 to -11.33 and -11.65 ppm showing that the local environment of the two phosphate groups is different. Furthermore, the spectra revealed that the J-coupling between the phosphorus atoms in the two phosphate groups is 22 Hz. Binding occurs in the slow-exchange regime since resonances for the free and bound states coexist. SIP interacts with both NADH and NADPH either inducing a conformational change and/or by binding. These spectral changes have been previously reported in the literature (Mano, Kuhn, Menu, & Dufourc, 2003). The upfield shift in

the phosphorus resonances has been attributed to either the distortion of the P-O-P bond or to the interaction of

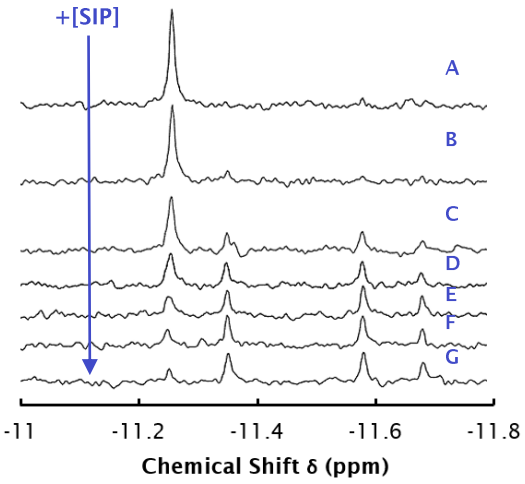

Figure 3.15: Spectral changes of NADPH (A to G) upon increasing amounts of SIP.

the anionic form of the phosphate group with arginine residues in the protein (Tsai, et al., 1989, Mas & Colman, 1984).

Experiments using overstoichiometric amounts of SIP, NADH/SIP ratio of 0.58, revealed the presence of two sets of resonances (Fig 3.16 B) corresponding to free and bound states of NAD(P)H. The concentrations of free and bound species were calculated from the relative intensity of the peaks (Fig.3.16) NADH presented a K_D of 20±5 μM and NADPH presented a K_D of 21±6 μM. A K_D in the micromolar range implies a relatively weak binding, characteristic of electron transfer reactions (Díaz-Quintana, Cruz-Gallardo, De La Rosa, & Díaz-Moreno, 2016).

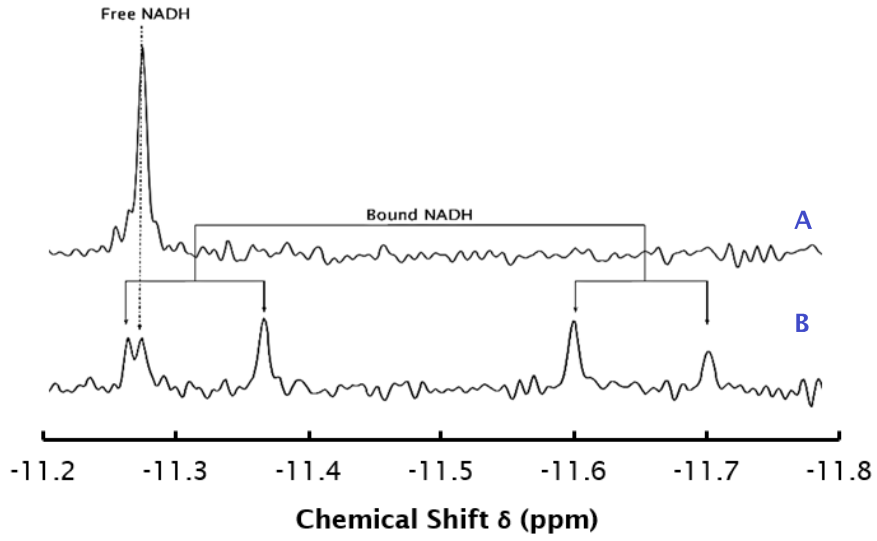

Figure 3.16: A) Proton-decoupled ^{31}P NMR spectra: top spectra corresponds to 100 μM of NADH and bottom spectra corresponds to a NADH/SIP ratio of 0.58. The addition of SIP leads to a symmetry break. Without SIP the two phosphorus of the NADH molecule are equivalent (A_2 system, same chemical shift) and become different in the addition of SIP (AB-type system).

Exploring the Bioactivity of SIP

In order to assess the bioactivity of SIP, anaerobic assays were performed. Contrary to what was expected, no direct reduction of SIP was observed with putative physiological electron donors NADH and NADPH (Fig.3.16). Instead, SIP reduction was observed with sodium dithionite and with a ferredoxin.

Upon mixing SIP with sodium dithionite, the absorption spectral changes were characterized by a decrease in 470 nm and by an increase at 600 nm (Fig.3.18 A). An isosbestic point was observed at 513 nm. In addition, it was also noted that in the presence of dithionite the solution of SIP changes from bright yellow to a clear blue solution. Altogether and in comparison to other described flavoproteins these observations suggest the decrease of the oxidized flavin and an increase in the semiquinone state over time (McMahon & Mayhew, 2007, Evans, et al., 2013). The rate constants for these processes are in the order of $10^{-4}s^{-1}$ (Fig.3.18 B). The data also suggest that over the period of 6000 s SIP did not achieve the fully reduced state since no decrease was found in the absorbance at 600 nm. The fully reduced state of SIP was achieved by increasing the amount of sodium dithionite, however this resulted in the precipitation of the protein. Since no reduction with NAD(P)H was observed, other possible biological relevant electron donors were considered.

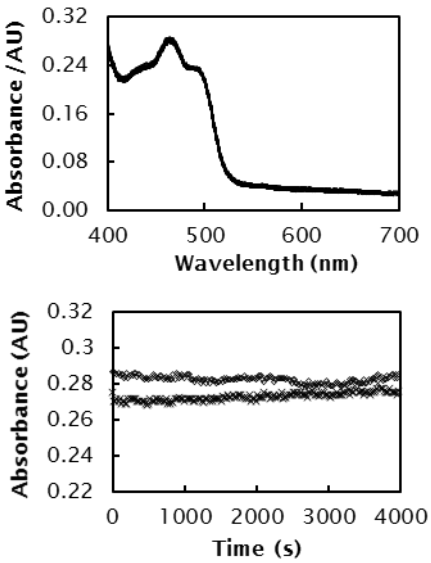

Figure 3.17: Attempt in reducing SIP with NADH (◇) and NADPH (χ). Top graph shows the stable SIP absorbance with NADH during 4000 s and bottom graph shows time-resolved trace of the absorbance of SIP at 470 nm.

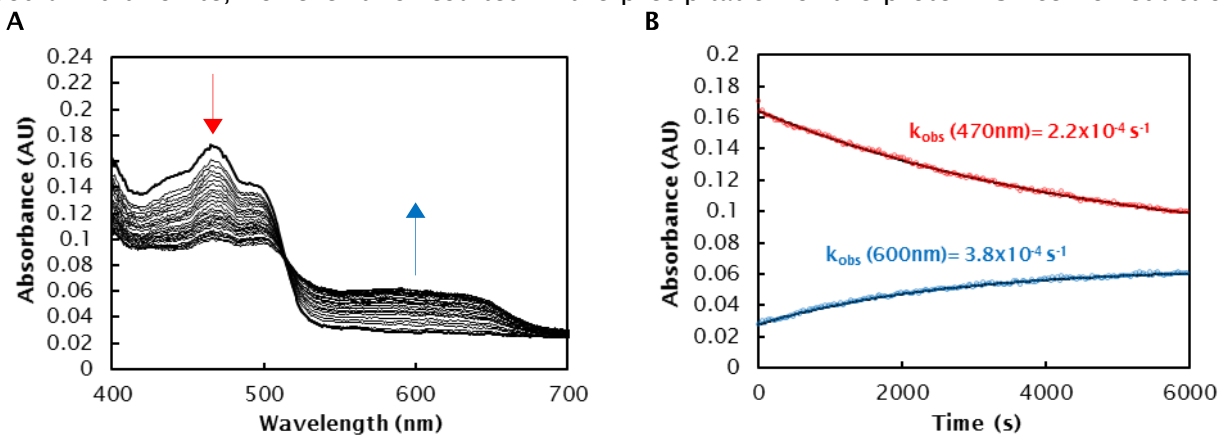

Figure 3.18: Stopped-flow analysis of the reduction of SIP with sodium dithionite at pH 7.6 for a period of 6000 s (100 min). A) Absorption spectral changes after mixing SIP (20 μM) with sodium dithionite (100 μM). Arrows indicate the change in absorbance with time. Red arrow indicates the decrease in absorbance at 470nm, the reduction of SIP. Blue arrow indicates the increase in absorbance at 600 nm, the formation of the semi-quinone state. B) Time-resolved reduction of SIP (red circles) and formation of the semi-quinone state (blue circles) and respective fits (black line) and rates obtained with Kinetic Studio..

It is reported in the literature that ferric reductases also utilize other electron donors including glutathione and ferredoxin (Miethke, et al., 2011). Having available a ferredoxin from *C. tetanomorphum* (GenBank: KAJ49949), which presents a high sequence identity (39%) to a ferredoxin encoded in the genome of *Shewanella* (Sequence ID: WP_059746450.1), the possibility of ferredoxin as a SIP electron donor was tested.

The purity of ferredoxin was assessed through SDS-PAGE gel, migrating as a single band at the bottom of the gel which was consistent with ferredoxin's molecular weight of ~6 KDa (Fig. 3.19 A). The ferredoxin rate of reduction with excess of sodium dithionite was 0.045 ±0.002 s^{-1} and this was determined from the decrease in the absorbance at 400 nm (Fig.3.19 B and C).

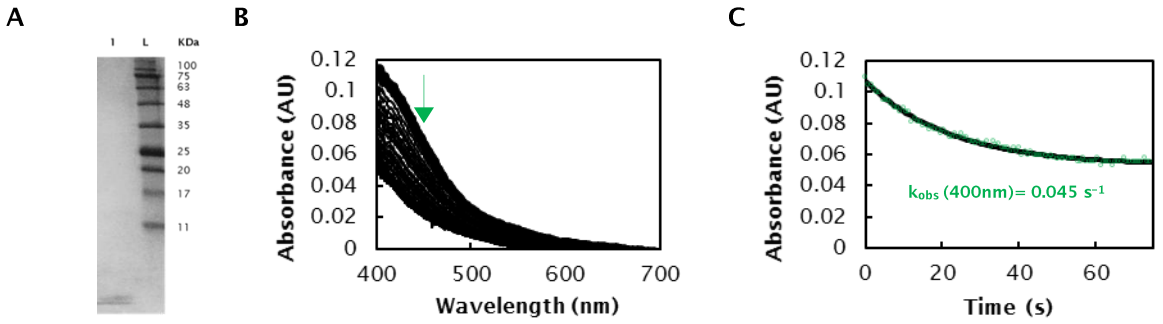

Figure 3.19: Ferredoxin, a 2Fe-2S protein from *Clostridium tetanomorphum*. A) SDS-PAGE gel of pure ferredoxin with single band (1) at the end of the gel (≈7KDa). B) Absorption spectral changes during 75 s after mixing ferredoxin with excess of dithionite. Green arrow indicates the decrease in absorbance with time, indicating the reduction of ferredoxin. C) Time-resolved reduction of ferredoxin (green circles) with respective fit (black line) and rate of reduction (0.045 ± 0.002 s^{-1}).

The ferredoxin was reduced in a 1:1 ratio using sodium dithionite. Subsequently the reduced ferredoxin (FDX_{red}) was mixed with equimolar amounts of SIP. The reduction of SIP using FDX_{red} revealed a biphasic kinetic trace (Fig. 3.20) characterized by a primary fast decrease in absorbance at 470 nm with a rate constant of 72±38 s^{-1} followed by a slower decrease with a rate

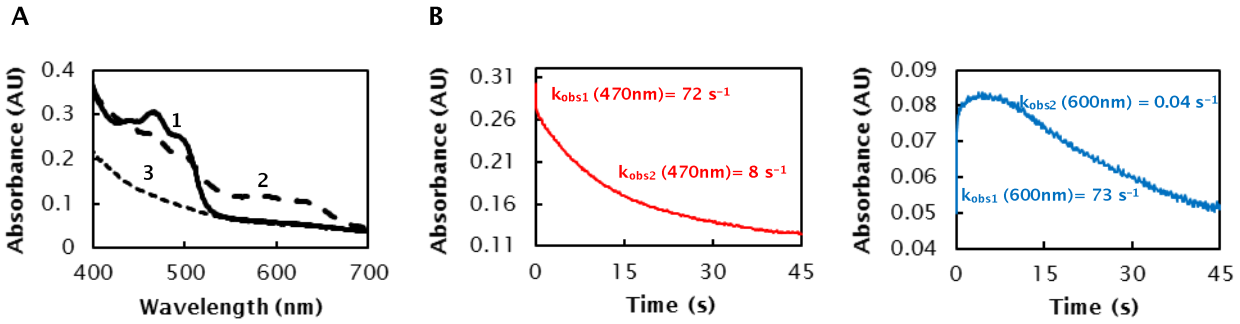

Figure 3.20: Reduction of SIP with Ferredoxin from *C.tetanomorphum*. A) Absorption spectral changes during 75 s after mixing ferredoxin with SIP. Numbers in the figure indicate significant spectral features: 1) initial spectrum at 0.0075 s showing the typical spectral features of oxidized SIP 2) spectrum after 2s, an increase in absorbance at 600 nm, typical feature of the formation of the semi-quinone 3) final spectrum at 75s, a decrease in absorbance at both 470 nm and 600 nm representing fully reduced SIP. B) Time-resolved kinetic trace of SIP reduction represented in red (470 nm) with respective rate constants and change in the semi-quinone state in blue, 600 nm with respective rate constants for a period of 45 s.

constant of 8±5 s^{-1}. These changes in absorbance at 470 nm indicate the reduction of SIP.

Additionally, significant spectral changes were also observed at 600 nm. A fast increase in absorbance (K_{obs1},600nm, of 73±15 s^{-1}) from 0 to ~ 0.3s, followed by a slower increase that reaches a maximum at 5 s, and then a decrease (K_{obs2},600nm, of 0.04±0.01 s^{-1}). These stages represent the formation of the semiquinone state (0-0.3s) followed by the transition to the fully reduced state of the flavin ($FADH_2$) (~11 to 45s) through time. Two isosbestic points were observed at 508 nm and at 450 nm. SIP reached the fully reduced state over a period of 75 s.

Ferric-Siderophore Reduction

Since no direct reduction was observed for the putative reducing agents NAD(P)H, SIP was reduced with sodium dithionite in a 1:1 ratio. Using previously reduced SIP (SIP_{red}), ferric siderophore reduction was observed for all siderophores with the exception of ferrioxamine E. Upon mixing of SIP_{red} with ferric siderophores (avaroferrin, bisucaberin, putrebactin) absorption spectral changes presented an increase at 470 nm and a decrease at 600nm (Fig.3.21). This is consistent with the single electron reaction where one electron flows from semi-quinone flavin to the ferric siderophore yielding fully oxidized SIP and Fe^{2+}. The rate constant of ferric siderophore

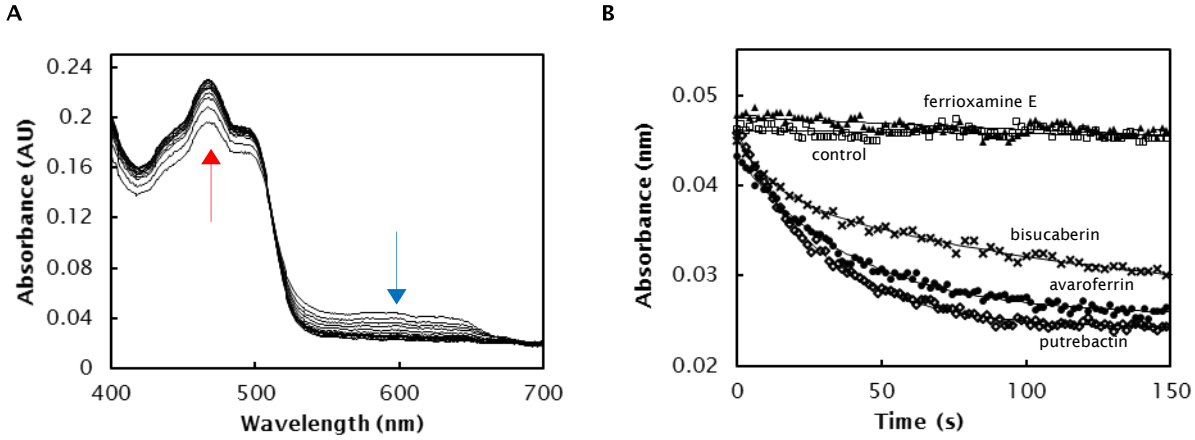

Figure 3.21: SIP-mediated reduction of ferric-siderophores. A) Absorption spectral changes during 150 s after mixing reduced SIP with ferric-siderophore avaroferrin. Red arrow indicates the increase in absorbance at 470 nm and blue arrow indicates a decrease in the absorbance at 600 nm. B) Time-resolved SIP-mediated reduction of ferric siderophores (600 nm): ▲ ferrioxamine E; ●- avaroferrin; ◇- putrebactin and x- bisucaberin □-control (apo-avaroferrin).

reduction was determined from the kinetic trace at 600 nm to avoid signal interference since ferric siderophores present a UV-Visible spectrum with maximum absorbance at 430 nm. All kinetic traces were monophasic with the exception of siderophore putrebactin which was best fit by a biphasic exponential. This might be explained by the presence of impurities in this siderophore sample (Appendix nr.1). The putrebactin sample provided by our collaborator in Japan contained traces of Avaroferrin and Bisucaberin blurring the interpretation of the kinetic results for this sample (Table 3.3). All siderophores presented similar rate constants with relative

differences which may result from the impurity of the ferric siderophores and differences in concentration.

Table 3.3: Rate constants ferric siderophore reduction.

Ferric siderophore	Rate constant (K_{obs})	R^2
Avaroferrin	0.033± 0.001	0.99
Bisucaberin	0.025 ±0.001	0.99
Putrebactin	0.08 ±0.001 and 0.007±0.005	0.99
Ferrioxamine E	-	-

Ferrozine Assay

In order to assess the production of ferrous iron, ferric reductase assays were performed with ferrozine. Absorption spectral changes were monitored up to a maximum of 1500 s and a gradual increase in absorbance at 562 nm (Fig.3.22) was observed. In contrast with previously performed experiments where no direct reduction of NADH and NADPH was observed, in the presence of ferrozine, ferric reductase activity was observed when both NADPH and NADH were used as reducing agents (Fig.3.22 and Fig.3.23). Rate constants were determined from the kinetic trace at 562 nm. Identical rates of ferrous iron formation were found for NAD(P)H, suggesting no preference of SIP

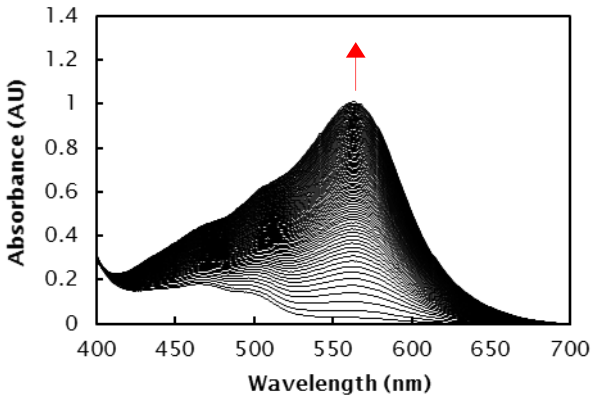

Figure 3.22: Absorption spectral changes during 1500 s after mixing ferrrozine, SIP, avaroferrin and NADPH. Red arrow indicates the increase in absorbance at 562nm, the formation of Fe(II)-ferrozine complex.

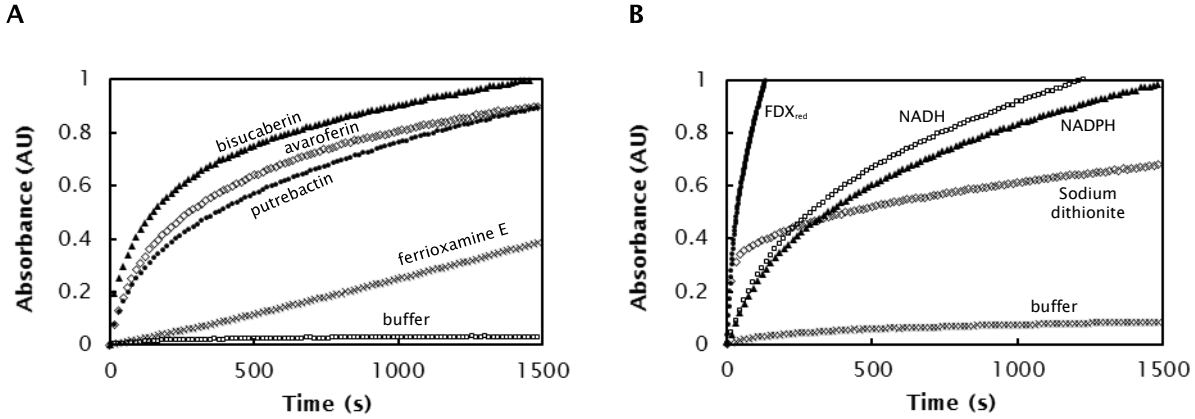

Figure 3.23: Time-resolved formation of the Fe(II)-ferrozine complex with different ferric siderophores (A) and with different reducing agents (B).

between these two reducing agents. These results are consistent with NMR data where the dissociation constants were identical as well.

Ferredoxin and dithionite as reducing agents were also tested. Ferredoxin presented the highest rate constants for the formation of ferrous iron. In the presence of ferrozine, SIP was able to reduce all ferric siderophores including the lower reduction potential ferrioxamine E. With the exception of ferrioxamine E, the formation of ferrous iron was biphasic in all three siderophores. These data tie in with the voltammetric results, suggesting the existence of two species of iron coordination with the siderophore in solution, one with a lower reduction potential (from –295 to -311) and another with a higher reduction potential (+25 to +35). Given the ability of SIP in reducing lower potential (-477mV) ferrioxamine E using NAD(P)H in the presence of ferrozine, it is possible that SIP is able to first reduce the iron coordinated species with the more positive potential at a faster rate and then reduce at a slower rate the species with lower reduction potential.

Overall these results suggest that the non-physiological reagent ferrozine has a dramatic influence in promoting ferric siderophore reduction, allowing the reduction of ferrioxamine E and the utilization of NADH and NADPH. This has been reported before in the literature, examples include FscN from *T.fusca* and YqjH from E.coli where ferric siderophore reductase activity and NAD(P)H reduction was only detected using ferene (ferrozine).

In most cases, there is a mismatch between reduction potentials of the ferric siderophores and free reduced flavoproteins, in the sense that ferric siderophores have lower reduction potentials causing these reactions to be thermodynamically unfavorable (Pierre, Fontecave, & Crichton, 2002). It has been argued in the literature that coupling this unfavorable reaction with the complexation of ferrous iron to a strong ferrous iron chelator such as ferrozine shifts the thermodynamic equilibrium enabling ferric siderophore reduction (Pierre, Fontecave, & Crichton, 2002). The biological relevance of this chemical coupling is questionable. However, this opens the possibility for an extra component in the pathway of ferric siderophore reduction, a ferrous iron acceptor, such as porphyrins or apoproteins. It is a logical view when considering the tight regulation mechanisms that exist across the siderophore pathway to avoid damage caused by free ferrous iron in the cell.

3.4. SIP crystallization and structural determination

From the ninety-six conditions tested in the screening crystallization experiments, twelve conditions yielded yellow crystals. Figure 3.24 (A), illustrates the variety of crystals obtained. The

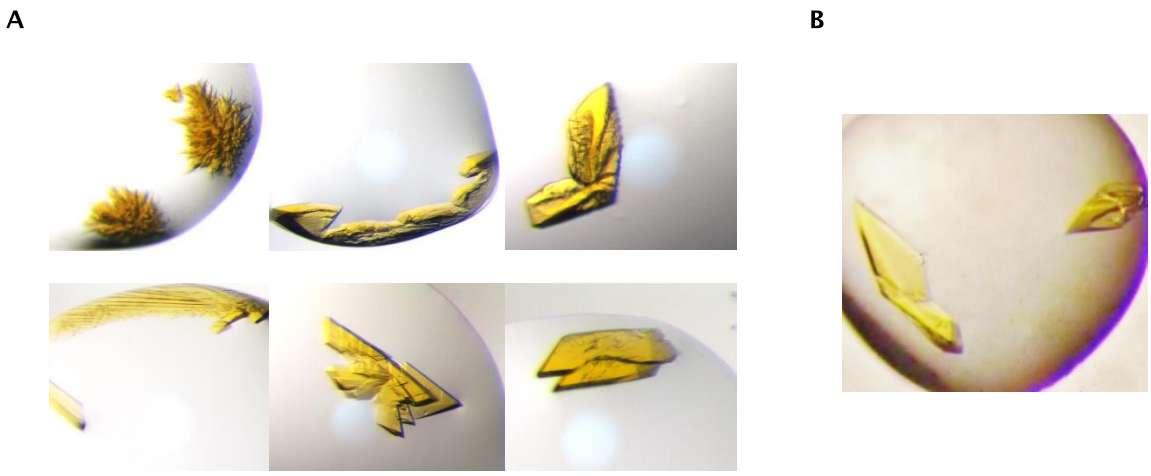

Figure 3.24: SIP crystals from the screening crystallization experiments. A) Representative variety of crystals obstained. B) Most promising SIP crystal obtained. Picture taken two days after set-up.

most promising crystal was obtained in 20% PEG 3350 0.2 M Magnesium formate dehydrate (Fig. 3.23 B).

In order to increase crystal size, hanging-drop optimization experiments were performed varying the concentration of PEG 3350 (18% to 22% w/v) and magnesium formate dihydrate (0.18 to 0.22 M). Crystals appeared after one day, and were fully grown after three days. Given that all crystals diffracted, no further optimization was performed at this level.

Crystals from various drops either from screening or optimization experiments were soaked in 22% (w/v) PEG 3350, 0.2 M Magnesium formate dihydrate before being flash-cooled in liquid nitrogen. Data collection was performed at Diamond Light Source (DLS), United Kingdom by Dr. Elin Moe.

In brief, data were collected up to a maximum resolution of 1.35 Å. This high resolution allowed the automatic determination of the preliminary three-dimensional structure of SIP (Fig.3.25 A). Analysis of the structure revealed great similarity with the computational model obtained (Fig. 3.9 and 3.25 A) and the FAD cofactor shows the typical conformation found in previously characterized SIPs. Full refinement is currently under way.

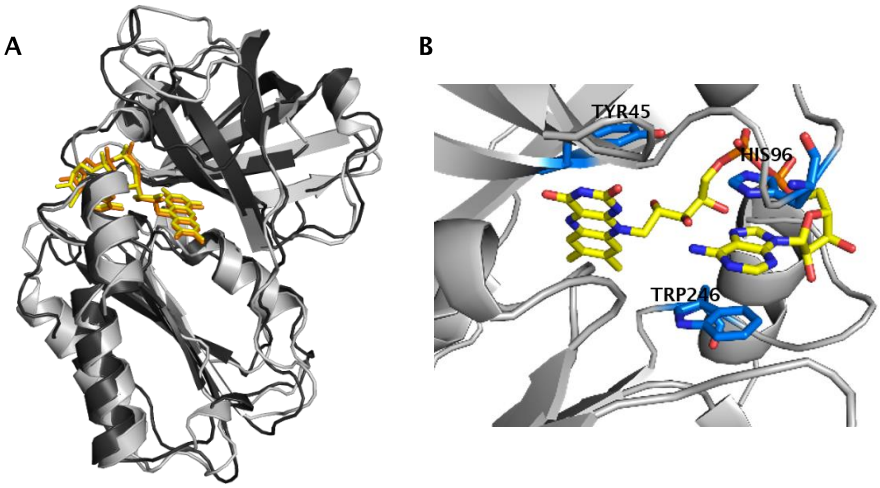

Figure 3.25: Preliminary analysis of three-dimensional structure of SIP: A) Preliminary structure of SIP determined by X-ray crystallization (colored in light grey) and corresponding FAD (yellow) versus SIP computational model structure and corresponding FAD (orange). B) View of the FAD binding pocket and key residues involved in its stabilization.

Further details can be found in appendix 3, a research article where this part of the thesis work was published with the title: "A putative siderophore-interacting protein from the marine bacterium *Shewanella frigidimarina* NCIMB 400: cloning, expression, purification, crystallization and X-ray diffraction analysis".

Conclusions and future perspectives

Life is an electron transport process that occurs in chemically active spatial enclosures, cells. Cells conserve and dissipate energy to maintain an inheritable order and element homeostasis (Schoepp-Cothenet, et al., 2013) (Williams, A chemical systems approach to evolution, 2007).

The selection of these elements is determined by the co-evolution of Life and Earth in geological timescales. Approximately two billion years ago, the massive production of oxygen by photosynthetic bacteria caused an environmental switch with dramatic consequences for living organisms and for the evolution of life (Ilbert & Bonnefoy, 2013, Zhang, et al., 2016). Oxygen rose as a dual-edged sword, on one hand providing the driving force for the evolution of the aerobic respiratory pathways which enabled the origin of new forms of life, and on the other hand, limiting the accessibility of essential nutrients such as iron. (Sessions, et al., 2009, Pierre, et al., 2002).

The GOE marked the end of an "iron age" where iron was the fundamental element for life (Crichton & Pierre, 2001). The development of siderophores and other ferric iron acquisition systems, made scarce iron, once again accessible to be incorporated in metabolic pathways together with copper, giving rise to the "iron-copper" age (Crichton & Pierre, 2001).

Since the discovery of the siderophore pathway, siderophores have been highly explored and this has provided both environmental and medicinal sciences with extraordinary findings (Saha, et al., 2016). However, its full potential has not yet been achieved (Miethke & Marahiel, Siderophore-based iron aquisition and pathogen control, 2007). The mechanism of ferric siderophore reduction in medicine may lead to the discovery of novel target-specific inhibition strategies ultimately providing novel pharmaceutical drugs that circumvent the emerging pathogens bacterial resistance. Additionally, for environmental sciences this knowledge is relevant for promoting a more efficient use of siderophores in bioremediation.

Overall, siderophore-interacting proteins, FSRs and SIPs are widely conserved across the genomes of Shewanella spp. (Pruitt, et al., 2005). SIP from *S.frigidimarina* is a flavoprotein which belongs to the SIP superfamily. Here it was shown that SIP has reduction potentials which are adequate to reduce ferric siderophores associated with *Shewanella.* This protein displays Redox-Bohr effect, performing proton-coupled electron transfer (Louro, Catarino, Salgueiro, LeGall, & Xavier, 1996).

Sequencing analysis, and NMR data indicate that SIP interacts and binds to both NADH and NADPH, the putative electron donors for siderophore interacting proteins. However, direct reduction of this protein, and of others characterized in the literature, using these electron donors has yet to be seen. Nevertheless, it should also be considered that these proteins, if included in

a larger network, can have other functions by interacting with different redox partners depending on the cell requirements for iron. Structural determination of SIP together with putative electron donors and acceptors is a future step which will provide crucial knowledge in understanding the interaction network of these proteins.

The functional characterization of SIP from *S.frigidimarina* brought to light novel aspects which were previously unknown for this type of proteins. The ability of SIP to utilize ferredoxin as electron donor broadens the spectrum of electron donors in this pathway. SIP-mediated siderophore reduction using ferredoxin as electron donor ties this pathway with the ROS cycle (Kiley & Beinerty, 2003). Iron-sulfur clusters are key to three major transcription regulators: FNR, IscR and SoxR. These mediate cellular responses to ROS and nitric oxide, with IscR being a global regulator essential in pathogenesis (Kiley & Beinerty, 2003). Ferrous iron has the ability to catalyze the formation of reactive species, and given the overall existing strict cellular iron regulation, it is feasible to speculate that if ferredoxins are the physiological electron donors of SIPs, these also play an essential role in maintaining cell homeostasis by controlling the fate of reactive ferrous iron (Papanikolaou & Pantopoulos, 2005, Mandin, et al., 2016). Additionally, the use of ferrozine, showed a dramatic influence in ferric siderophore reduction by promoting the reduction of lower reduction potential ferrioxamine E and the utilization of NADH and NADPH. This chemical coupling has not been very highlighted in the literature although it might be of biological relevance if one considers the possible role of downstream partners in the pathway of ferric siderophore reduction. For example, ferrous iron acceptors such as porphyrins or apoproteins that can drive ferric iron reduction, and prevent the undesired release of ferrous iron (Pierre, Fontecave, & Crichton, 2002) (Baysse, et al., 2003). These two findings are tied together, suggesting that the mechanism of ferric siderophore reduction can be part of a larger network of cell processes that include iron release from the siderophores, iron uptake and iron regulation working in close communication to maintain iron homeostasis.

In this thesis, another important feature that should be considered in the mechanism ferric siderophore reduction is its location. SIPs and FSRs can be found in various locations inside the cell (Schröder, Johnson, & Vries, 2003) and the determination of the reduction potential of Shewanella's ferric siderophores enhanced an important chemical feature of these small iron chelators and ferric siderophore reduction. As with analogous siderophore alcaligin these siderophores display speciation, that is, the iron coordination species in solution change with pH and with ratio of ligand to metal abundance (Nishio, Hou, Raymound, O'Sullivan, & Esker, 1998). This property of siderophores remains unexploited from the biological point of view, although is it another extraordinary reminder of iron's versatility as a redox center. The reduction potential of siderophores can be changed in three ways: the structure of the apo-siderophore, iron-

coordination and pH. These properties determine ferrous iron release from the siderophore and can determine its fate upon cellular iron acquisition.

The production of a ferredoxin from *S. frigidimarina* and of a FSR from *S.algae* (appendix 2) will be pursued in the future. With the characterization of this SIP from *S. frigidimarina*, the next step is to understand the role of these proteins in iron acquisition and virulence of *Shewanella* by performing gene mutations within its genome and check for the resulting phenotypes.

The comprehensive characterization of SIP from *S.frigidimarina* brings out novel aspects to the pathway of ferric siderophore reduction. Further knowledge on this class of proteins can unravel mechanistic details which are crucial to attain insights about *Shewanella*'s emergent pathogenicity and about the colonization of microorganisms in iron limited environments.

Bibliography

Abergel, R., Zawadzka, A., Hoette, T., & Raymond, K. (2009). Enzymatic hydrolysis of trilactone siderophores: where chiral recognition occurs in enterobactin and bacillibactin iron transport. *J. Am. Chem. Soc. , 131*, 12682–12692.

Altschul, S., Gish, W., Miller, W., Myers, E., & Lipman, D. (1990). Basic local alignment search tool. *J. Mol. Biol. , 215*, 403-410.

Anderson, G., Frazer, D., Wilkins, S., Becker, E., Millard, K., Murphy, T., & Vulpe, C. (2002). Relationship between intestinal iron-transporter expression, hepatic hepcidin levels and the control of iron absorption. *Biochem. Soc. Trans., 30*, 724-726.

Andrews, N. (2005). Iron metabolism: disorders. *eLS*.

Andrews, S., Robinson, A., & Rodríguez-Quiñones, F. (2003). Bacterial iron homeostasis. *FEMS Microbiol. Rev., 27*, 25-237.

Arceneaux, J., & Bryers, B. (1980). Ferrisiderophore reductase activity in *Bacillus megaterium*. *J. Bacteriol., 141*, 715-721.

Archibald, F. (1983). *Lactobacillus plantarum*, an organism not requiring iron. *FEMS Microbiol. Lett., 19*, 29-32.

Armstrong, F., Heering, H., & Hirst, J. (1997). Reactions of complex metalloproteins studied by protein-film voltammetry. *Chem. Soc. Rev., 26*, 169.

Bamford, V., Armour, M., Mitchell, S., Cartron, M., Andrews, S., & Watson, K. (2008). Preliminary X-ray diffraction analysis of YqjH from *Escherichia coli*: a putative cytoplasmic ferri-siderophore reductase. *Acta Cryst, F64*, 792–796.

Baysse, C., Matthijs, S., Schobert, M., Layer, G., Jahn, D., & Cornelis, P. (2003). Co-ordination of iron acquisition, iron porphyrin chelation and iron–protoporphyrin export via the cytochrome c biogenesis protein CcmC in *Pseudomonas fluorescens*. *Microbiol., 149*, 3543–3552.

Beleneva, I., Magarlamov, T., Eliseikina, M., & Zhukova, N. (2009). Biochemical and pathogenic properties of the natural isolate of *Shewanella algae* from Peter the Great Bay, Sea of Japan. *J. Invertebr. Pathol., 102*, 250-255.

Birrell , J., & Hirst, J. (2013). Investigation of NADH Binding, Hydride Transfer,and NAD(+) Dissociation during NADH Oxidation by Mitochondrial Complex I Using Modified Nicotinamide Nucleotides. *Biochem., 52*, 4048-4055.

Blommel, P., Becker, K., Duvnjak, P., & Fox, B. (2007). Enhanced bacterial protein expression during auto-induction obtained by alteration of lac repressor dosage and medium composition. *Biotechnol Prog, 23*, 585-598.

Botelho-Nevers, E., Gouriet, F., Rovery, C., Paris, P., Roux, V., Raoult, D., & Brouqui, P. (2005). First case of osteomyelitis due to *Shewanella algae*. *J. Clin. Microbiol., 43*, 5388-5390.

Brown, K., & Ratledge, C. (1975). Iron transport in mycobacterium smegmatis: ferrimycobactin reductase (NAD(P)H: ferrimycobactin reductase), the enzyme releasing iron from its carrier. *FEBS lett., 53*, 262-266.

Butterton, J., & Calderwood, S. (1994). Identification, cloning, and sequencing of a gene required for ferric vibriobactin utilization by *Vibrio cholerae*. *J. Bacteriol., 176*, 5631-5638.

Cartron, M., Maddocks, S., Gillingham, P., Craven, C., & Andrews, S. (2006). Feo — transport of ferrous iron into bacteria. *BioMet., 19*(143-157).

Carvalho, C., & Fernandes, P. (2014). Siderophores as "Trojan Horses": tackling multidrug resistance? *Front. Microbiol., 5*, 1-3.

Caza, M., & Kronstad, J. (2013). Shared and distinct mechanisms of iron acquisition by bacterial and fungal pathogens of humans. *Front. Cel. Inf. Microbiol., 3*, 1-23.

Charles, M., Srirangaraj, S., & Kali, A. (2015). Neonatal sepsis caused by *Shewanella algae*: A case report. *Austral. Med. J., 8*, 64-66.

Chifman, J., Laubenbacher, R., & Torti, S. (2014). A systems biology approach to iron metabolism. *Adv Exp Med Biol., 844*, 201-225.

Constant, J., Chernev, I., & Gomez, E. (2014). *Shewanella putrefaciens* infective endocarditis. *Braz. J. Infect. Dis., 18*, 686-688.

Coves, J., & Fontecave, M. (1993). Reduction and mobilization of iron by a NAD(P)H:flavin oxidoreductase from *Escherichia coli*. *Eur. J. Biochem., 211*, 635-641.

Crichton, R., & Pierre, J. (2001). Old iron, young copper: from Mars to Venus. *BioMetals, 14*, 99-112.

Crosa, J. (1989). Genetics and molecular biology of siderophore-mediated iron transport in bacteria. *Microbiol. Rev., 53*, 517-530.

Crosa, J., & Walsh, C. (2002). Genetics and assembly line enzymology of siderophore. *Microbiol. Mol. Biol. Rev., 66*, 223-249.

Crumbliss, A., & Harrington, J. (2009). Iron sequestration by small molecules: thermodynamic and kinetic studies of natural siderophores and synthetic model compounds. *Adv. Inorg. Chem., 61*, 179-242.

Deneer, H., Healey, V., & Boychuk, I. (1995). Reduction of exogenous ferric iron by a surface-associated ferric reductase of *Listeria* spp. *Microbiology, 141*, 1985-1992.

Derby, H., & Hammer, B. (1931). Bacteriology of butter: IV - Bacteriological studies on surface taint butter. *Res. Bull., 141*(387-416).

Díaz-Quintana, A., Cruz-Gallardo, I., De La Rosa, M., & Díaz-Moreno, I. (2016). Diversity of interactions in redox systems: from short- to long-lived complexes. In R. Louro, & I. Díaz-Moreno (Eds.), *Redox proteins in supercomplexes and signalosomes* (pp. 35-60). Oxon, UK: CRC Press.

Doherty, C. (2007). Host-pathogen interactions: the role of iron. *J. Nutr. , 137*, 1341-1344.

Drewniak, L., Stasiuk, R., Uhrynows, W., & Sklodowska , A. (2015). *Shewanella* sp. O23S as a driving agent of a system utilizing dissimilatory arsenate-reducing bacteria responsible for self-cleaning of water contaminated with arsenic. *Int. J. Mol. Sci. , 16*, 14409-14427.

Duan, M., Wang, D., Wang, J., Xiao, X., Han, L., & Zhang, F. (2014). A case report of intracranial infection caused by *Shewanella putrefaciens*. *Neurol Sci*.

Ernst, J., & Winkelman, G. (1977). Enzymatic release of iron from sideramines in fungi: NADH: sideramine oxidoreductase in neurospora crassa. *Biochim. Biophys. Acta., 500*, 27-41.

Evans, E., Dodson, C., Maeda, K., Till Biskup, T., Wedge, C., & Timmel, C. (2013). Magnetic field effects in flavoproteins and related systems. *Inter. Foc. 3, 3*, 1-17.

Faou, A., & Morse , S. (1991). Characterization of a soluble ferric reductase from *Neisseria gonorrhoeae*. *Biol. Metals., 126-131*, 4.

Fielding, L. (2007). NMR methods for the determination of protein-ligand dissociation constants. *Prog. Nucl. Mag. Res. Sp., 51*, 219-242.

Fontecave, M., Covès, J., & Pierre, J. (1994). Ferric reductases or flavin reductases? *BioMetals, 7*, 3-8.

Fontecave, M., Eliasson, R., & Reichard, P. (1987). NAD(P)H:Flavin oxidoreductase of *Escherichia coli*. *J. Biol. Chem., 262*, 12325-12331.

Francis, J., Madinaveitia, J., Macturk, H., & Snow, G. (1949). Isolation from Acid-Fast Bacteria of a Growth-Factor for *Mycobacterium johnei* and of a Precursor of Phthiocol. *Nature, 163*, 365-366.

Fredrickson, J., Romine, M., Beliaev, A., Auchtung, J., Driscoll, M., Gardner, T., Reed, J. (2008). Towards environmental systems biology of *Shewanella*. *Nat. Rev. Microbiol., 6*, 592-603.

Fujita, M., & Sakai, R. (2014). Production of avaroferrin and putrebactin by heterologous expression of a deep-sea metagenomic DNA. *Mar. Drugs, 12*, 4799-4809.

Furukawa , A., Konuma, T., Yanaka, S., & Sugase, K. (2016). Quantitative analysis of protein–ligand interactions by NMR. *Prog. Nucl. Mag. Res. Sp.*

Gasteiger , E., Hoogland, C., Gattiker A., A., Duvaud, S., Wilkins, M., Appel, R., & Bairoch, A. (2005). Protein Identification and Analysis Tools on the ExPASy Server. In J. M. Walker (Ed.), *The Proteomics Protocols Handbook* (pp. 571-607). Humana Press.

Ghisla, S., & Massey, V. (1989). Mechanisms of flavoprotein-catalyzed reactions. *Eur. J. Biochem., 181*, 1-17.

Górska, A., Sloderbach, A., & Marszaff, M. (2014). Siderophore-drug complexes: potential medicinal applications of the ´Trojan horse´ strategy. *Trends Pharmacol. Sci. , 35*, 442-449.

Gram, L. (1994). Siderophore-mediated iron sequestering by Shewanella putrefaciens. *Appl. Environ. Microb., 60*, 2132-2136.

Gressier, M., Mbayo, D., Deramond, H., Grados, F., Eb, F., & Canarelli, B. (2010). First case of human spondylodiscitis due to *Shewanella algae*. *Int. J. Infec. Dis., 145*, 261-264.

Gründlinger, M., Gsaller, F., Schrettl, M., Lindner, H., & Haas, H. (2013). Aspergillus fumigatus SidJ mediates intracellular siderophore hydrolysis. *Appl. Environ. Microb., 79*, 7534 – 7536.

Hallé, F., & Meyer , J. (1989). Ferripyoverdine-reductase activity in *Pseudomonas fluorescens*. *Biol. Metals, 2*, 18-24.

Hallé, F., & Meyer, J. (1992). Ferrisiderophore reductases of *Pseudomonas*: Purification, properties and cellular location of the Pseudornonas aeruginosa ferripyoverdine reductase. *Eur. J. Biochem., 209*, 613-620.

Hantke, K. (1987). Ferrous iron transport mutants in *Escherichia coli* K-12. *FEMS Microbiol. Lett., 44*, 53-57.

Harrington, J., & Crumbliss, A. (2009). The redox hypothesis in siderophore-mediated iron uptake. *BioMetals, 22*, 679-689.

Heering, H., Hirst, J., & Armstrong, F. (1998). Interpreting the catalytic voltammetry of electroactive enzymes adsorbed on electrodes. *J. Phys. Chem. B. , 102*, 6889–6902.

Hesseltine, C., Pidacks, C., Whitehill, A., Bohonos, N., Hutchings, B., & Williams, J. (1952). Coprogen, a new growth factor for coprophilic fungi. *J. Am. Chem. Soc., 74*, 1362-1362.

Hider, R., & Kong, X. (2010). Chemistry and biology of siderophores. *Nat. Prod. Rep., 27*, 637-657.

Hirst, J. (2006). Elucidating the mechanisms of coupled electron transfer and catalytic reactions by protein film voltammetry. *Biochim. Biophys. Acta, 1757*, 225-239.

Holland, H. (2006). The oxygenation of the atmosphere and oceans. *Phil. Trans. R. Soc. B, 361*, 903-915.

Holt, H., Gahrn-Hansen, B., & Bruun, B. (2005). *Shewanella algae* and *Shewanella putrefaciens*: clinical and microbiological characteristics. *Clin. Microbiol. Infec., 11*, 347-352.

Homuth, M., Valentin-Weigand, P., Rohde, M., & Gerlach, G. (1998). Identification and characterization of a novel extracellular ferric reductase from *Mycobacterium paratuberculosis*. *Infect. Immun., 66*, 710-716.

Huston , D., & Logan, G. (2004). Barite, BIFs and bugs: evidence for the evolution for the evolution of Earth's early hydrosphere. *Earth Planet. Lett., 220*, 41-55.

Huyer, M., & Page, W. (1989). Ferric reductase activity in *Azotobacter vinelandii* and its inhibition by Zn^{2+}. *J. Bacteriol., 171*, 4031-4037.

Ilbert, M., & Bonnefoy, V. (2013). Insight into the evolution of the iron oxidation pathways. *Biochim. Biophys. Acta, 1827*, 161-175.

Ingelman, M., Ramaswamy, S., Nivière, V., Fontecave, M., & Eklund, H. (1999). Crystal Structure of NAD(P)H:Flavin Oxidoreductase from *Escherichia coli*. *Biochemistry, 38*, 7040-7049.

Janda, J. (2014). *Shewanella*: a marine pathogen as an Emerging cause of human disease. *Clin. Microbiol. Newslett., 36*, 25-29.

Jeuken, L., McEvoy, J., & Armstrong, F. (2002). Insights into gated electron-transfer kinetics at the electrode-protein interface: A square-wave voltammetry study of the blue copper protein azurin. *J. Phy. Chem. B, 106*, 2304-2313.

Kammler , M., Schön, C., & Hantke, K. (1993). Characterization of the ferrous iron uptake system of Escherichia coli. *J. Bacteriol., 175*, 6212-6219.

Khashe, S., & Janda, J. (1998). Biochemical and pathogenic properties of *Shewanella algae* and *Shewanella putrefaciens*. *J. Clin. Microbiol., 36*, 783-787.

Kiley, P., & Beinerty, H. (2003). The role of Fe–S proteins in sensing and regulation in bacteria. *Curr. Opin. Microbiol., 6*, 181-185.

Kim, B., Cho, S., Kang, B., Kim, I., Byun, J., Park, C., & Choi, S. (2014). A Case of spontaneous bacterial peritonitis with bacteremia caused by *Shewanella algae*. *Infect. Chemother., 46*, 264-268.

Koonin, E. (2014). Carl Woese's vision of cellular evolution and the domains of life. *RNA Biol., 11*, 197-204.

Kristiansen, M., Graversen, J., Jacobsen, C., Sonne, O., Hoffman, H., Lawk, S., & Moes, S. (2001). Identification of the haemoglobin scavenger receptor. *Nature, 409*, 198-201.

Kumari, K., Kaviyasarasan, V., Srividhya, R., & Sathishkumar, C. (2016). Devulging the treasure of hydroxamate siderophore on keratinocyte migration; its implications for wound healing. *Int. J. Adv. Res., 4*, 810-829.

Lau, C., Krewulak, K., & Vogel, H. (2015). Bacterial ferrous iron transport: the Feo system. *FEMS Microbiol. Rev.*, 273-298.

Lee , W., Ou , T., Chen, F., & Hsu, W. (2014). *Shewanella putrefaciens* bacteremia in a uremic patient receiving hemodialysis. *J. Microbiol. Immun. Infect., 49*, 59-60.

Lee, G., Lee, J., Kim, D., Yun, N., & Kim, S. (2013). A fatal *Shewanella algae* infection after an open tibial fracture following a tropical storm. *JBJS Case Conn., 3*, 1-4.

Levy, P., & Tessier, J. (1998). Arthiritis due to *Shewanella putrefaciens*. *Clin. Infect. Dis., 26*, 536.

Lewis, K., Epstein, S., D'Onofrio, A., & Ling, L. (2010). Uncultured microorganisms as a source of secondary. *J. Antibiot., 63*(468-476).

Li, K., Chen, W., & Bruner, S. (2015). Structure and mechanism of the siderophore-interacting protein from the fuscachelin gene cluster of *Thermobifida fusca*. *Biochemistry, 54*, 3989-4000.

Liu, J., Chakraborty, S., Hosseinzadeh, P., Yu, Y., Tian, S., Petrik, I., Lu, Y. (2014). Metalloproteins containing cytochrome, iron−sulfur, or copper. *Chem. Rev., 114*, 4366−446.

Liu, P., Shi, Z., Shyu, C., Wu, Z., Lai, K., Chang, C., Tung, K. (2014). Cobra bite wound infection caused by *Shewanella algae*. *Int. J. Infec. Dis., 20*, 11-12.

Lodge, J., Gaines, C., Arceneaux, E., & Byers, B. (1982). Ferrisiderophore reductase activity in *Agrobacterium tumefaciens*. *J. Bacteriol., 149*, 771-774.

Long, H., & Hammer, B. (1941). Classification of the organisms important in dairy products: III - *Pseudomonas putrefaciens*. *Res. Bulletin, 285*, 176-195.

Louro, R., Catarino, T., Salgueiro, C., LeGall, J., & Xavier, A. (1996). Redox-Bohr effect in the tetrahaem cytochrome c3 from *Desulfovibrio vulgaris*: a model for energy transduction mechanisms. *JBIC, 1*, 34-38.

Lyons, T., Reinhard, C., & Planavsky, N. (2014). The rise of oxygen in Earth's early ocean and atmosphere. *Nature, 506*, 307-315.

Mandin, P., Chareyre, S., & Barras, F. (2016). A regulatory circuit composed of a transcription factor, IscR, and a regulatory RNA, RyhB, controls Fe-S Cluster Delivery. *MBio., 7*, 1-9.

Mano, N., Kuhn, A., Menu, S., & Dufourc, E. (2003). Ca2+ enhanced catalytic NADH oxidation: a coupled 31P-NMR and electrochemistry study. *Phys. Chem. Chem. Phys., 5*, 2082-2088.

Martinez, J., & Butler, A. (2007). Marine amphiphilic siderophores: marinobactin structure, uptake and microbial partitioning. *J. Inorg. Biochem., 101*, 1692-1698.

Martinez, J., Carter-Franklin, J., Mann, E., Martin, J., Haygood, M., & Butler, A. (2003). Sttructure and membrane affinity of a suite of amphilic siderophores produced by a marine bacterium. *PNAS, 100*, 3754-3759.

Mas, M., & Colman, R. (1984). Phosphorus-31 nuclear magnetic resonance studies of the binding of nucleotides to to NADP+ specific isocitrate dehydrogenase. *Biochemistry, 23*, 1675-1683.

Matzanke, B., Anemüller , S., Schünemann, V., Trautwein, A., & Hantke, K. (2004). FhuF, part of a siderophore-reductase system. *Biochemistry, 43*, 1386-1392.

McHugh, J., Rodríguez-Quiñones, F., Abdul-Tehrani, H., Poole, R., Svistunenko, D., Cooper, C., & Andrews, S. (2003). Global iron-depedent gene regulation in *Escherichia coli*: a new mechanism for iron homeostasis. *J. Biol. Chem., 278*, 29478-29486.

McMahon, B., & Mayhew, S. (2007). Identification and properties of an inducible phenylacyl-CoA dehydrogenase in Pseudomonas putida KT2440. *FEMS Microbiol. Lett., 273*, 50-57.

Miethke, M., Kraushaar, T., & Marah, M. (2013). Uptake of xenosiderophores in *Bacillus subtilis* occurs with high affinity and enhances the folding stabilities of substrate binding proteins. *FEBS Lett., 587*, 206–213.

Miethke, M., & Marahiel, M. (2007). Siderophore-based iron aquisition and pathogen control. *Microbiol. Mol. Biol. Rev., 71*, 413-451.

Miethke, M., Hou, J., & Marahiel, M. (2011). The siderophore-interacting protein YqjH acts as a ferric reductase in different iron assimilation pathways of *Escherichia coli*. *Biochemistry, 50*, 10951-10964.

Miethke, M., Pierik, A., Peuckert, F., Seubert, A., & Marahiel, M. (2011). Identification and characterization of a novel-type ferric siderophore reductase from Gram-positive extremophile. *J. Biol. Chem. , 286*, 2245-2260.

Moody, M., & Dailey, H. (1985). Ferric iron reductase of *Rhodopseudomonas sphaeroides*. *J. Bacteriol., 163*, 1120-1125.

Müller, K., Matzanke, B., Schünemann, V., Trautwein, A., & Hantke, K. (1998). Fhuf, an iron-regulated protein of *Escherichia coli* with a new type of [2Fe-2S] center. *Eur. J. Biochem., 258*, 1001-1008.

Muñoz-Gallego, I., Chaves, F., & Angeles , M. (2016). Epidemiological and clinical characteristics of *Shewanella* spp. infections in a tertiary hospital in Madrid. *Infec. Dis.*, 2374-4243.

Myers, C., & Nealson, K. (1988). Bacterial manganese reduction and growth with manganese oxide as the sole electron acceptor. *Science, 240*, 1319-1321.

Nagoba, B., & Vedpathak, D. (2011). Medical applications of siderophores. *Eur. J. Gen. Med., 8*, 229-235.

Neilands, J. (1952). A crystalline organo-iron pigment from a rust Fungus (ustilago sphaerogena). *J. Am. Chem. Soc., 74*, 4846-4847.

Neilands, J. (1981). Microbial iron compounds. *Ann. Rev. Biochem., 50*, 715-731.

Nemeth, E., Tuttle, M., Powelson, J., Vaughn, M., Donovan, A., Ward, D., Kaplan, J. (2004). Hepcidin regulates cellular iron efflux by binding to ferroportin and inducing its internalization. *Science, 306*, 2090-2093.

Nishio, T., Hou, Z., Raymound, K., O'Sullivan, B., & Esker, T. (1998). A preorganized siderophore: thermodynamic and structural characterization of alcaligin and bisucaberin, microbial macrocyclic dihydroxamate chelating agents. *Inorg. Chem., 37*, 6630-6637.

O'Brien, S., Hodgson, D., & Buckling, A. (2014). Social evolution of toxic metal bioremediation in *Pseudomonas aeruginosa*. *Proc. R. Soc. B, 281*.

Ochiai, E.-I. (1986). Iron versus copper. *J. Chem. Ed., 63*, 942-944.

Oh, H., Kum, K., Kim, E., Lee, H., Choe, K., & Oh, M. (2008). Outbreak of *Shewanella algae* and *Shewanella putrefaciens* infections caused by a shared measuring cup in a general surgery unit in Korea. *Infect. Control. Hosp. Epidemiol., 29*, 742-748.

Otvos, J., Krum, D., & Masters, B. (1986). Localization of the free radical on the flavin mononucleotide of the air-stable semiquinone state of NADPH-cytochrome P-450 reductase using 31P NMR spectroscopy. *Biochemistry, 25*, 7220-7228.

Papanikolaou, G., & Pantopoulos, K. (2005). Iron metabolism and toxicity. *Toxicol. App. Pharmacol., 202*, 199-211.

Paulsen, K., Stankovich, M., Stockman, B., & Markley, J. (1990). Redox and Spectral Properties of a Flavodoxin from *Anabaena* 7120. *Arch. Biochem. Biophys., 290*, 68-73.

Pierre, J., Fontecave, M., & Crichton, R. (2002). Chemistry for an essential biological process: the reduction of ferric iron. *BioMetals, 15*, 341-346.

Poch, M., & Johnson , W. (1993). Ferric reductases of Legionella pneumophila. *BioMetals, 6*, 107-114.

Pope, T., Teague, W., Kossack, R., Bray, S., & Flannery, D. (1982). *Pseudomonas*: Sacroiliac osteomyelitis: diagnosis by gallium citrate Ga 67 scan. *Am. J. Dis. Child., 136*, 649-450.

Pruitt, K., Tatusova, T., & Maglott, D. (2005). NCBI Reference Sequence (RefSeq): a curated non-redundant sequence database of genomes, transcripts and proteins. *Nucleic Acids Res., 33*, 501–504.

Raines, D., Sanderson, T., Wilde, E., & Duhme-Klair, A.-K. (2015). Siderophores. *Ref. Mod. Chem. Mol. Sci. Chem. Eng.*

Reissbrodt, R., Heier, H., Tschape , H., Kingsley , R., & Williams, P. (2000). Resuscitation by ferrioxamine E of stressed *Salmonella enterica* serovar typhimurium from soil and water microcosms. *App. Env. Microbiol., 66*, 4128-4130.

Roger, S., Chen, S., Lawrence, S., & Sorrell, T. (1991). *Pseudomonas Putrefaciens* bacteraemia in a peritoneal dialysis patient. *Nephrol. Dial. Transplant., 6*.

Ryndak, M., Wang, S., Smith, I., & Rodriguez, G. (2010). The mycobacterium tuberculosis high-affinity iron importer, ItrA, contains an FAD-binding domain. *J. Bacteriol., 192*, 861-869.

Saha, M., Sarkar, S., Sarkar, B., Sharma, B., Bhattacharjee, S., & Tribedi, P. (2016). Microbial siderophores and their potential applications: a review. *Environ. Sci. Pollut. Res., 23*, 3984–3999.

Satomi, M. (2014). *Shewanella*. *Encycl. Food Microbiol., 3*, 397-407.

Schaible, U., & Kaufmann, S. (2004). Iron and microbial infection. *Nature Revi. Microbiol., 2*, 946-953.

Schoepp-Cothenet, B., Lis, R., Atteia, A., Baymann, F., Capowiez, L., Ducluzeau, A., Nitschke, W. (2013). On the universal core of bioenergetics. *Biochim. Biophys. Acta, 1927*, 79-73.

Schröder, I., Johnson, E., & Vries, S. (2003). Microbial ferric reductases. *FEMS Microbiol. Rev., 27*, 427-247.

Sedláček , V., Spanning, R., & Kučera, I. (2009). Ferric reductase A is essential for effective iron acquisiition in *Paracoccus dentrificans*. *Microbiology, 155*, 1294-1301.

Sessions, A., Doughty, D., Welander, P., Summons, R., & Newman, D. (2009). The continuing puzzle of the great oxidation event. *Curr. Biol., 19*, 567-574.

Sharma, K., & Kalawat, U. (2010). Emerging infections: *Shewanella* - A series of five cases. *J. Lab. Phys., 2*, 61-65.

Silva, J., & Williams, R. (1991). *The biological chemistry of elements* (1st ed.). Oxford: Oxford University Press.

Skaar, E. (2010). The battle for iron between bacterial pathogen and their vertebrate host. *PLoS Pathog., 6*, 1-4.

Smith, E., Davis, C., & Barber, M. (2003). Voltammetric simulations of multiple electron transfer/proton transfer coupled reactions: flavin adenine dinucleotide as a model system. *Anal. Biochem., 323*, 114-123.

Spasojević, I., Armstrong, S., Brickman, T., & Crumbliss, A. (1999). Electrochemical Behavior of the Fe(III)Complexes of the cyclic hydroxamate siderophores alcaligin and desferrioxamine E. *Inorg. Chem., 38*, 449-454.

Stephen, J. (2014). *Shewanella dysentery* in a patient with underlying malignancy. *Med J Malaysia , 69*, 284-285.

Studier, F. (2005). Protein production by auto-induction in high-density shaking cultures. *Protein Expression and Purification , 41*, 207-234.

Sutak, R., Chamot, C., Tachezy, J., Camadro, J., & Lesuisse, E. (2004). Siderophore and haem iron use by *Tritrichomonas foetus*. *Microbiology, 150*, 3979-3987.

Taberzadeh, M., Katouli, M., Amirinejad, R., Fazarneh, M., & Gharibi, O. (2014). A case of wound infection caused by *Shewanella algae* in the south of Iran. *New Microbes and New Infections, 2*, 29-30.

Tan, C., Lai, C., Kuar, W., & Hsueh, P. (2008). Purulent pericarditis with greenish pericardial effusion caused by *Shewanella algae*. *Journal of Clinical Microbiology, 46*, 2817-2819.

Tandara, L., & Salamunic, I. (2012). Iron metabolism: current facts and future directions. *Biochemia Medica, 22*, 311-328.

Trindade, I., Louro, R., Moe, E., Fonseca, B., & Matias, P. (2016). A putative siderophore-interacting protein from the marine bacterium *Shewanella frigidimarina* NCIMB 400: cloning, expression, purification,crystallization and X-ray diffraction analysis. *Acta Cryst. F, 72*.

Tsai, C., Senior, D., & Al-Kassim, L. (1989). Comparative studies on coenzyme specificity of dehydrogenases. *Comp. Biochem. Physiol., 94*, 655-659.

Tu, J., Lu, F., Miao, S., Ni, X., Jiang, P., Yu, H., Hu, Q. (2014). The siderophore-interacting protein is involved in iron acquisition and virulence of *Riemerella anatipestifer* strain CH3. *Veterinary Microbiology, 168*, 395–402.

Vadas, A., Johnson, E., Monbouquette, H., & Schröder, I. (1999). Identification and characterization of a novel ferric reductase from the hyperthermophilic archaeon *Archaeoglobus fulgidus*. *The Journal of Biological Chemistry , 274*, 36715–36721.

Vignier, N., Barreau, M., Olive, C., Baubion, E., Théodose, R., Hochedez, P., & Cabié, A. (2013). Human Infection with *Shewanella putrefaciens* and *S.algae*: report of 16 cases in Martinique and review of the literature. *Am. J. Trop. Med. Hyg., 89*, 151-156.

Viollier, E., Inglett, P., Hunter, K., Roychoudhury, A., & Cappellen, P. (2000). The ferrozine method revisited: Fe(II)/Fe(III) determination in natural waters. *Applied Geochemistry, 15*, 785-790.

Wagner, N., Otto, L., Podda, M., Schmitt, Y., & Tappe, D. (2013). Travel-related chronic hemorrhagic leg ulcer infection by *Shewanella algae*. *Journal of Travel Medicine, 262*, 1195-1982.

Wandersman , C., & Delepelaire , P. (2004). Bacterial iron sources: From siderophores to hemophores.58: 611–647. *Annu Rev Microbiol , 58*, 611-647.

Williams, R. (2007). A chemical systems approach to evolution. *Dalton Trans, 991*, 991-1001.

Williams, R. (2012). Iron in evolution. *FEBS Letters, 586*, 479-484.

Wu, W., Swanner, E., Hao, L., Zeitvogel, F., Obst, M., Pan, Y., & Kappler, A. (2014). Characterization of the physiology and cell–mineral interactions of the marine anoxygenic phototrophic Fe(II) oxidizer *Rhodovulum iodosum* – implications for Precambrian Fe(II) oxidation. *FEMS Microbiol Ecol , 88*, 503-515.

Wyckoff, E., Allred, B., Raymond, K., & Paynea, S. (2015). Catechol Siderophore Transport by *Vibrio cholerae*. *Journal of Bacteriology, 197*, 2840-2849.

Xia, M., Wei, J., Lei, Y., & Ying, L. (2007). A novel ferric reductase purified from *Magnetospirillum gryphiswaldense* MSR-1. *Current Microbiology, 55*, 71–75.

Yan, L., Zhang, S., Chen, P., & Li, H. (2012). Magnetotactic bacteria, magnetosomes and their application. *Microbiological Research , 167*, 507-519.

Yang, Y., Harris, D., Luo, F., Xiong, W., Joachimiak, M., Wu, L., Zhou, J. (2009). Snapshot of iron response in *Shewanella oneidensis* by gene network reconstruction. *BMC Genom., 10*, 1-17.

Zhang, S., Wang, X., Wang, H., & Bjerrum, C. (2016). Sufficient oxygen for animal respiration 1,400 million years ao. *PNAS, 113*, 1731-1736.

Appendice

Appendix nr.1: LC-MS profile of the ferric siderophores provided by Dr.Masaki Fujita.

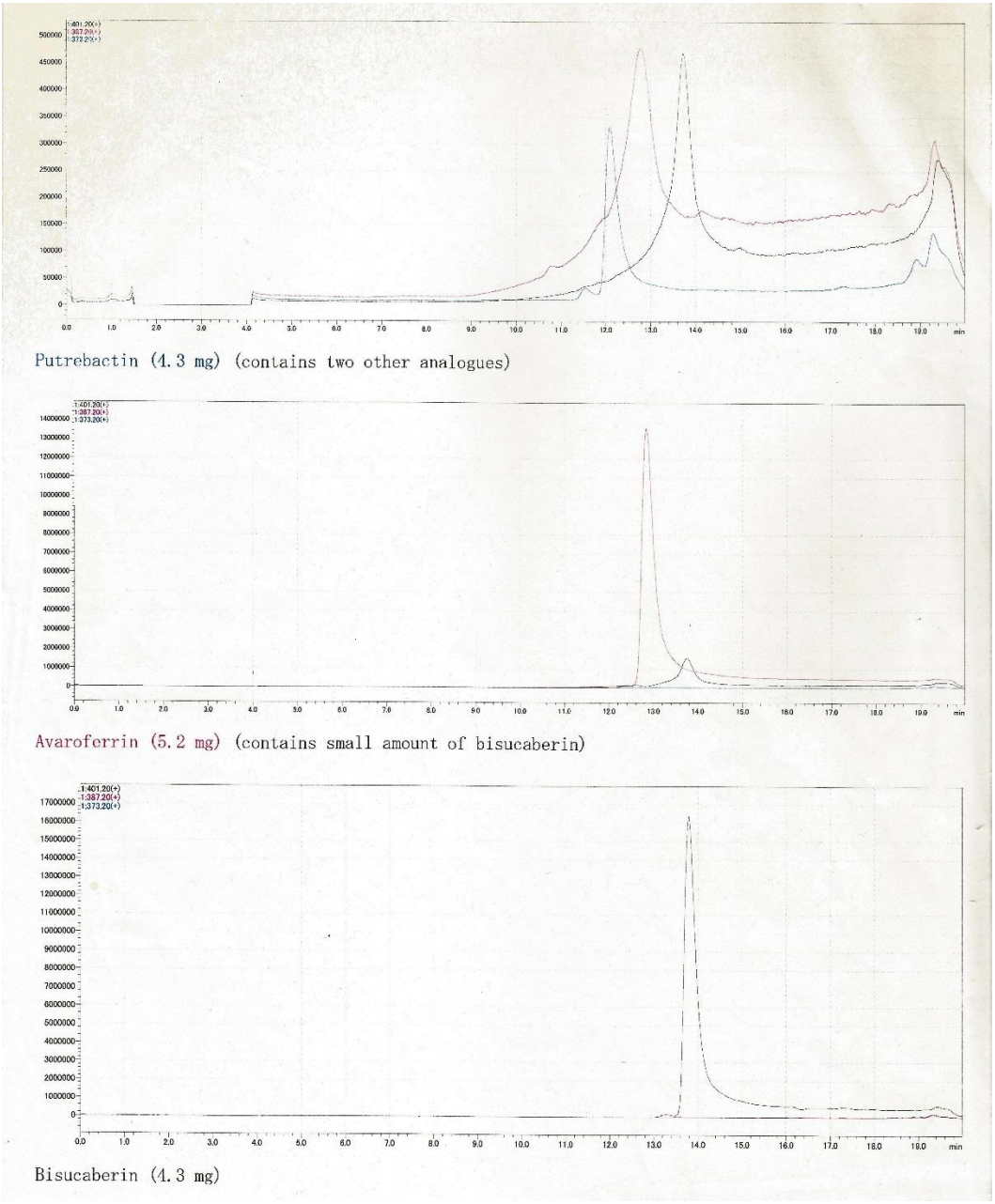

Appendix nr.2: On-going work, production of a ferrireductase from *Shewanella algae*

```
S. algae        MGISIASELNQL-----LAQKAAFYGEHFKA-----KESLEQLPQ--EAISLNSV-LSQA
E. coli         MAYRSAPLYEDIIWRTHLQPQDAGLAQAVRATIAKHREHLLEFIRLDEPAPLNAMTLAQW

S. algae        HYPVLLQQFALSYQAKVSTTCATKPEI--DARALHSMWSQWFFGLQLPPLLLWLFASQPG
E. coli         SSPNALSSLLAVYSDHI---YRNQPTMIRENKPLISLWAQWYIGLMVPPLMLALLTQEK-

S. algae        SALNRAIAAAACSGNWYLEPFDNGRAETFYLLLDADVSHPAPAGQLASWESLLEQLLIPI
E. coli         -------ALDVSPEHFHAEFHETGRVACFWVDMCED-KNATPHSPQQRMETLISQALVPV

S. algae        VERLAELGPVPSKLHFSHQAYIVHWYLGELSLPVSWRQQLIREMFEQAELQPRTYVAPIA
E. coli         VQALEATGEINGKLIWSNTGYLINWYLTEMKQLLG---EATVESLRHALFFEKTLTNGED

S. algae        HPFWRKLRLKQQ-SPRIACCLRHKLPCTQMCADCPLDKDGRKGKGQKACG
E. coli         NPLWRTVVLRDGLLVRRTCCQRYRLPDVQQCGDCTLK------------
```

Figure 1: Homology of ferrireductase from *S.algae* with Fhuf, FSR from *E.coli*. Golden highlighted residues represent unusual 2Fe-2S binding motif, blue capitals represent conserved residues.

The genome of *S. algae JCM*21037 encodes for ferrireductase (FR) (Reference PATRIC-Pathosystems Resource Integration Center), has a 28% identity with Fhuf from *E.coli* sharing its unusual 2Fe-2S cluster (Fig.1) with the binding motif C-C-$x_{10/11}$-C-x_2-C.

The ferrireductase gene was amplified via polymerase chain reaction (PCR) from the genomic DNA of Shewanella algae JCM21037 using the primers: 5' ATGGGAATAAGTATTGCCAGCGAGCTCAAC 3' and 5' CTAACCGCAGGCCTTTTGCCCTTTG 3'. The PCR product was ligated into the expression vector pETBlue-1 (Novagen) (Fig.2) and transformed into various competent cells including: *E.coli Tuner* (DE3) pLacI and *E.coli BL21* (DE3). Expression tests using different media, temperature, aeration and induction types have been performed but so far no overexpression of FR has been found.

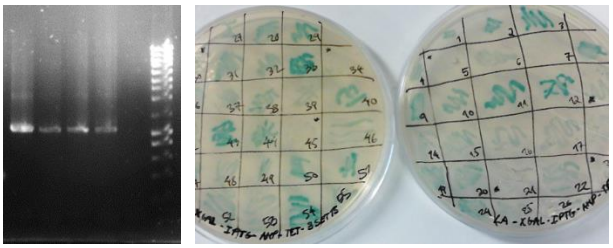

Figure 2: Positive gene amplification and insertion in pET BLUE (left-hand side). Positive colony-screening (right-hand side).

Appendix nr.3: Published article: ""A putative siderophore-interacting protein from the marine bacterium *Shewanella frigidimarina* NCIMB 400: cloning, expression, purification, crystallization and X-ray diffraction analysis".

STRUCTURAL BIOLOGY COMMUNICATIONS
ISSN 2053-230X

A putative siderophore-interacting protein from the marine bacterium *Shewanella frigidimarina* NCIMB 400: cloning, expression, purification, crystallization and X-ray diffraction analysis

Inês B. Trindade,[a] Bruno M. Fonseca,[a] Pedro M. Matias,[a,b] Ricardo O. Louro[a] and Elin Moe[a]*

[a]Instituto de Tecnologia Química e Biológica António Xavier, Universidade Nova de Lisboa, Avenida da República (EAN), 2780-157 Oeiras, Portugal, and [b]Instituto de Biologia Experimental e Tecnológica (iBET), Apartado 12, 2780-901 Oeiras, Portugal. *Correspondence e-mail: elinmoe@itqb.unl.pt

Received 1 June 2016
Accepted 13 July 2016

Edited by M. S. Weiss, Helmholtz-Zentrum Berlin für Materialien und Energie, Germany

Keywords: siderophore-interacting protein; *Shewanella frigidimarina*; crystallographic analysis.

Siderophore-binding proteins (SIPs) perform a key role in iron acquisition in multiple organisms. In the genome of the marine bacterium *Shewanella frigidimarina* NCIMB 400, the gene tagged as SFRI_RS12295 encodes a protein from this family. Here, the cloning, expression, purification and crystallization of this protein are reported, together with its preliminary X-ray crystallographic analysis to 1.35 Å resolution. The SIP crystals belonged to the monoclinic space group $P2_1$, with unit-cell parameters a = 48.04, b = 78.31, c = 67.71 Å, α = 90, β = 99.94, γ = 90°, and are predicted to contain two molecules per asymmetric unit. Structure determination by molecular replacement and the use of previously determined ~2 Å resolution SIP structures with ~30% sequence identity as templates are ongoing.

1. Introduction

The Great Oxygenation Event (GOE) was marked by a profound transition in ocean chemistry, where the previously readily available iron became a limiting nutrient worth battling for (Holland, 2006). In an oxygen-rich atmosphere, two redox states of iron are accessible to biology: an oxidized, insoluble ferric state, iron(III), and a highly reactive reduced ferrous state, iron(II). The reversibility of this redox pair, iron(II)/iron(III), plays a crucial role in several metabolic processes including the electron-transport chain, photosynthesis, oxidative phosphorylation and the tricarboxylic acid cycle (Miethke & Marahiel, 2007).

To circumvent low iron bioavailability, organisms have found diverse strategies for importing and utilizing iron, including direct extracellular reduction (Deneer *et al.*, 1995), the acquisition of iron-bound or haem proteins using specific receptors (Wandersman & Delepelaire, 2004) and the synthesis and extracellular release of small molecules with high affinity for ferric iron named siderophores (Neilands, 1981).

These iron siderophores are strong ferric chelators and can be used in various applications, including the cultivation of uncultured microorganisms, as ecofriendly substitutes for pesticides, as enhancers in the bioremediation of heavy metals, in iron-overload therapy, in cancer therapy and as Trojan horse antibiotics (Saha *et al.*, 2016).

Given their vast applications, considerable efforts have been made in research to understand the mechanistic details behind siderophore synthesis, transport and regulation (Miethke *et al.*, 2011; Schalk & Guillon, 2013; Crosa & Walsh,

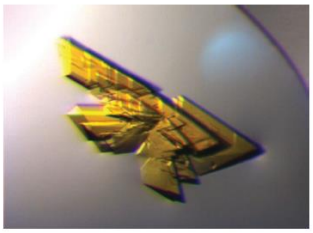

OPEN ACCESS

Table 1
Macromolecule-production information.

Source organism	*S. frigidimarina* NCIMB 400
DNA source	*S. frigidimarina* NCIMB 400
Forward primer (5′–3′)	ATG AAT AAC CAA TCA GCT AAA AAA TCT CC
Reverse primer (5′–3′)	CTA CAA CGG CTG CAT CTG CTT TTG
Cloning vector	pETBlue-1 (Novagen)
Expression vector	pETBlue-1 (Novagen)
Expression host	*E. coli* Tuner (DE3) pLacI
Complete amino-acid sequence of the construct produced	MNNQSAKKSPTRLTYISDIIEISPYLRRLVLSGE-QLANFPADQQGAYVKVLIPQPGETTVNMTLTG-PNAAIKRSYTIREFDPVRGQLSLDFVINKHTG-PATDWAKLANVGDTVAIAGPGPLKMNRFDFND-YLLFGDSTSINAVDALIKRLPATAKGHIIMLV-NSHQEQALLSQHPLLKTHWLVLNDSITAEQQI-DWLLDKLELFGDLPAVTQVFVGLEATQVRVIK-QYLLEQQQLPLSSISATGYWKRNTDADTFGKQ-KQMQPL
Theoretical pI†	7.6

† Calculated using *Protein Calculator* (http://protcalc.sourceforge.net/).

2002). At the molecular level, one of the least explored aspects of siderophore use is the release of the imported iron from ferric siderophore complexes. In order to be utilized, iron needs to be released from these high-affinity complexes. Two strategies have been reported so far. One is the release of iron through hydrolytic cleavage of the siderophore complex by esterases (Brickman & McIntosh, 1992). The other is single-electron reduction, also known as siderophore recycling, which is either mediated by unspecific endogenous reducing agents (Brickman & McIntosh, 1992) or by specific siderophore ferric reductases (Miethke *et al.*, 2011).

In 2015, Li and coworkers suggested that two families of specific siderophore reductases exist. One is the FAD-containing siderophore-interacting protein (SIP) family and the other is the ferric siderophore reductase (FSR) protein family, which contains an iron–sulfur cluster as a redox centre (Li *et al.*, 2015). Several members of the SIP family have been characterized [for example, ViuB from *Vibrio cholerae* (Butterton & Calderwood, 1994), IrtA from *Mycobacterium tuberculosis* (Ryndak *et al.*, 2010), YqjH from *Escherichia coli* (Miethke *et al.*, 2011) and FscN from *Thermobifida fusca* (Li *et al.*, 2015)]. Presently, catalytic mechanisms have been proposed for the SIP family, namely for its members YqjH and FscN. Both of these proteins indicate a preference for NADPH as a reducing agent, although YqjH is able to reduce various iron chelates, whereas FscN is only able to reduce the endogenous siderophore fuscachelin (Miethke *et al.*, 2011; Li *et al.*, 2015). Two structures of SIPs have been deposited in the PDB: the 1.89 Å resolution structure of FscN from the Gram-positive *T. fusca* (PDB entry 4yhb; Li *et al.*, 2015) and the 2.2 Å resolution structure of a SIP from the Gram-negative bacterium *Shewanella putrefaciens* (PDB entry 2gpj; Joint Center for Structural Genomics, unpublished work). Here, we report the cloning, expression, purification and crystallization of a SIP from the marine bacterium *S. frigidimarina* NCIMB 400. Further knowledge of the mechanistic and structural details of this family of proteins, namely with respect to the ligand-binding pockets, may provide new strategies for controlling the performance of siderophore recycling and utilization. This knowledge is relevant for the development of new drugs that inhibit the growth and virulence of pathogens and also for promoting a more efficient use of siderophores in bioremediation *via* the protein engineering of SIPs.

2. Materials and methods

2.1. Macromolecule production

The SFRI_RS12295 gene fragment was amplified *via* polymerase chain reaction (PCR) from the genomic DNA of *S. frigidimarina* NCIMB 400 using the primers listed in Table 1. The PCR product was ligated into the expression vector pETBlue-1 (Novagen) and transformed into competent *E. coli* Tuner (DE3) pLacI cells for expression. Protein over-expression was achieved using an autoinduction method (Blommel *et al.*, 2007; Studier, 2005). The cells were first grown overnight in Luria–Bertani (LB) medium supplemented with 35 mg l^{-1} chloramphenicol and 100 mg l^{-1} ampicillin at 303 K and 170 rev min^{-1}. 2% of this culture served as the inoculum. The auto-induction medium was made by adding 50 ml 20× NPS stock solution [1 *M* Na_2HPO_4, 1 *M* KH_2PO_4, 500 m*M* $(NH_4)_2SO_4$] and 20 ml 50× 5052 stock solution consisting of 25%(*w*/*v*) glycerol, 2.5%(*w*/*v*) glucose, 10%(*w*/*v*) α-lactose monohydrate to 1 l LB medium supplemented with 1 m*M* $MgSO_4$, 35 mg l^{-1} chloramphenicol and 100 mg l^{-1} ampicillin (Blommel *et al.*, 2007; Studier, 2005). The cells were allowed to grow continuously for 30 h at 303 K and 170 rev min^{-1}.

Cells were harvested by centrifugation for 10 min at 11 305*g* and were then cooled to 193 K. The cells were later defrosted and resuspended in 20 m*M* Tris–HCl buffer pH 7.6 with a protease-inhibitor cocktail (Roche) and DNase I (Sigma) prior to a three-pass cell disruption at 6.9 MPa using a French press. The lysate was centrifuged at 11 305*g* to remove undisrupted cells and then ultracentrifuged at 204 709*g* for 90 min at 277 K to remove cell membranes and debris. The supernatant was dialyzed overnight against 20 m*M* Tris–HCl buffer pH 7.6 and concentrated using an Amicon Ultra Centrifugal Filter (Millipore) with a 10 kDa cutoff. The SIP was purified from the supernatant using two ion-exchange chromatography columns: a Q Sepharose Fast Flow column (GE Healthcare) followed by an SP Sepharose Fast Flow column (GE Healthcare). Both columns had previously been equilibrated with 20 m*M* Tris–HCl buffer pH 7.6 and were used with a stepwise elution method. The fraction containing the SIP eluted from the Q Sepharose column at 150 m*M* NaCl. This fraction was dialyzed against 20 m*M* Tris–HCl buffer pH 7.6, concentrated and loaded onto the SP Sepharose column. The fraction containing the SIP was eluted at 100 m*M* NaCl.

Eluted fractions were analysed by SDS–PAGE with Blue-Safe staining (NZYTech) and UV–visible spectroscopy to select fractions containing the purified SIP.

2.2. Crystallization

Purified protein (30 mg ml^{-1}) in 20 m*M* Tris–HCl pH 7.6, 150 m*M* NaCl was diluted to 10 mg ml^{-1} with 20 m*M* Tris–HCl pH 7.6 (final salt concentration 50 m*M* NaCl) and used for

crystallization experiments on a Honeybee Cartesian crystallization robot (Genomic Systems) with MDL3 plates (100 nl protein solution and 40 µl reservoir solution) and the JCSG-*plus* crystallization screen (Molecular Dimensions). Yellow crystals appeared in 12 out of 96 crystallization conditions. The most promising crystals were found in well A5 with the following reservoir solution: 20% PEG 3350, 0.2 *M* magnesium formate dihydrate. In an attempt to improve the crystal size, hanging-drop optimization experiments were performed by hand, varying the concentration of PEG 3350 from 18 to 22%(*w*/*v*) and of magnesium formate dihydrate from 0.18 to 0.22 *M*. Crystals appeared in all conditions after 1 d and were fully grown after 3 d. In order to confirm that the crystals obtained consist of the SIP, crystals were collected from some of the drops, washed twice in reservoir solution and analysed by SDS–PAGE. The crystallization conditions for the crystal used for data collection are described in Table 2.

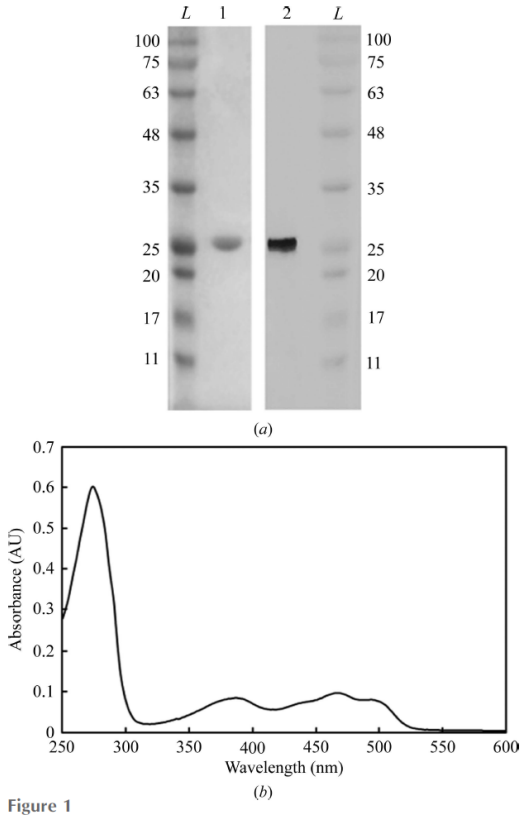

Figure 1
(*a*) 12% SDS–PAGE gels. Lanes 1 and 2 correspond to the purified SIP fraction before crystallization and dissolved multiple crystals of the SIP, respectively. Lane *L* corresponds to the protein ladder (labelled in kDa). (*b*) UV–visible profile of the purified protein. The UV–visible spectrum was measured in a Shimadzu UV-1800 UV–Vis spectrophotometer using a fast scan rate.

Table 2
Crystallization conditions.

Method	Hanging drop
Plate type	EasyXtal 15-Well Tool (Qiagen)
Temperature (°C)	18
Protein concentration (mg ml^{-1})	10
Buffer composition of protein solution	20 m*M* Tris–HCl pH 7.6, 50 m*M* NaCl
Composition of reservoir solution	22% PEG 3350, 0.22 *M* magnesium formate dihydrate
Volume and ratio of drop	2 µl, 1:1
Volume of reservoir (µl)	500

Table 3
Data collection and processing.

Diffraction source	Beamline I04, DLS
Wavelength (Å)	0.9795
Temperature (K)	100
Detector	Pilatus 6M-F
Rotation range per image (°)	0.10
Total rotation range (°)	180
Exposure time per image (s)	0.040
Space group	$P2_1$
a, *b*, *c* (Å)	48.04, 78.31, 67.71
α, β, γ (°)	90, 99.94, 90
ISa	12.0
Resolution range (Å)	18.6–1.35 (1.39–1.35)
Total No. of reflections	357812 (26206)
No. of unique reflections	107545 (7947)
Completeness (%)	99.4 (99.6)
Multiplicity	3.3 (3.3)
$\langle I/\sigma(I)\rangle$†	7.1 (1.3)
R_{meas}	0.098 (0.970)
Overall *B* factor from Wilson plot (Å^2)	15.2

† Mean $I/\sigma(I) < 2.0$ at 1.45 Å.

2.3. Data collection and processing

Crystals from several drops were briefly soaked in 22%(*w*/*v*) PEG 3350, 0.2 *M* magnesium formate dihydrate before being flash-cooled in liquid nitrogen or were cooled directly from the crystallization drop in cases where the PEG 3350 concentration was 22%. The best diffracting crystal grew in 22% PEG 3350, 0.22 *M* magnesium formate dehydrate, and data to 1.35 Å resolution were collected on beamline I04 at Diamond Light Source (DLS), UK. A total of 1800 images were collected using 0.1° oscillation width and the data were autoprocessed by *xia*2 (Winter, 2010), which makes use of *XDS* (Kabsch, 2010) and the *CCP*4 suite (Winn *et al.*, 2011) for integration and truncation of the data. The data-collection and processing statistics are listed in Table 3.

3. Results and discussion

The SIP was purified to apparent purity (>95%) by ion-exchange chromatography as described in §2. The purified protein appeared yellow and migrated as a single band at ~30 kDa on a 12% SDS–PAGE gel, as expected from theoretical calculations (Fig. 1*a*). Yellow-coloured crystals were dissolved and migrated as a 30 kDa protein on an SDS–PAGE gel, as observed for the purified protein (Fig. 1*a*), and confirmed that the crystals consist of the SIP. The purified protein was also analysed by UV–visible spectroscopy and

showed typical spectral features of an oxidized flavoprotein in the UV–visible region (Fig. 1*b*), with absorption peaks at 387 and 470 nm.

The crystal which was used for data collection was multiple, similar to that shown in Fig. 2. However, it was possible to obtain good-quality diffraction data from one of the single-crystal components, and no special precautions were needed in processing despite the apparent split crystal. No colour change of the crystal was observed during data collection, indicating an unchanged redox state of the FAD throughout X-ray exposure.

The 22% PEG 3350 concentration was sufficient to provide adequate crystal cryoprotection. In the partial diffraction image shown in Fig. 2, the lack of ice rings can be appreciated; although a weak diffuse scattering ring from the solvent is present, the maximum number of counts per pixel is not greater than 3.

The SIP crystals belonged to the monoclinic space group $P2_1$, with unit-cell parameters $a = 48.04$, $b = 78.31$, $c = 67.71$ Å, $\beta = 99.94°$. Cell-volume considerations (Matthews, 1968; Kantardjieff & Rupp, 2003) indicate that there are two SIP monomers in the asymmetric unit, with a V_M of 2.13 Å^3 Da^{-1} and an estimated solvent content of 42.4%. Although a self-rotation plot failed to reveal any significant trace of non-crystallographic twofold rotation axes, a native Patterson map calculated using data to 2.5 Å resolution displayed a strong non-origin peak at coordinates (1/2, 0, 1/2) with a peak height 61% of that of the origin, suggesting translational noncrystallographic symmetry consistent with a pseudo-*B*-centred lattice (Fig. 3). The overall twinning score was 2.28; thus, the data do not appear to be twinned.

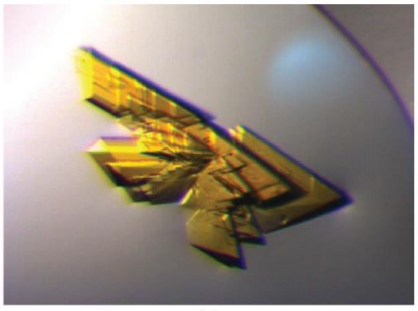

(*a*)

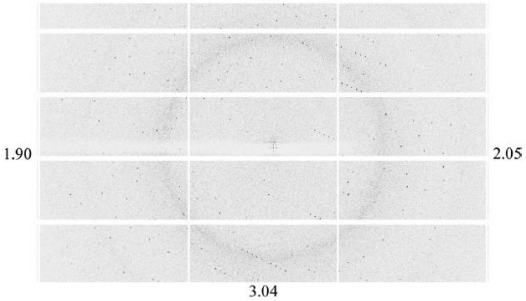

(*b*)

Figure 2
(*a*) Example of a multiple crystal of the SIP similar to that used for data collection on beamline I04 at DLS. (*b*) Detailed view of a SIP diffraction image obtained using a Pilatus 6M-F detector on beamline I04 at DLS. The numbers at the edge indicate the corresponding resolution limits. In the faintly visible diffuse scattering ring at ∼3.8 Å resolution, the maximum number of counts per pixel away from Bragg reflections is 3.

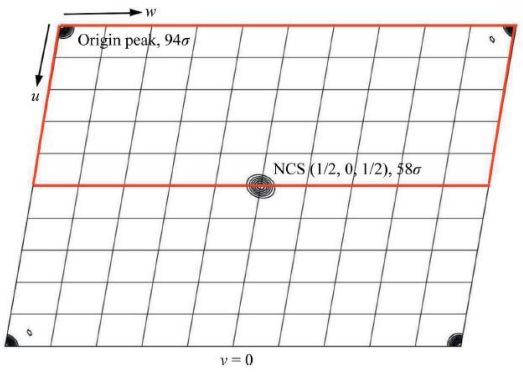

Figure 3
$v = 0$ section of a native Patterson map calculated using data to 2.5 Å resolution showing the presence of a strong non-origin peak at coordinates (1/2, 0, 1/2) consistent with pseudo-*B*-centring. Contour levels are drawn every 10 map r.m.s.d. units between 5 and 100 r.m.s.d. units. The section is drawn between $0 \le u \le 1$ and $0 \le w \le 1$ and the asymmetric unit is outlined in red.

Attempts will be made to determine the crystal structure by molecular replacement (MR) using the previously determined SIP structures PDB entries 2gpj (2.2 Å resolution) and 4yhb (1.89 Å resolution), which show 32 and 28% sequence identity, respectively, as templates. The higher resolution crystal structure of the SIP from *S. frigidimarina* will provide crucial information regarding the molecular mechanism underlying iron acquisition in microorganisms.

Acknowledgements

This work was financially supported by Project LISBOA-01-0145-FEDER-007660 (Microbiologia Molecular, Estrutural e Celular) funded by FEDER funds through COMPETE2020 – Programa Operacional Competitividade e Internacionalização [POCI, the European Community's Seventh Framework Program (FP7/2007-2013)] under Grant Agreement 283570 (BioStruct-X), and by national funds and postdoctoral fellowships SFRH/BPD/94050/2013 and SFRH/BPD/93164/2013 to EM and BFM, respectively, through FCT (Fundação para a Ciência e a Tecnologia). Beamtime at I04 at Diamond Light Source (DLS) and assistance from the beamline staff are gratefully acknowledged (http://www.diamond.ac.uk/Beamlines/Mx/I04.html).

References

Blommel, P. G., Becker, K. J., Duvnjak, P. & Fox, B. G. (2007). *Biotechnol. Prog.* **23**, 585–598.

Brickman, T. J. & McIntosh, M. A. (1992). *J. Biol. Chem.* **267**, 12350–12355.
Butterton, J. R. & Calderwood, S. B. (1994). *J. Bacteriol.* **176**, 5631–5638.
Crosa, J. H. & Walsh, C. T. (2002). *Microbiol. Mol. Biol. Rev.* **66**, 223–249.
Deneer, H. G., Healey, V. & Boychuk, I. (1995). *Microbiology*, **141**, 1985–1992.
Holland, H. D. (2006). *Philos. Trans. R. Soc. Lond. B Biol. Sci.* **361**, 903–915.
Kabsch, W. (2010). *Acta Cryst.* D**66**, 125–132.
Kantardjieff, K. A. & Rupp, B. (2003). *Protein Sci.* **12**, 1865–1871.
Li, K., Chen, W.-H. & Bruner, S. D. (2015). *Biochemistry*, **54**, 3989–4000.
Matthews, B. W. (1968). *J. Mol. Biol.* **33**, 491–497.
Miethke, M., Hou, J. & Marahiel, M. A. (2011). *Biochemistry*, **50**, 10951–10964.
Miethke, M. & Marahiel, M. A. (2007). *Microbiol. Mol. Biol. Rev.* **71**, 413–451.
Neilands, J. B. (1981). *Annu. Rev. Biochem.* **50**, 715–731.
Ryndak, M. B., Wang, S., Smith, I. & Rodriguez, G. M. (2010). *J. Bacteriol.* **192**, 861–869.
Saha, M., Sarkar, S., Sarkar, B., Sharma, B. K., Bhattacharjee, S. & Tribedi, P. (2016). *Environ. Sci. Pollut. Res. Int.* **23**, 3984–3999.
Schalk, I. J. & Guillon, L. (2013). *Amino Acids*, **44**, 1267–1277.
Studier, F. W. (2005). *Protein Expr. Purif.* **41**, 207–234.
Wandersman, C. & Delepelaire, P. (2004). *Annu. Rev. Microbiol.* **58**, 611–647.
Winn, M. D. *et al.* (2011). *Acta Cryst.* D**67**, 235–242.
Winter, G. (2010). *J. Appl. Cryst.* **43**, 186–190.